MAXWELL-STEFAN MODELING OF MASS TRANSFER EFFECTS IN REACTIVE CHROMATOGRAPHY

by

JOSÉ IGNACIO MEZA PEREIRA

A thesis submitted as a partial fulfillment
of the requirements for the degree of

DOCTOR OF PHILOSOPHY

IN

CHEMICAL ENGINEERING

UNIVERSITY OF PUERTO RICO
MAYAGÜEZ CAMPUS
2009

Approved by:

Lorenzo Saliceti Piazza, Ph.D. Member, Graduate Committee	Date
Gilberto Villafañe Ruiz, Ph.D. Member, Graduate Committee	Date
Jaime Benítez Rodríguez, Ph.D. Chairman, Graduate Committee	Date
Félix Román, Ph.D. Representative of Graduate School	Date
David Suleiman Rosado, Ph.D. Chairperson of the Department and Member, Graduate Committee	Date

ABSTRACT

A rigorous dynamic theoretical model was developed and implemented for simultaneous diffusion, reaction, and adsorption inside porous solids for the fixed bed chromatographic reactor (FBCR), true moving bed chromatographic reactor (TMBCR), and simulated moving bed chromatographic reactor (SMBCR). It takes into account multicomponent inter-particle and intra-particle mass-transfer effects using the Maxwell-Stefan approach. In all the simulation results, this model proved to be robust and in all cases predicted very accurately the experimental data for several chromatographic reactor case studies from the recent literature with nonlinear multicomponent adsorption isotherms catalyzed by the acid resin Amberlyst 15. They included the synthesis of diethylacetal from ethanol and acetaldehyde; the production of triacetine, from glycerol and acetic acid; the production of dimethylacetal from methanol and acetaldehyde; the synthesis of ethyl lactate, from ethanol and lactic acid; and the synthesis of methylacetate from methanol and acetic acid.

The model based on the Maxwell-Stefan approach was found to predict the behavior of the FBCR, TMBCR, and SMBCR significantly better than the previous linear driving force (LDF) and Fickian diffusivity approximations. It was also used to compare the predictions of the TMBCR and SMBCR for any given application. It was found that, for some applications, the TMBCR approximation of the SMBCR performance is not justified.

The influence of feed composition, switching time, and reaction separation region on the performance of a SMBCR for diethylacetal synthesis was analyzed by simulation. The best operational point in terms of productivity (24.29 kg of acetal/L of adsorbent-day) and desorbent consumption (5.15 L ethanol/kg acetal) for 97% purity of both raffinate and extract was found to

be a switching time of 3.75 min, feed concentration of 80% mol of acetaldehyde, and fluid/solid flow ratios in sections II and III of γ_{II} = 2.625, γ_{III} =3.5, respectively.

The numerical solution of all model equations was obtained for transient (in the FBCR, TMBCR, and SMBCR) and steady state (in the TMBCR) using MATLAB®7.

RESUMEN

Se desarrolló e implementó un modelo teórico dinámico y riguroso para describir procesos simultáneos de difusión, reacción y adsorción dentro de sólidos porosos para reactores cromatográficos de lecho fijo (FBCR, por sus siglas en inglés), de flujo real contra-corriente (TMBCR, por sus siglas en inglés) y de flujo contra-corriente simulado (SMBCR, por sus siglas en inglés). El mismo toma en consideración efectos de transferencia de masa dentro y fuera de la partícula en sistemas multicomponentes usando el enfoque de Maxwell-Stefan. En todas las simulaciones, el modelo demostró ser robusto y predijo con gran precisión los datos experimentales para varios casos de reactores cromatográficos, tomados de la literatura reciente, con isotermas no lineares de adsorción multicomponente catalizadas por la resina ácida Amberlyst 15. Estos casos incluyeron la síntesis de dietilacetato, a partir de etanol y acetaldehído; la producción de triacetina, a partir de glicerol y ácido acético; la producción de dimetilacetato, a partir de metanol y acetaldehído; la síntesis de lactato de etilo, a partir de etanol y ácido láctico; y la síntesis de metilacetato, a partir de metanol y ácido acético.

El modelo basado en el enfoque de Maxwell-Stefan predijo el comportamiento de FBCRs, TMBRs y SMBRs significativamente mejor que las aproximaciones previamente usadas en la literatura de potencial linear (LDF, por sus siglas en inglés) y difusividad de Fick. También fue usado para comparar las predicciones del comportamiento TMBCR y SMBCR para cada una de las aplicaciones. Se encontró que, para algunos casos, no se justifica aproximar el comportamiento de un SMBCR con el de un TMBCR.

Se estudió mediante simulaciones la influencia que tienen en el rendimiento de un SMBCR para la síntesis de dietilacetato variables como la composición de la alimentación, el

tiempo de cambio (“switch time”) y la región operacional de reacción/separación. El punto óptimo de operación en términos de productividad (24.29 kg de producto/L de adsorbente-día) y consumo de desorbente (5.15 L etanol/kg de producto), para una pureza de 97% de ambos extracto y rafinado, resultó ser un tiempo de cambio de 3.75 minutos, concentración de la alimentación de 80% molar de acetaldehído, y razones de flujo líquido/sólido en las secciones II y III de γ_{II} = 2.625, γ_{III} =3.5, respectivamente.

Las soluciones numéricas de todas las ecuaciones del modelo fueron obtenidas para el estado transitorio (en los FBCR, TMBCR y SMBCR) y para el estado estacionario (en el TMBCR) usando MATLAB®7.

Table of Contents

List of Figures viii
List of Tables xiv
Chapter 1 Introduction to Reactive Chromatography 1
1.1 Motivation 1
1.2 Previous works on chromatographic reactors 4
1.2.1 Fixed bed chromatographic reactor (FBCR) 6
1.2.2 Continuous rotating annular chromatographic reactor (CRACR) 10
1.2.3 Countercurrent True Moving Bed Chromatographic Reactor 14
1.2.4 Simulated Moving Bed Chromatographic Reactor (SMBCR) 17
1.3 Modeling of Chromatographic Reactors 22
1.4 Research objectives 26
Chapter 2. Mathematical Description of Fixed Bed Chromatographic Reactors 28
2.1 Modeling of chromatographic reactors 28
2.1.1 Mass balance or continuous models 31
2.1.2 Model Solution 46
2.1.3 Parameters Estimation 54
2.2 FBCR Simulation with Maxwell-Stefan Approach 56
2.2.1 Application 1: Diethylacetal Synthesis 56
2.2.2 Application 2: Production of Triacetin 62
2.3 Conclusions 76
Chapter 3. Maxwell-Stefan in Continuous Reactive Chromatography: Simulated Moving Bed Chromatographic Reactor 78
3.1 Introduction 78
3.2 Modeling Strategies for the SMBCR Process 80
3.2.1 Model Equations Using a SMBCR Strategy 81
3.2 Numerical Solution 86
3.3 SMBCR Simulation with Maxwell-Stefan Approach 86

3.3.1 Application 1: Dimethylacetal Synthesis 86
3.3.2 Application 2: Ethyl Lactate Synthesis 94
3.4 Conclusions 99
Chapter 4. Modeling SMBCR Performance Using the True Moving Bed Chromatographic Reactor (TMBCR) Approach 101
4.1 Introduction 101
4.2 Transient and Steady State Models for the TMBCR Strategy 103
4.3 TMBCR Simulation with the Maxwell-Stefan Approach 107
4.3.1 Model Validation for TMBCR at Steady State. 107
4.4. Comparison of True and Simulated Moving Bed Chromatographic Reactor 114
4.4.1 Comparison of True and Simulated Moving Bed Chromatographic Reactor Predictions with the LDF Model 114
4.4.2 Comparison of True and Simulated Moving Bed Chromatographic Reactor Using the Maxwell-Stefan Approach Model 117
4.5 Conclusions 120
Chapter 5. Performance Assessment of SMBCR Operational Parameters 121
5.1 Introduction 121
5.2 Criteria for Performance Assessment of SMBCR Parameters 121
5.3 Performance of a SMBCR: synthesis of diethylacetal as case study 125
5.3.1 Effect of feed composition 125
5.3.2 Effect of switching time 132
5.3.3 Effect of flow rate ratios on development of reaction/separation region 138
Chapter 6. Conclusions and Recommendations for Further Research 142
6.1 Conclusions 142
6.2 Recommendations for further research 144
REFERENCES 146

List of Figures

Figure 1.1 Classifications of chromatographic reactors..... 5

Figure 1.2: Characteristics of fixed bed chromatographic reactor..... 6

Figure 1.3 Batch chromatography; angular time. 11

Figure 1.4 Conceptual view of continuous annular chromatographic reactor; rectangular time is shown. 11

Figure 1.5: True countercurrent chromatographic reactor (Lode et al., 2001). 15

Figure 1.6: Simulated moving bed chromatographic reactor 19

Figure 2.1 Classification of different models used for FBCRs..... 29

Figure 2.2 Schematic of a chromatographic column. 33

Figure 2.3 Knudsen diffusion mechanism. 38

Figure 2.4 Continuum bulk diffusion mechanism. 38

Figure 2.5 Schematic of the dusty fluid model. 39

Figure 2.6 Solution strategy. 48

Figure 2.7 Two elements in the domain [0, 1]. 51

Figure 2.8 Production step in a FBCR modeled with the Maxwell-Stefan approach. Experimental data are from Silva and Rodrigues (2002)..... 63

Figure 2.9 Production step in a FBCR modeled with the LDF approximation. Experimental data are from Silva and Rodrigues (2002). 64

Figure 2.10 Production step in a FBCR modeled with the Maxwell-Stefan approach. Experimental data are from Silva and Rodrigues (2005)..... 65

Figure 2.11 Production step in a FBCR modeled with the LDF approximation. Experimental data are from Silva and Rodrigues (2005). 66

Figure 2.12 Production step in a FBCR modeled with the LDF approximation. Experimental data are from Gelosa et al. (2003). 71

Figure 2.13 Production step in a FBCR modeled with a Fickian diffusion approximation. Experimental data are from Gelosa et al. (2003). 73

Figure 2.14 Production step in a FBCR modeled with the Maxwell-Stefan approach. Experimental data are from Gelosa et al. (2003). 74

Figure 2.15 Regeneration step in a FBCR modeled with the Maxwell-Stefan approach. Experimental data are from Gelosa et al. (2003). 75

Figure 2.16 Production step in a previously regenerated FBCR modeled with the Maxwell-Stefan approach. Experimental data are from Gelosa et al. (2003). 76

Figure 3.1 Schematic diagram of an eight-columns SMBCR; t is the time variable and t* is the switching time of the SMBCR ports. 79

Figure 3.2 Classification of models for SMBCR analysis. 80

Figure 3.3 Schematic diagram of an eight-column SMBC. 82

Figure 3.4 Solution strategy of the SMBCR 87

Figure 3.5 Bulk concentration profile during (A) the fifth and (B) the eighth cycles in a SMBCR modeled with the LDF approach. Experimental data are from Gandi et al, (2008). 92

Figure 3.6 Bulk concentration profile during (A) the fifth and (B) the eighth cycles in a SMBCR modeled with the Maxwell-Stefan approach. Data are from Gandi et al, (2008). 95

Figure 3.7 Bulk concentration profile in a TMBCR at cycle steady state modeled with the Maxwell-Stefan approach. Experimental data are from Pereira et al., 2009. 100

Figure 3.8 Bulk concentration profile in a TMBCR at cycle steady state modeled with the LDF approach. Experimental data are from Pereira et al., 2009. 100

Figure 4.1. True moving bed chromatographic reactor for the reaction $A + B \leftrightarrow C + D$..... 102

Figure 4.2 Bulk concentration profile in a TMBCR at steady state modeled with the LDF approach. Experimental data are for the SMBCR from Silva and Rodrigues (2005)..... 109

Figure 4.3 Bulk concentration profile in a TMBCR at steady state modeled with the Fickian diffusion approach. Experimental data are for the SMBCR from Silva and Rodrigues (2005). 110

Figure 4.4 Bulk concentration profile in a TMBCR at steady state modeled with the Maxwell-Stefan approach. Experimental data are for the SMBCR from Silva and Rodrigues (2005). 111

Figure 4.5 Bulk concentration profile in a TMBCR at cycle steady state modeled with the Maxwell-Stefan approach. Experimental data are from Silva and Rodrigues (2005, Run 3). 113

Figure 4.6 Transient bulk concentration profile in a TMBCR (A) θ = 1; (B) θ = 6; (C) θ = 12; and (D) steady state modeled with the Maxwell-Stefan approach at θ = 55. Experimental data are from Silva and Rodrigues (2005). 113

Figure 4.7 Comparison in steady state of the TMBCR model (dashed lines) and SMBCR (solid lines) in the middle of the switching time using the LDF model for the production of diethylacetal. 115

Figure 4.8 Comparison in steady state of the TMBCR model (dashed lines) and SMBCR (solid lines) at the middle of the switching time using the LDF model for the production of dimethylacetal. 115

Figure 4.9 Comparison in steady state of the TMBCR model (dashed lines) and SMBCR (solid lines) at the middle of the switching time using equilibrium theory for the synthesis of methylacetate. 116

Figure 4.10 Comparison in steady state of the TMBCR model (dashed lines) and SMBCR (solid lines) at the middle of the switching time using the LDF model for the synthesis of ethyl lactate. 116

Figure 4.11 Comparison in steady state of the TMBCR model (dashed lines) and SMBCR (solid lines) in the middle of the switching time using the Maxwell-Stefan approach model for the production of diethylacetal. 118

Figure 4.12 Comparison in steady state of the TMBCR model (dashed lines) and SMBCR (solid lines) at the middle of the switching time using the Maxwell-Stefan approach model for the production of dimethylacetal. 118

Figure 4.13 Comparison in steady state of the TMBCR model (dashed lines) and SMBCR (solid lines) at the middle of the switching time using the Maxwell-Stefan approach model for the synthesis of methylacetate. 119

Figure 4.14 Comparison in steady state of the TMBCR model (dashed lines) and SMBCR (solid lines) at the middle of the switching time using the Maxwell-Stefan approach model for the synthesis of ethyl lactate (experimental data are from Pereira et al., 2009). 119

Figure 5.1 $\gamma 2$ - $\gamma 3$ plane for linear isotherms (Lode et al., 2001)..... 124

Figure 5.2 Effect of the feed composition on purity and acetaldehyde conversion..... 127

Figure 5.3 Effect of the feed composition on productivity and desorbent consumption..... 127

Figure 5.4 Effect of the feed composition (30 mol% acetaldehyde) in the middle of switching time at cyclic steady state. 128

Figure 5.5 Effect of the feed composition (40 mol% acetaldehyde) in the middle of switching time at cyclic steady state. 128

Figure 5.6 Effect of the feed composition (50 mol% acetaldehyde) in the middle of switching time at cyclic steady state. 129

Figure 5.7 Effect of the feed composition (60 mol% acetaldehyde) in the middle of switching time at cyclic steady state. 129

Figure 5.8 Effect of the feed composition (70 mol% acetaldehyde) in the middle of switching time at cyclic steady state. 130

Figure 5.9 Effect of the feed composition (80 mol% acetaldehyde) in the middle of switching time at cyclic steady state. 130

Figure 5.10 Effect of the feed composition (90 mol% acetaldehyde) in the middle of switching time at cyclic steady state. 131

Figure 5.11 Effect of the feed composition (100 mol% acetaldehyde) in the middle of switching time at cyclic steady state. 131

Figure 5.12 Effect of switching time on purity and acetaldehyde conversion. 133

Figure 5.13 Effect of switching time on productivity and desorbent consumption. 133

Figure 5.14 Cyclic steady state concentration profiles in the middle of switching time of 2.75 min for a feed composition of 80 mol% acetaldehyde. 134

Figure 5.15 Cyclic steady state concentration profiles in the middle of switching time of 3 min for a feed composition 80 mol% acetaldehyde. 134

Figure 5.16 Cyclic steady state concentration profiles in the middle of switching time of 3.25 min for a feed composition 80 mol% acetaldehyde. 135

Figure 5.17 Cyclic steady state concentration profiles in the middle of switching time of 3.5 min for a feed composition 80 mol% acetaldehyde. 135

Figure 5.18 Cyclic steady state concentration profiles in the middle of switching time of 3.6 min for a feed composition 80 mol% acetaldehyde. 136

Figure 5.19 Cyclic steady state concentration profiles in the middle of switching time of 3.75 min for a feed composition 80 mol% acetaldehyde. 136

Figure 5.20 Cyclic steady state concentration profiles in the middle of switching time of 4 min for a feed composition 80 mol% acetaldehyde. 137

Figure 5.21 Cyclic steady state concentration profiles in the middle of switching time of 4.5 min for a feed composition 80 mol% acetaldehyde. 137

Figure 5.22 Flow rate ratios that describe the reaction/separation region for a switching time of 3.75 min and a feed composition 80 mol% acetaldehyde. 140

Figure 5.23 Effect of the flow rate ratios on productivity and desorbent consumption for a switching time of 3.75 min and a feed composition 80 mol% acetaldehyde. 140

Figure 5.24 Cyclic steady state concentration profiles in the middle of switching time of 3.75 min for a feed composition 80% mol acetaldehyde (γ_{II} = 2.625 and γ_{III} = 3.5). 141

List of Tables

Table 2.1 Reaction equilibrium constant and kinetic parameters 58

Table 2.2 Relative molecular volume and surface area of pure species parameters..... 59

Table 2.3 Interaction parameters..... 59

Table 2.4 Characteristics of FBCR column 60

Table 2.5 Adsorption equilibrium isotherms and component parameters at 288 K 60

Table 2.6 Reaction equilibrium constant and kinetic parameters at 353 K (Gelosa et al., 2003). 68

Table 2.7 Relative molecular volume and surface area of pure species parameters..... 68

Table 2.8 Interaction parameters..... 69

Table 2.9 Characteristics of FBCR column (Gelosa et al., 2003)..... 69

Table 2.10 Adsorption isotherms parameters at 353 K (Gelosa et al., 2003). 69

Table 3.1 Relative molecular volume and surface area of pure species parameters..... 89

Table 3.2 Interaction parameters..... 89

Table 3.3 Characteristics of FBCR Column 90

Table 3.4 Adsorption equilibrium isotherms and component parameters at 288 K 90

Table 3.5 Operating conditions and characteristics of the SMBCR (Gandi et al., 2008). 93

Table 3.6 Operating conditions and characteristics of the SMBCR (Pereira et al., 2008). 97

Table 3.7 Relative molecular volume and surface area of pure species parameters..... 98

Table 3.8 Adsorption equilibrium isotherms and component parameters at 323.15 K 98

Table 4.1 Operating conditions and characteristics of the SMBCR (Run 1 of Silva and Rodrigues, 2005)..... 108

Table 4.2 Operating conditions and characteristics of the SMBCR (Run 3 of Silva and Rodrigues, 2005). 112

Table 5.1 Operational conditions and characteristics of the SMBCR for diethylacetal synthesis (Silva and Rodrigues, 2005) 126

C H A P T E R 1

1. Introduction to Reactive Chromatography

1.1 Motivation

In the pharmaceutical, chemical, biochemical, agrochemical, fragrances, food, and biotechnology industries, life science products are considered to be the most promising market for the near future. Many of these products are made using conventional processes with sequentially structured chains of operational units and can be significantly improved by integrated processes using multifunctional reactors. These integrated processes aim to save capital investment, energy and operating cost, reduce equipment size, minimize waste and pollution and, most importantly, improve selectivity and productivity. For the last three decades, there has been a large amount of research focused on the chemical engineering domain to develop new concepts of the multifunctional reactors (Agar, 1999), in particular, and integrated processes in general. The multifunctional reactors are divided into three principal categories:

A. Integration of heat transfer and chemical reaction.

- High-temperature endothermic processes in heat integrated fixed-bed reactors.
- High-temperature fuel cells with internal reforming, i.e., molten carbonate fuel cell (MCFC).

B. Integration of separation processes and chemical reactions

- Reactive distillation processes.
- Reactive chromatography.
- Reactive stripping.

- Reactive crystallization.

C. Integration of mechanical unit operations and chemical reactions

- Reactive extraction.
- Reactive comminution.
- Filtration and chemical reactions.

Due to the fact that most chemical reactions are reversible with two or more products, separation processes are always required to take the desired products out of unconverted reactants and other by-products. Therefore, the integration of chemical reactions and separation processes into a single unit is more convenient and widely applicable than the other integrations. The main advantage of these integrated systems lies in a possible shift of chemical equilibrium to the product side by simultaneous separation of the reaction products and the possibility of optimizing process selectivity. Other advantages are the following: reduced energy consumption, improved operational safety, and improved ecological harmlessness by avoidance of auxiliary agents and chemical wastes. However, due to the coupling of two or many process steps into one apparatus, the number of degrees of freedom for adjusting the integrated processes can be decreased and the control is often much more complex than for non-integrated units. The advantages of coupling chemical reaction and separation have been exploited since 1921 (Backaus, 1921) for methyl acetate production with reactive distillation (RD) process (Agreda and Partin, 1984) and have been applied in the petrochemical industry. RD technology is also being applied for production of oxygenates such as methyl tert-butyl ether (MTBE), (Sneesby et al., 1998 and

Sundmacher et al., 1999) ethyl tert-butyl ether (ETBE), (Oudshoorn et al., 1999) or tertiary amyl methyl ether (TAME) (Oost, 1996). However, there are constraints and difficulties in RD implementation, mainly volatility constraints. It is necessary that both products have different boiling points to ensure the separation, therefore, the production of some products (diethylacetal) using RD technology is not feasible, given the close boiling points of several components. The versatility of the fractionating column in the dual role of continuous reactor and separator as applied to chemical processing was well established (Berman et al., 1948a).

An alternative reaction-separation unit is the chromatographic reactor, which utilizes differences in adsorptivity of the different components involved rather than differences in their volatility. It is particularly attractive as an alternative to RD when the species involved are either non-volatile or sensitive to temperature, as is the case in some fine chemical, or pharmaceutical applications, or exhibit small volatility differences. However, until now, there are few integrated processes with industrial applications. For example, reactive distillation (Agreda and Partin, 1984), reactive extraction (Bart, 2001), and reactive absorption (Kenig and Górak, 2005) have been reported in the literature. The other developing concepts of multifunctional reactors are not yet commercialized because of technical barriers. In these cases, reactive chromatography is paid more attention than the others because of its potential for efficient production of high purity products and many impressive industrial applications of preparative chromatographic separations. Although there are several investigations related to reactive chromatography, its theoretical basis and

experimental database are still not sufficient for commercialization. Hence, much research is motivated in an effort to provide profound insights into all aspects of reactive chromatography. The ultimate aim is to possibly scale it up for industrial applications.

1.2 Previous works on chromatographic reactors

Chromatographic systems are traditionally used for separating one or more components from mixtures. The separation principle of the system depends on the interaction of the individual components in the mixture with the stationary phase. A chromatographic reactor, on the other hand, can be defined as a chromatographic system that is used to convert one or more components partially or totally, and simultaneously separate one or more of the products that are formed. The reaction can either be chemical or biochemical, taking place on the stationary phase, in the mobile phase, or both. Normally, chromatographic reactors consist of a stationary and mobile phase in continuous contact, and when the stationary phase acts as adsorbent and catalyst, the reaction and the separation take place simultaneously inside the reactor. The chromatographic reactors can be classified as gas chromatographic reactors or liquid chromatographic reactors, depending on gases or liquids used as mobile phase. The gas chromatographic reactors are not as developed due to the deficiency of interesting reactions from the application point of view in the gas phase, compared to the very interesting reactions in the liquid phase. From now, in this thesis, we will always speak of liquid chromatographic reactors. Reactive chromatography also can be classified according to the operation mode, depending if the reactant, or the reactant mixture, are dosed continuously or periodically into the reactor as shown in Figure 1.1.

Chromatographic reactors have been studied since the 1960s (Dinwiddie and Morgan 1961). Relevant publications include a wide variety of fundamental studies in the

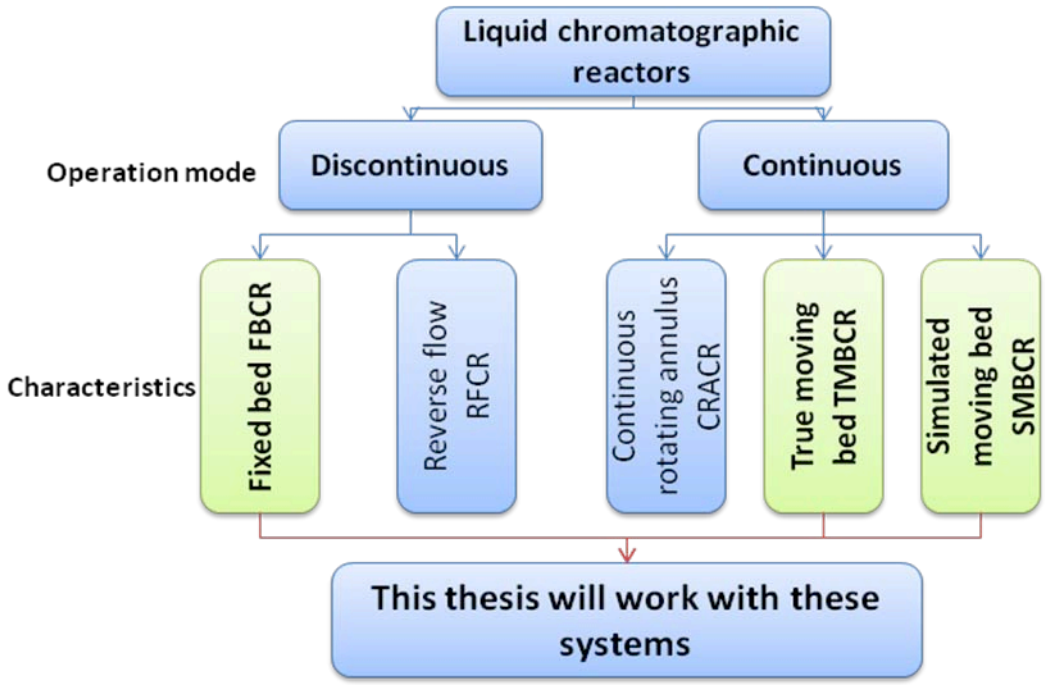

Figure 1.1 Classifications of chromatographic reactors

implementation of reaction equations and need to make a distinction between heterogeneous and homogeneous systems. A chromatographic column can be described in two different ways, the column can be divided into theoretical plates that are connected in series or can be based on the differential mass balance.

The adsorption on the stationary phase can be described by an adsorption isotherm, which can exhibit a linear or nonlinear behavior. The mass transfer resistance can be taken into consideration, or equilibrium between liquid and solid phases can be assumed. This section reviews relevant works which have served as support basis for the development of the present investigation.

1.2.1 Fixed bed chromatographic reactor (FBCR)

The operation principle of a batch chromatographic reactor for a reversible reaction $A \Leftrightarrow B + C$ is shown in Figure 1.2. The reactant A is injected as a pulse into a fixed bed column and it is converted to B and C during its propagation in the column. The different adsorptions of components B and C leads to different propagation velocities, and the products are separated from each other. This separation takes place because the component with the lower affinity migrates faster along the column in comparison to the component with the higher affinity.

Schweich and Villermaux (1982) studied yield enhancement by equilibrium displacement in a chromatographic catalytic reactor. Evidence for yield enhancement in the

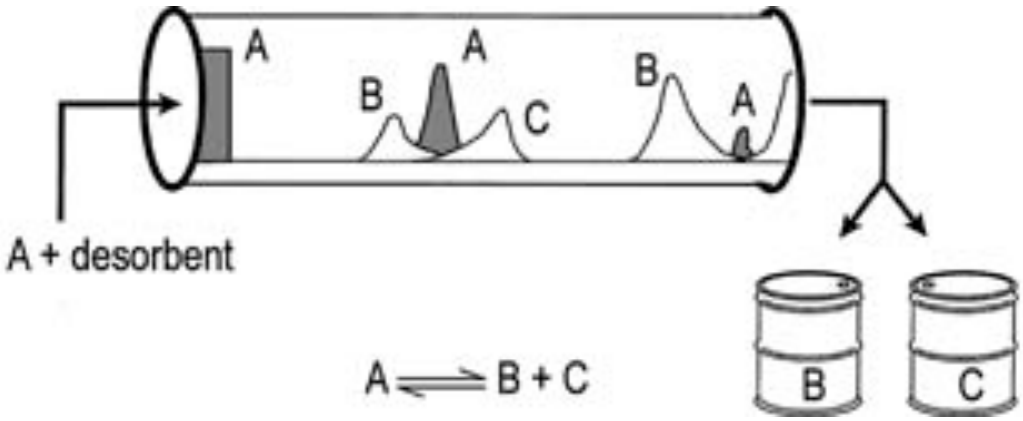

Figure 1.2: Characteristics of fixed bed chromatographic reactor

equilibrium $C_6H_{12} \leftrightharpoons C_6H_6 + 3H_2$ was obtained from the effects on the degree of conversion to benzene of flow rate, bed length, carrier gas composition, and pulse duration. They observed significant differences between their experimental results and equilibrium-based predictions. They ruled out any temperature effect on their results. One of the most important aspects of their work is that it places doubt in the assumption of local reaction equilibrium made in several analytical studies of chromatographic reactors.

Mazzotti et al., 1997 analyzed the dynamic behavior of chromatographic reactors in order to evidence a few peculiarities of these units and to provide a better understanding of their behavior, for which a complete analysis has been lacking. The experiments were performed in a laboratory-scale chromatographic reactor. The unit behavior was described by means of an equilibrium dispersive mathematical model, which implies the assumption of local absorption equilibrium, i.e., negligible mass transport resistances, on the basis of a characteristic time analysis. Axial dispersion was accounted for as well as changes of the swelling ratio of the resin as a consequence of composition variations. Temperature and fluid flow rate were assumed to be constant and uniform. The reaction rate was finite in the resin, due to its catalytic role, whereas it was negligible in the fluid phase (pseudo-homogeneous).

Experimental data were in good agreement with the results obtained using a fully predictive equilibrium dispersive model. It was observed that the agreement between experiment and theory was satisfactory, in particular if one takes into account that the model was fully predictive. The chromatographic reactor exhibits a rather rich dynamical behavior, which was a consequence of the dual role, as a catalyst and as a selective sorbent, played by the resin.

A dynamics of fixed bed adsorptive reactor for synthesis of diethylacetal was studied by Silva and Rodrigues in 2002. Diethylacetal is an important raw material for fragrances and pharmaceutical products and is used in the flavoring of spirit drinks and is produced by a reversible liquid phase reaction and was synthesized from ethanol and acetaldehyde, catalyzed by the acid resin Amberlyst 18. Adsorption and reaction experiments were performed in a fixed bed adsorptive reactor, operating isothermally at 15ºC and at atmospheric pressure. Experimental results of dynamic absorption of binary nonreactive

mixtures were used to obtain multicomponent adsorption equilibrium isotherms of the Langmuir type. The reaction kinetic reported earlier (Silva and Rodrigues, 2001) were used in the model of the adsorptive reactor, which also included axial dispersion, external and internal mass transfer resistance, and multicomponent Langmuir isotherms. The model equations were solved by orthogonal collocation on finite elements implemented by the PDECOL package, using the measured model parameters, and was validated by experimental data for reaction and regeneration steps, with good accuracy.

Falk and Seidel in 2002 analyzed the discontinuous operation of a chromatographic reactor. The principle of a discontinuously operated chromatographic reactor was studied experimentally and theoretically. The heterogeneously catalyzed hydrolysis of methylformate was chosen as a model reaction. An acidic ion exchange resin was used as catalyst and adsorbent. The relevant adsorption equilibrium constants were available from a previous study. In this work the reaction rates were quantified on the basis of batch reactor experiments. Subsequently, systematic experiments were carried out using a fixed bed. The influence of temperature, residence time, and feed concentration on the reactor performance was studied. It was attempted to analyze the observations using a simplified pseudo-homogeneous cell model. Since the model was found to be capable of describing the reactor behavior over a wide parameter range, it was applied to perform extensive parametric calculations. From the results obtained a few generally applicable rules to evaluate the potential of discontinuously operated chromatographic reactors could be derived.

Gelosa et al., 2003 discussed a new application of chromatographic reactors that addresses some unique features. They studied the synthesis of glycerol triacetate (triacetine) by the esterification of glycerol with acetic acid. This requires a series of three esterification

steps, each producing a molecule of water, with glycerol monoacetate (monoacetine) and glycerol diacetate (diacetine) as intermediate products, according to the following kinetic scheme:

Glycerol + acetic acid ⇔ monoacetine + water

Monoacetine + acetic acid ⇔ diacetine + water

Diacetine + acetic acid ⇔ triacetine + water

This process is strongly limited by equilibrium; the triacetine is typically used as a plasticizer in various applications, such as filters for cigarettes, which require it to be of food grade. The experimental apparatus consisted of a single column with an internal diameter of about 1.5 cm and a length of 44 cm that was packed with resin Amberlyst 15 with an internal porosity of 0.36 and interparticle bed void fraction of 0.42. The good agreement between the predicted results and the experimental data for the chromatographic reactor demonstrates the reliability of the model. This model could provide a useful tool for the investigation of the possible performance of more efficient continuous units, such as annular chromatographic or simulated moving beds, and for their scale-up, which is needed to assess the economic performance that can be expected from these processes.

The esterification of acrylic acid with methanol using Amberlyst 15 as a stationary phase has been investigated using a chromatographic reactor (Ströhlein et al., 2006). Several experimental runs at various operating conditions have been conducted in a batch column. The model parameters have been determined in a fast and reliable way by directly fitting the batch column experiments. In general, a good agreement between experimental and calculated results was obtained. Based on the detailed batch column model, a complete

model of a simulated-moving-bed reactor has been implemented and its optimal point of operation for the synthesis of methyl acrylate from acrylic acid has been determined. Particularly when considering the low-operating temperature, we can regard this process as a possible competition for current technologies.

Common to all reactive chromatography processes operated in the classical batch mode are low efficiency in utilizing the stationary phase inventory and large effluent (or desorbent) consumption resulting in an excessive dilution of the final products, in addition to the usual disadvantages connected with discontinuous operation (Lode et al., 2001). This same problem is encountered in the case of purely separate chromatography, but significant improvements have been accomplished recently by transforming these operations into continuous processes. Technically, this has been done in two different ways: through annular as well as simulated moving bed (SMB) chromatography, both of which have their specific advantages and drawbacks. Nevertheless, these developments have indeed been successful in establishing the industrial application of chromatographic separation, especially in the field of chiral and bioseparations (Juza et al., 2000).

1.2.2 Continuous rotating annular chromatographic reactor (CRACR)

By using a cylindrical annulus, the chromatographic reactor can be operated continuously. The annular space is formed by employing two concentric cylinders. The annulus, packed with adsorbent and/or catalyst, is rotated continuously. A small quantity of mixture is introduced onto the top of the column and is separated into its components which elute from the apparatus at different times (Figure 1.3). The first approach to continuity is the cyclic operation of several batch columns as shown in Figure 1.4. Therefore, the columns are

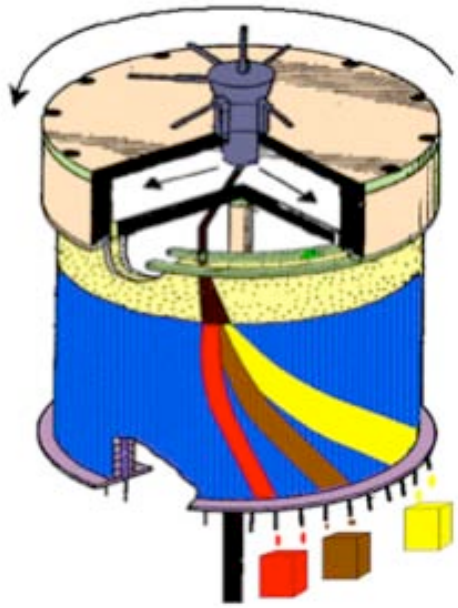

Figure 1.3 Batch chromatography, angular time.

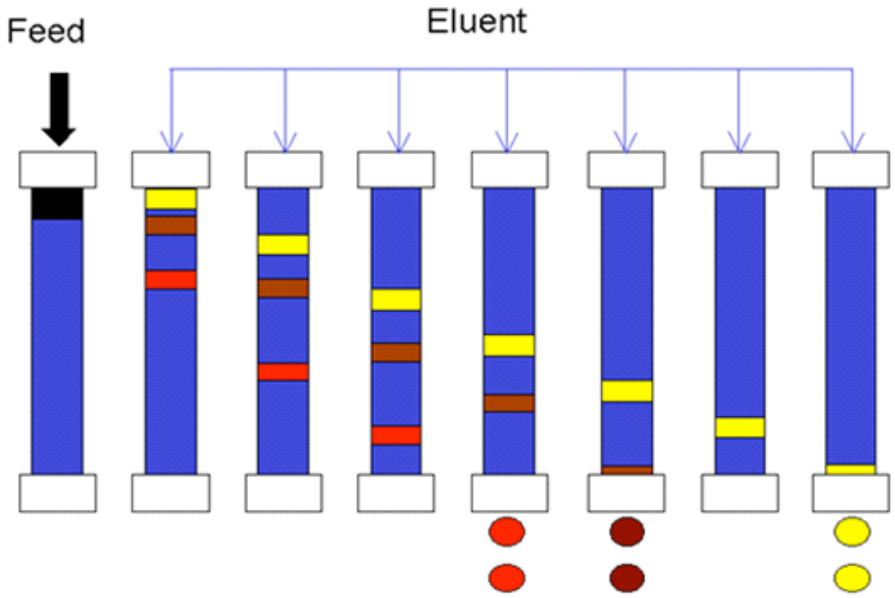

Figure 1.4 Conceptual view of continuous annular chromatographic reactor, rectangular time is shown.

arranged in a circle. After one column is charged with mixture the system will be rotated to the next position. Thereby the components will elute at different angles. If the number of batch columns is raised to infinity and the dividing walls between the columns are removed we obtain an annulus which rotates continuously. This rotating annulus is then the continuous rotating annular chromatograph, CRAC (Herbsthofer and Bart, 2003). Martin in 1949 was the first to propose the concept of annular chromatography. In the CRAC, the stationary phase is packed into the annular space formed by two concentric cylinders. The apparatus is rotated slowly and the annular bed is uniformly supplied with eluent. The feed nozzle does not rotate, though the feed is introduced continuously at a fixed point at the top of the bed. Like in the batch column the feed is carried through the bed by the mobile phase. During the residence time a single feed molecule spends in the mobile phase its movement will be axial due to gravity and, because of the rotation relative to the fixed feed inlet, also tangential. For the time the molecule is adsorbed on the stationary phase its movement is only tangential. These two effects and the different affinities of the components to the stationary phase cause the components to appear as helical bands with characteristic stationary exit points. Because of diffusion effects, the helical bands will be spreaded to the exit. Here the jacket of the CRAC is cut and projected on a length from 0° to 360°. Several separation problems in the CRAC have already been discussed (Bart et al., 1996, Reissner et al., 1997, and Takahashi, and Goto in 1992), but the application of the CRAC as a reactor (CRACR) raises several questions and may give some benefits. One advantage is that reaction and separation take place in one single unit leading to lower investment costs. For a reversible reaction, chemical equilibria may be shifted, because due to the continuous separation of the products, the reverse reaction is avoided. This leads to higher yields than archived in non-separating

reactors. The disadvantage of the heterogeneous catalyst is the additional influence of the diffusion transport resistance. In this case the macro kinetics have to be investigated instead of the actual reaction velocity of homogeneous reactions. Simultaneous biochemical reaction and separation was carried out successfully for the first time in a continuous rotating annular chromatograph (CRAC) by Sarmidi and Barker in (1993), inverting sucrose to glucose and fructose using the enzyme invertase. The chromatograph was packed with 14.5 dm^3 Dowex 50W-X4 calcium form ion exchange resin. Results from the initial experiments indicated that complete conversion could be achieved for feed concentrations of up to 50% w/v sucrose and at feed throughputs of up to 15 kg sucrose per m^3 resin/h.

Lang in 2003 studied a continuous rotating annular chromatographic reactor. The reactive system used as a model system for this application was the esterification of glycerol and acetic acid (glycerol triacetate). The reactions are reversible and the maximal yield of triacetin was limited by chemical equilibrium. The production of triacetin is usually a costly and time-consuming process that involves several steps. The possibility of applying a chromatographic reactor for this purpose would be a major achievement. Stipulations were to keep the process simple and to avoid unwanted by products. This led to the use of acetic acid as an eluent, while the glycerol was applied in the feed. The use of ion-exchange resins as heterogeneous catalysts therefore facilitates the separation of the products from the catalyst. Based on the thermodynamic and kinetic research data that was measured in other similar studies, a model to reflect the behavior of the continuous rotating annular chromatographic reactor was developed, in order to analyze the processes inside the reactor and to get a better understanding of its dynamic behavior. This model was also used as a means to check the influence of the operating parameters on the product yield, purity, and overall productivity. It

was confirmed that the annular chromatographic reactor does indeed have a high and very promising potential in this application. As a number of the long term experiments under controlled conditions showed, the process was well reproducible and it reached the steady state in a short time compared to other separation techniques. The conversion of glycerol to triacetin was just fractionally lower than 100% and the triacetin was separated successfully from all of the other products. Investigations on the influence of different operating conditions on the product yield and purity, were also carried out and documented. These could be used in further attempts to improve this process and/or technique if it was desired. The triacetin that was produced in the continuous rotating annular chromatographic reactor only has to be separated from the eluent acetic acid by means of simple distillation. The other costly purifications steps, which were usually involved in conventional production methods, could thus be eliminated. The CRACR demonstrated that it was the most effective process for the production of triacetin.

A major drawback of the CRACR is the large amount of eluent needed to operate the process. This also leads to a high dilution of the products. Another disadvantage is the poor use of the adsorbent. These drawbacks led to the development of continuous countercurrent processes.

1.2.3 Countercurrent True Moving Bed Chromatographic Reactor

The true moving bed chromatographic reactor (TMBCR), also called countercurrent moving bed chromatographic reactor, was first mentioned by Takeuchi et al., 1977 (see Fig. 1.5). The solid phase is moved in the opposite direction to the liquid flow. The unit is divided into four sections, each of them with different functions to achieve complete conversion and separation. The reactant A is fed to the unit between the two central sections

of the unit (sections 2 and 3), a chemical reaction is triggered and the product species are formed. The product B with higher affinity is conveyed downwards with the solid phase and is withdrawn from the extract port, and the product C with less affinity is carried in the direction of fluid flow, toward the raffinate port. Before being recycled, both the fluid and the solid phases are regenerated within sections 1 and 4. The main advantage of such an arrangement is the countercurrent flow, as in a heat exchanger or distillation column, which maximizes the average driving force. Thus, the efficiency with which the stationary phase is used increases.

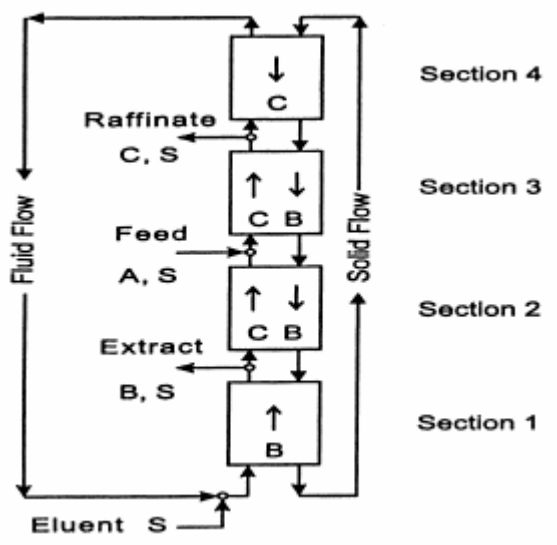

Figure 1.5: True countercurrent chromatographic reactor (Lode et al., 2001).

The first countercurrent moving bed reactor was studied by Takeuchi et al., 1977. On the basis of theoretical studies on a reaction of type $A \Leftrightarrow B$ an improvement in the conversion compared to equilibrium was found. Seven years later Petroulas et al., in 1985 analyzed a countercurrent moving bed chromatographic reactor. They investigated theoretically and experimentally a countercurrent moving bed chromatographic reactor. In

this reactor, a reversible heterogeneous reaction takes place on catalyst particles passing downward through an upcoming gas stream. The behavior of an ideal reactor model was examined for different values of feed concentrations and reactor length. It was predicted that reaction and separation can be achieved simultaneously and that under appropriate operating conditions, a reactor fed at the bottom with the species more favored by thermodynamic equilibrium can lead to 100% product purity with overall conversions lower than a conventional fixed bed reactor. The effect of nonidealities on the reactor performance was also discussed. Finite adsorption and axial dispersion had a generally deteriorating effect on overall conversion and product purity. An improved reactor configuration with a bottom stripping section was suggested. Its operating conditions can be tailored so that predicted performance exceeds that of a fixed bed both in yield and product purity. The hydrogenation of mesitylene with excess hydrogen over a Pt on alumina catalyst was used for an experimental investigation of the reactor. The experiments, performed in a ½ in inside diameter, 7 ft long column, resulted in products of higher purity than the equilibrium prediction, and overall conversions comparable to a fixed bed reactor.

In 1989, Fish et al. investigated experimentally a countercurrent moving bed reactor. The test reaction was the hydrogenation of 1,3,5-trimethylbenzene vapor at 190°C by Pt supported on 30–50 mesh Al_2O_3. Simultaneous reaction and separation of the reactant and product, 1,3,5,-trimethylcyclohexane, occurred during the continuous contacting, giving good product purity. Conversions could, in some cases, significantly exceed the equilibrium conversion expected in a tubular reactor operating at the same temperature and feed conditions. The dependence of product purity and conversion upon experimental conditions was investigated. A dispersionless, adsorption equilibrium model was presented for the two

cases of a linear isotherm and a Langmuir isotherm. The trends of observed reactor behavior with changes in feed rate and feed position were satisfactorily accounted for by the models.

In the 90s, the technology of the countercurrent moving bed reactor attracted more and more interest in the fine chemical and pharmaceutical industry. Van der Wielen et al., in 1990 integrated bioconversion and continuous product separation by means of countercurrent adsorption. Selective product removal from the reaction zone by means of adsorption was advantageous in case of unfavorable thermodynamic equilibrium as could be encountered for enzymatic conversions. The application of a multi-stage fluid bed contactor as a continuous device for adsorptive bioconversion was investigated as a possible solution. In this reactor-adsorber, two solid flows (adsorbent and immobilized biocatalyst) could be controlled independently. As a first step in the process design a mathematical model describing the steady state performance of the reactor was developed. The design and construction of a laboratory scale multi-stage fluid bed reactor-adsorber was illustrated for the reversible first order glucose-fructose isomerization with a zeolitic adsorbent as model system. This proved the reactor-adsorber to be a useful tool in the design of bioconversion processes.

The movement of the solid particles is difficult to achieve. One reason is the unavoidable backmixing of the solid that reduces the efficiency of the process. Another problem is the abrasion of the particles caused by the movement. Note, however, that there is an alternative to this setup, which is described next.

1.2.4 Simulated Moving Bed Chromatographic Reactor (SMBCR)

In order to overcome the difficulties of TMBCR in conveying solid particles, an invention of Universal Oil Products Company for a simulated moving bed separation was

registered for the patent US 2985589 (Broughton and Gerhold, 1961). The countercurrent flow of the solid phase can be simulated by periodically switching the valves of interconnected columns in the direction of the liquid flow. The inlet and outlet ports are switched for one bed distance in the direction of the fluid flow in a time interval called the switching time period. The principle of a simulated moving bed chromatographic reactor can be explained by considering a reversible reaction of type A↔B + C. According to the position of the inlet and outlet stream the unit can be divided in four sections as shown in Figure 1.6. In section I, placed between the desorbent and extract nodes, the adsorbent is regenerated by desorption of the more strongly adsorbed product (C) from the solid, which justifies the fact that this section has the highest flow rate in the system. In section II (between the extract and feed node) and section III (between the feed and raffinate node), the reaction is occurring and products (B and C) are formed. The more strongly adsorbed product (C) is adsorbed and transported with the solid phase to the extract port. The less strongly adsorbed product (B) is desorbed and transported with the liquid in the direction of the raffinate port. In section IV, which is placed between the raffinate and desorbent node, the desorbent is regenerated before being recycled to section I.

The application of SMBCR to liquid-phase reactions had already been reported more than two decades ago. Most of the early work found in the literature, though, is directed towards enzymatic sugar hydrolysis and isomerizations (Hashimoto et al., 1983). They worked in a process for producing a higher-fructose syrup containing more than 50% fructose. A process was developed that involves a new system combining selective adsorption of fructose and an immobilized glucose isomerase reaction. Continuous countercurrent contact of the liquid stream with the solid adsorbent was simulated by

advancing adsorption columns against the fixed inlets and outlets of liquid streams without actual movement of the solid adsorbent, while the immobilized enzyme reactors are stationary. Two mathematical models, an intermittent moving-bed and a continuous moving-bed model, were presented for calculation of the concentration profiles of glucose and fructose in the system. The validity of the models was experimentally confirmed, and a criterion for good production in the system was presented. This system requires less desorbent than a process using a fixed-bed adsorber and a simulated moving-bed process to produce the syrup with 45-65% fructose content, the level desired in food manufacture.

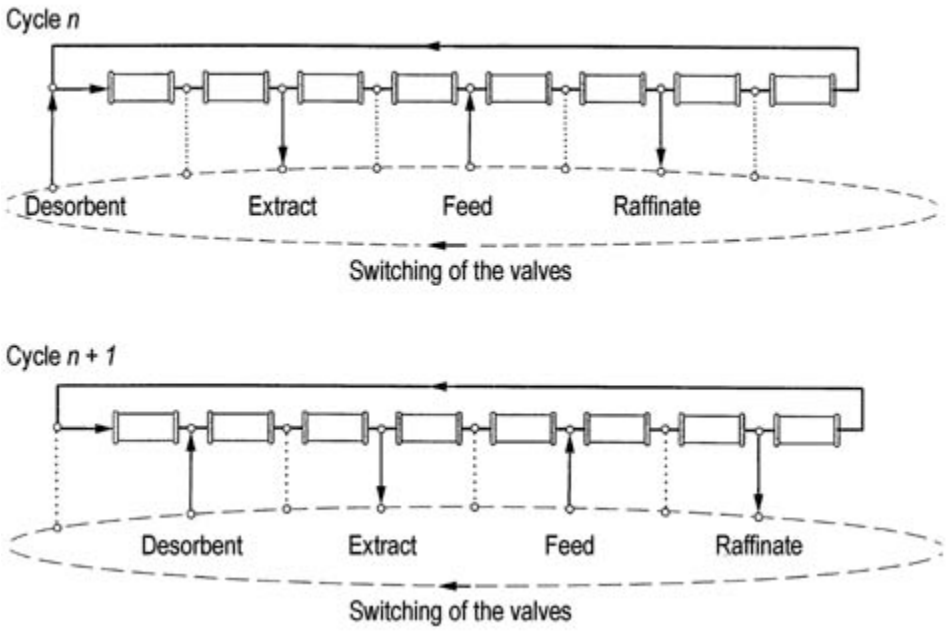

Figure 1.6: Simulated moving bed chromatographic reactor.

This work was then followed by extensive experimental investigations on the inversion of sucrose by Barker et al., 1992. The combination of bioreaction and separation was carried out successfully on a simulated moving column continuous countercurrent

chromatographic reactor-separator (SCCR-S) system. The continuous inversion of sucrose to glucose and fructose using invertase and the biosynthesis of dextran from sucrose in the presence of the enzyme dextransucrase was studied. Complete sucrose conversions were achieved and product purities of up to 95% w/v were obtained in the inversion studies. The operation was carried out on a preparative scale with throughputs in excess of 16 kg of dry sugar solids per cubic meter of resin per hour used. The simultaneous inversion and product separation was found to overcome problems associated with substrate inhibition. Complete reaction and separation was obtained at feed concentrations as high as 55% w/v. Previous studies on the biosynthesis of dextran on batch chromatographic systems showed significant improvements in product yields. The simultaneous removal of the acceptor by product fructose from the reaction mixture led to the formation of greater amounts of high molecular weight dextran (over 80% more than the conventional process at 20% w/v sucrose concentration). To carry out dextran biosynthesis on the SCCR-S system, it was necessary to repack it with larger-size resin to allow for the high pressures caused by the more viscous dextran. Complete conversions were achieved at sucrose concentrations of 5% w/v with dextran and fructose product purities of up to 100% and 97%, respectively, obtained under certain conditions.

The hydrolysis of lactose and maltose was investigated by Shieh and Barker in (1995, 1996) and the lactosucrose produced from sucrose and lactose using an enzyme β-fructosyfuranosidase was reported by Kawase et al., 2001. Lode et al., in 2003 compared the true countercurrent and simulated moving bed reactors. Simulated moving bed reactors (SMBR) combine chemical reaction and adsorptive separation within one single continuous

and countercurrent unit. This integration promises substantial improvements in process performance, especially when applied to equilibrium-limited reactions involving such heat-sensitive products as fine chemicals and pharmaceuticals. In this work, the interplay among the relevant process design parameters (dimensionless ratios of the fluid and solid flow rates, and the Damköhler numbers for each section of the unit) was investigated. For this, an analytical solution of differential mass-balance equations for the corresponding true countercurrent process (TCC), using as a model system the reaction $A \Leftrightarrow B + C$ with each species exhibiting linear adsorption behavior, was developed. Based on this solution, criteria were derived for the optimum process design with respect to productivity and solvent consumption. Comparing these results with numerical simulations of an SMBR unit shows that the TCC model does not apply to SMBR units with a finite number of columns per section, that is, units of practical relevance, because the two units exhibit different residence time distributions and, hence, lead to different degrees of conversion.

Liquid-phase reactions also include acetic acid esterifications catalyzed by sulfonated ion-exchange resins. A process where one of the reactants, i.e. ethanol, is also used as solvent was investigated using a four-section SMBCR under open-loop conditions with pure acetic acid in the feed (Mazzotti et al., 1996, Lode et al., 2001). A similar process based on the same stationary phase was utilized for the esterification of phenethyl alcohol but now using a non-reactive species as solvent, 1,4-dioxane, also resulting in complete conversion and withdrawal of the products in pure, though diluted, form (Kawase et al., 1996). Most recently, also the production of bisphenol-A in a SMBR unit was reported (Kawase et al., 1999) and the production of MTBE was reported by Zhang et al., (2001).

In (2005) Silva and Rodrigues presented the development of a novel process for the production of diethylacetal from the reaction between ethanol and acetaldehyde catalyzed by the acid resin Amberlyst 15 using simulated moving-bed reactor (SMBCR) technology. The methodology used combines modeling/simulation with laboratory and pilot-scale experiments. The kinetic law of the reaction was measured from experiments in a batch catalytic reactor. The adsorption parameters were obtained from experiments performed in a fixed-bed adsorption column. Laboratory experiments in fixed-bed adsorptive reactors were performed and used to validate the model and simulation tools. The SMBCR technology was applied for diethylacetal production and separation with 87% purity and the acetaldehyde conversion was about 98%. The influence of feed composition, switching time, and mass-transfer resistance on the SMBCR performance was analyzed by simulation. The reaction/separation region was determined using separation zone methodology. Simulated results show that high acetal purities can be achieved for 100% acetaldehyde conversion.

1.3 Modeling of Chromatographic Reactors

The models for the reactors classification mentioned above have been summarized by (Borren and Fricke, 2005 and Fricke et al., 1999). The models are based on conservative mass balances or divided into theoretical plates, and can be considered as an extension of models used for preparative chromatography with reaction kinetics additionally taken into account. The simplest models (called the ideal model) with an analytical solution, are very unrealistic for most systems. Models for the FBCR were surveyed initially by Villermaux in 1981 and Sardin et al., 1993 and the most recent were for Mazzotti et al., 1996, Lode et al., 2001, Gelosa et al., 2003, and Silva and

Rodrigues, 2002 and 2005. In the 1996 work, Mazzotti et al. studied the synthesis of ethyl acetate and water from ethanol and acetic acid on a commercial polystyrene-divinylbenzene acidic resin. The behavior of the chromatographic reactor was described by means of an equilibrium dispersive mathematical model, which implies the assumption of local sorption equilibrium, i.e., negligible mass-transport resistances, on the basis of a characteristic time analysis. Axial dispersion was accounted for as well as changes of the swelling ratio of the resin as a consequence of composition variations. Experimental data were in good agreement with the results obtained using a fully predictive equilibrium dispersive model. This exploits an accurate description of both the multicomponent sorption equilibria on the resin, based on the extended Flory-Huggins model, and the kinetics of the heterogeneously catalyzed chemical reaction. Four years later Lode et al., 2001 used the same reaction, and a model for a reactive chromatographic column was developed and validated.

Later, Silva and Rodrigues, 2002 synthesized diethylacetal from ethanol and acetaldehyde catalyzed by the acid resin amberlyst 18. The mathematical model used to describe the dynamic behavior of the fixed-bed adsorber/reactor considers the following assumptions: the flow pattern is described by the axial dispersed plug-flow model (Chung and Wen, 1968); external and internal mass-transfer for adsorbable species are combined in a global resistance; isothermal process; constant column length and packing porosity were assumed. The model equations were solved by orthogonal collocation on finite elements implemented by the PDECOL package, using the measured model parameters, and was validated by experimental data for reaction and regeneration step, with good accuracy.

One year later, Gelosa et al., 2003 worked the synthesis of triacetine, starting from glycerol and acetic acid, using reactive chromatography on acidic polymeric resins. To describe quantitatively the behavior of the chromatographic reactor discussed above, a suitable mathematical model was developed. The overall model includes the assumptions of equilibrium partitioning, intraparticle transport, and reaction kinetics developed in the sections above. In addition, axial dispersion was introduced to account for deviations from plug-flow behavior. Accordingly, the model includes the mass balances in the bulk liquid phase flowing along the reactor and in the liquid inside the pores of the resin. The adsorbed phase was assumed to be at equilibrium with the liquid in the pores. The change in the resin volume due to swelling was taken into account by using a constant average value of the swelling ratio, and the superficial liquid velocity of the liquid, was assumed to be constant. It was found that the presence of water in the resin at the end of the regeneration step has a strongly detrimental effect on the final triacetine purity.

Recently, Silva and Rodrigues, 2005, presented the diethylacetal synthesis in a fixed-bed adsorptive reactor packed with Amberlyst 15. A mixture of ethanol and acetaldehyde was continuously fed to the chromatographic reactor initially saturated with ethanol. The dynamic behavior of a fixed bed for the synthesis of diethylacetal was predicted by mathematical model for the adsorptive reactor. The assumptions in this model were the same used by Silva and Rodrigues, 2002.

The modeling for SMBCR consists of two different approaches: the first combines the model of several batch columns with mass balance for inlet and outlet streams of the whole system (Fricke et al., 1999, Dünnebier et al., 2000, Kawase et al., 2001, Lode et al., 2001, and Toumi and Engell, 2004); the second assumes that a SMBCR is

equivalent to a TMBCR, thus this approach is called the TMBCR model. For example, the TMBCR have been applied successfully by Azevedo and Rodrigues, 2001, Lode et al., 2003, Silva and Rodrigues, 2005, and Minceva and Rodrigues, 2005.

In 1999, Fricke et al. studied the effect of the process parameters on the performance of a chromatographic SMB reactor for a reversible decomposition reaction of type A ↔ B + C. All process simulations presented here were based upon a rigorous model of the SMB chromatographic reactor, where axial back mixing, mass transfer resistance within the fluid and solid phase, as well as the periodic fluid node switching of the SMB process were all accounted for (Meurer et al., 1997). Using such a detailed model of the process, a good agreement between real reactor behavior and simulation results was expected. Later, Dünnebier et al., 2000 presented a novel optimization and design strategy for simulated moving bed (SMB) chromatographic processes in general and SMB reactors in particular. The optimization strategy was based on mathematical optimization, a rigorous dynamic process model, and a detailed cost function. Potential savings in operating cost of up to 20% and in desorbent consumption of up to 60% were identified.

Minceva and Rodrigues, 2005 worked on the design of a SMBCR where the reactive-separation regions were determined for two reactive systems: inversion of sucrose, with enzyme introduced in the unit through the eluent stream and Michaelis-Menten reaction kinetics; and A ↔ B + C reaction, with immobilized enzyme and linear reaction kinetic law. The steady state equivalent TMBCR analogy was applied in the algorithm used for determination of the reactive-separation regions.

The reactive chromatography technology is still developing and there is a deficit in accurate data to achieve reliable predictions of chromatographic reactors. More systematic

studies are needed. Actually, all researches about the SMBCR use equilibrium theory in the interface liquid-solid and for diffusion and reaction inside porous catalyst use pseudo-homogeneous analysis. The pseudo-homogeneous analysis prevents an explicit and quantitative interpretation of the reactive process purely in terms of equilibrium theory. These interactions require a fundamental study of the behavior of the molecules with respect to adsorption and transport processes in porous media, which constitute the basic ingredients for developing a reliable model of a chromatographic reactor. The current knowledge in the literature is not sufficient for the derivation of simulation models, on which a design procedure can be based. For this reason, the study of SMBCR utilizing the more rigorous theory of diffusion inside porous for homogeneous reaction, and diffusion and reaction inside porous catalyst for heterogeneous reaction (the “dusty fluid model”), and the mass transfer effects based on the Maxwell-Stefan approach proposed in this work, constitutes a significant contribution to the field of Chemical Engineering.

1.4 Research objectives

The main objective is to study and implement a rigorous dynamic theoretical model of simultaneous diffusion, reaction, and adsorption inside porous solids for both homogeneous and heterogeneous reactions, and to understand the effects of mass transfer based on the Maxwell-Stefan approach on the synthesis and optimization strategies in systems of liquid reactive chromatography.

A list of the specific objectives of this work follows.

- To develop a rigorous model for the FBCR, TMBCR, and SMBCR taking into account multicomponent mass-transfer effects using the Maxwell-Stefan approach.
- To validate the modeling results in the FBCR, TMBCR, and SMBCR using experimental data from the literature.
- To compare the predictions of the Maxwell-Stefan approach model of the FBCR, TMBCR, and SMBCR with those available in the literature for other models.
- To compare the predictions of the TMBCR and SMBCR for any given application.
- To study the influence of feed composition, and switching time in the SMBCR performance.

C H A P T E R 2

2. Mathematical Description of Fixed Bed Chromatographic Reactors

In this chapter, computer modeling of the fixed bed chromatographic reactor (FBCR) is presented. Model formulations, parameter estimation, and the numerical solutions are introduced.

2.1 Modeling of chromatographic reactors

In the field of chemical engineering, computer modeling of chromatography is an important part of design and process development. One of the reasons is that the validated models allow virtual prediction of conditions studied or not studied experimentally, optimization, and scale-up of the process. In many cases, expensive plant trials can be replaced by cheap simulation, and feasibility studies are principally based on computer calculations. To quantify chromatographic separations, the first mathematical models were presented during World War II. Gu in 1995 and Dünnebier et al., 2000, have summarized recent developments.

Different models to describe chromatographic reactors have been published. In general, models used to describe chromatographic reactors can be considered as extended models of chromatographic separation columns taking into account reactions. They can be classified according to the modeling approach and the effects that are taken into account by the model (Figure 2.1).

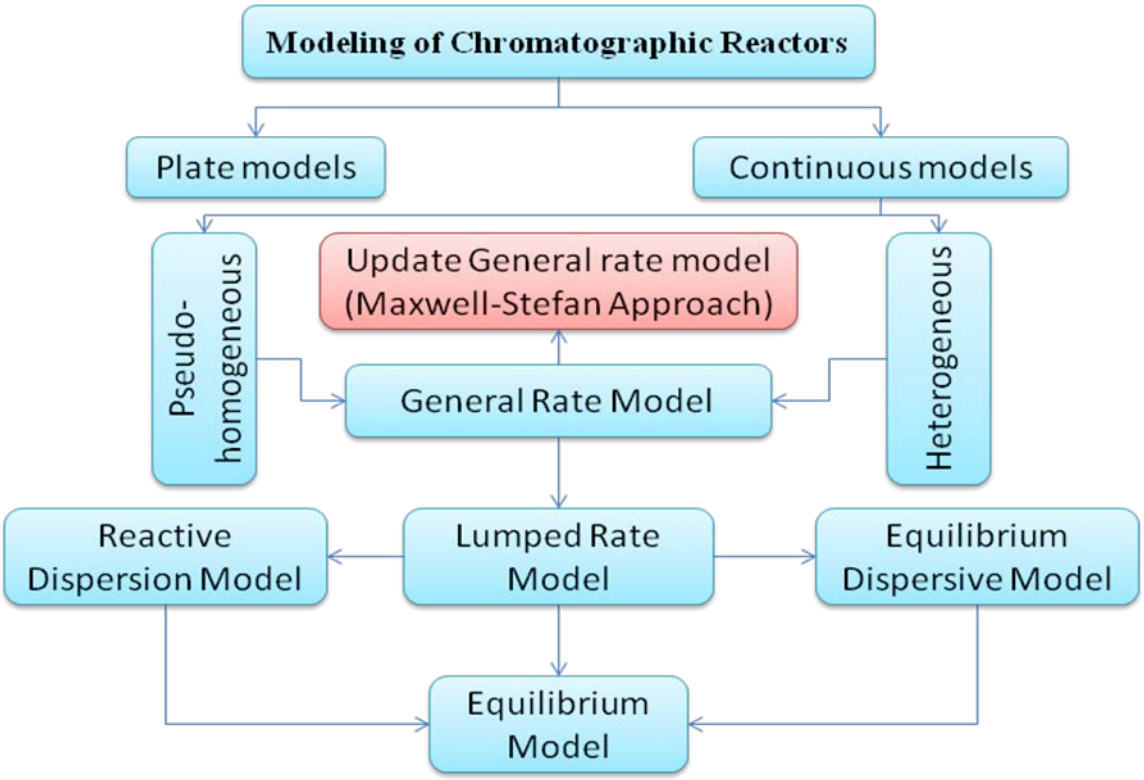

Figure 2.1 Classification of different models used for FBCRs.

As shown in Figure 2.1, a chromatographic column can be described by two different modeling approaches. In the first model, the column is divided into theoretical plates that are connected in series. The second model is based on the differential mass balance.

The plate model supposes that the chromatographic column contains a large number of separate layers, called *theoretical plates*. Separate equilibrations of the sample between the stationary and mobile phase occur in these "plates." The analysis moves down the column by transfer of equilibrated mobile phases from one plate to the next. It is important to remember that the plates do not really exist; they are a figment of the imagination that helps us understand the processes at work in the column. This gives a set of first order ODEs that describe the adsorption and interfacial mass transfer. The following assumptions are made: the column consists of a certain number of equivalent theoretical plates, in each of which the

ratio of the volume of the stationary phase to that of the mobile phase is the same; the flow is continuous without mixing between the plates; and the equilibrium of solutes between the two phases is instantaneously attained. Although plate models offer a simple way to describe chromatographic processes, they have some drawbacks. These models cannot be used easily to describe separately different physical kinetic phenomena causing band broadening. In principle the number of theoretical plates depends on specific interactions between each components and the stationary phase. Using an average number of theoretical plates for all components reduces the accuracy of calculations.

Mass balance or continuous models, also called rate models are based on the differential mass balance equation, which allows considering simultaneously all possible contributions to mass transfer kinetics. The models consist of a set of nonlinear coupled partial differential equations of the convection-diffusion (or hyperbolic-parabolic) type. The properties of this type of equation, in particular very steep gradients, make the application of many standard discretization procedures difficult. A lot of research has been devoted to the development of suitable discretization schemes, like finite difference or orthogonal collocation methods (Kaczmarski et al., 1997, Kaczmarski and Antos, 1996, Gu in 1995, Dünnebier et al., 2000, and Gomes et al., 2007). Common to most of the previously known approaches is the need for extreme computational power, which makes it difficult, even with modern computers, to perform simulations substantially below real time.

In Figure 2.1, depending on the initial assumptions, the general rate model can be simplified into simpler models. In addition to compulsory terms of convection, adsorption and reaction, other terms as dispersion and limited mass transfer rate can

be considered. Otherwise, two or more effects of dispersion, adsorption kinetic and mass transfer resistances can be lumped into a single effective kinetic parameter. Due to the nonlinearity in the mass balance equations, numerical methods are needed to solve these models. However, special cases with linear adsorption isotherms and first order reaction rate expressions can be solved analytically.

In the updated general rate model, all mass transfer effects in the chromatographic column are modeled in terms of the Maxwell-Stefan approach, which is the rigorous method to describe multicomponent mass transfer processes (Higler et al., 2000). In this thesis, only the continuous models based on the updated general rate will be applied to simulate chromatographic reactors.

2.1.1 Mass balances for continuous models

In a liquid chromatographic column packed with porous particles, the distribution of phases is very important for detailed modeling and simulation. When the pore network is fully filled with liquid, the volume of a column V_{col} can be divided into a volume of liquid phase V_L and a solid material volume in the form of particles, V_S.

$$V_{col} = V_S + V_L \tag{2-1}$$

The volume of the liquid phase includes the interstitial liquid volume, V_{inert} and the intraparticle liquid volume, V_{intra}.

$$V_{col} = V_S + V_{inter} + V_{intra} \tag{2-2}$$

The volume of particle, V_{solid} consists of the intraparticle liquid and the volume of solid material:

$$V_{Solid} = V_S + V_{intra} \tag{2-3}$$

If the column is homogeneously and well packed, the total porosity ε_t of a fixed-bed is:

$$\varepsilon_t = \frac{V_L}{V_{col}} \tag{2-4}$$

Also, it is possible to define external and internal porosities of following form:

Bulk or external porosity $\varepsilon_b = \frac{V_{inter}}{V_{col}}$ (2-5)

Particle or internal porosity $\varepsilon_p = \frac{V_{intra}}{V_S}$ (2-6)

Determining the total porosity in terms of bulk and particle porosities:

$$\varepsilon_t = \frac{V_{inter} + V_{intra}}{V_{col}} = \varepsilon_b + (1 - \varepsilon_b)\varepsilon_p \tag{2-7}$$

2.1.1.1. Conservation Equation in the Flowing Mobile Phase for FBCRs

A schematic diagram of the chromatographic column for a liquid-porous catalyst system is shown in Figure 2.2. It is assumed that the bulk of the liquid phase is ideally mixed and that the mass transfer resistance is located in films near the liquid/solid interface. To model mass transfer in this film the Maxwell-Stefan equations are used. Mass transfer inside the porous catalyst will be described with the Dusty Fluid Model, which is also based on the Maxwell-Stefan equations.

The equations of continuity for a multicomponent reacting mixture describe the change in mass concentration of each of species with time at a fixed point in space by diffusion, convection, and mass transfer of all components, as well as by chemical reactions that produce or consume components (Bird et al., 2002). The system we consider is a differential volume element of a column, $\boldsymbol{dV_{col}}$, fixed in space, through which the bulk fluid mixture is

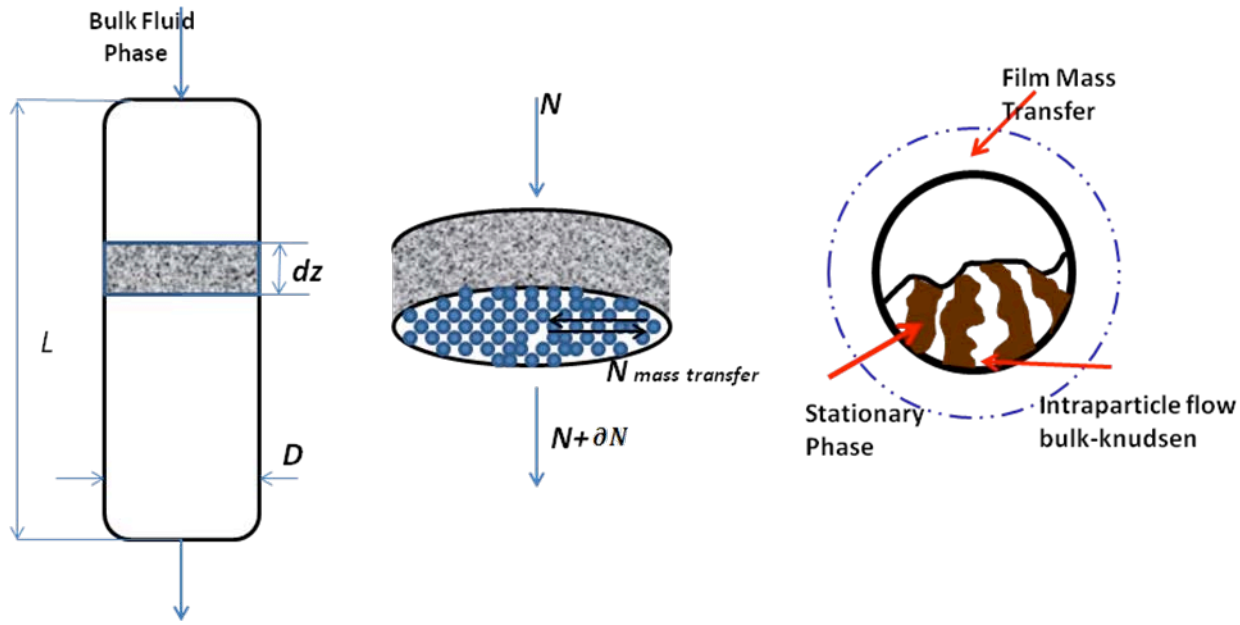

Figure 2.2 Schematic of a chromatographic column.

flowing (see Fig. 2.2). This differential element has a length ***dz***, and the cross section area $\boldsymbol{A_{col}}$ with a diameter of the column ***D***:

$$dV_{col} = A_{col}\, dz = \frac{\pi D^2}{4} dz \tag{2-8}$$

The equations of mass balances for all species *i* present in molar quantities is

$$\varepsilon_b \frac{\partial C_{b,i}}{\partial t} = -\varepsilon_b \left(\nabla \cdot N_{b,i}\right) - (1-\varepsilon_b) N_{film,i}\Big|_{r=d_p/2} + R_{Hom} \qquad i = 1, 2, 3 \cdots n \tag{2-9}$$

where $\boldsymbol{N_{b,i}}$ and $\boldsymbol{N_{film,i}}$ are the molar flow rates of component *i* in the bulk and film, respectively. The molar flux combines convective and diffusive fluxes of the following form (Bird et al., 2002):

$$N_{b,i} = J_{b,i} + \bar{u} C_{b,i} \tag{2-10}$$

Replacing equation (2-10) in (2-9)

$$\varepsilon_b \frac{\partial C_{b,i}}{\partial t} = -\varepsilon_b \nabla \cdot J_{b,i} - \varepsilon_b \bar{u} \nabla \cdot C_{b,i} - (1-\varepsilon_b) N_{film,i}\Big|_{r=d_p/2} + R_{Hom} \quad i = 1 \cdots n \qquad (2\text{-}11)$$

where $\boldsymbol{J_{b,i}}$, $\bar{u}$, and $\boldsymbol{C_{b,i}}$ are the diffusive fluxes, average velocity, and molar concentrations in the bulk liquid phase for each component. The diffusive fluxes in the bulk liquid phase are turbulent fluxes and, to solve this problem, empirical expressions found in the literature must be used. We present here the most popular one, called the Boussinesq's hypothesis. It implies, by analogy with Fick's first law of diffusion,

$$J_{b,i} = -D_{eddy} \frac{\partial C_{b,i}}{\partial z} \qquad (2\text{-}12)$$

This is the defining equation for the turbulent diffusivity D_{eddy}, also called the eddy diffusivity. This diffusivity is not a physical property characteristic of the fluid, but depends on position, direction, and the nature of the flow field. In other words, all components are transported by the same mechanism (Taylor and Krishna, 1993). In chromatography the eddy diffusivity is referred to as *axial dispersion coefficient*. Replacing equation (2-12) in (2-11) we have:

$$\varepsilon_b \frac{\partial C_{b,i}}{\partial t} = \varepsilon_b D_{eddy} \frac{\partial {C_{b,i}}^2}{\partial^2 z} - \varepsilon_b \bar{u} \frac{\partial C_{b,i}}{\partial z} - (1-\varepsilon_b) N_{film,i}\Big|_{r=d_p/2} + R_{Hom} \quad i = 1 \cdots n$$

(2-13)

For the implementation of the reaction equations, we need to make a distinction between heterogeneous and homogeneous systems. Homogeneous reactions take place in the liquid bulk and liquid transfer film. Adding the term of reaction in the equation 2-13 we have:

$$\boxed{\varepsilon_b \frac{\partial C_{b,i}}{\partial t} = \varepsilon_b D_{eddy} \frac{\partial {C_{b,i}}^2}{\partial^2 z} - \varepsilon_b \bar{u} \frac{\partial C_{b,i}}{\partial z} - (1-\varepsilon_b) N_{film,i}\Big|_{r={d_p}/{2}} + \sum_{j=1}^{N_R} \nu_{i,j} r_j^{hom} \quad i = 1 \cdots n}$$

(2-14)

where $\boldsymbol{\nu_{i,j}}$ and $\boldsymbol{r_j}$ are stoichiometry coefficients and the reaction numbers, respectively.

The liquid/solid interphase mass transfer rates in the above conservation equations are evaluated using the Maxwell-Stefan theory (Krishna and Wesselingh, 1997; Taylor and Krishna, 1993). The Maxwell-Stefan equations for mass transfer in liquid phase are:

$$\frac{x_i}{RT} \frac{\partial \mu_i^L}{\partial \eta} = \sum_{j=1}^{n} \frac{x_i N_j^{film} - x_j N_i^{film}}{C_t k_{i,j}} \qquad \text{for} \qquad i = 1 \cdots n \tag{2-15}$$

In this equation, $\boldsymbol{x_i}$ is the mole fraction of species $\boldsymbol{i}$, $\boldsymbol{R}$ is the gas constant, $\boldsymbol{\mu_i}$ is the chemical potential of species $\boldsymbol{i}$, $\boldsymbol{\eta}$ is a dimensionless film coordinate, $\boldsymbol{C_t}$ is the total liquid phase concentration, and $\boldsymbol{k_{i,j}}$ is the liquid phase binary pair mass transfer coefficient.

We may express the chemical potential in equation (2-15) in terms of activity coefficients, $\boldsymbol{\gamma}$ and mole fraction gradients as

$$\frac{x_i}{RT} \frac{\partial \mu_i^L}{\partial \eta} = \sum_{j=1}^{n} \Gamma_{i,j} \nabla \cdot x_j = \Gamma \nabla \cdot x_i \quad \text{and} \quad \Gamma_{i,j} = \delta_{i,j} + x_i \frac{\partial \ln(\gamma_i)}{\partial x_i} \tag{2-16}$$

Replacing equation (2-16) in (2-15) we have

$$\Gamma \nabla \cdot x_i = \sum_{j=1}^{n} \frac{x_i N_j^{film} - x_j N_i^{film}}{C_t k_{i,j}} \qquad \text{for} \qquad i = 1 \cdots n \tag{2-17}$$

Equation (2-17) is expressed conveniently in matrix form as (Taylor and Krishna, 1993)

$$\overline{N_{film}} = -\left[\overline{B_b(x_b)}\right]^{-1} \left[\overline{\Gamma(x_b)}\right] \nabla \overline{C_b} \qquad \text{for} \qquad i = 1 \cdots n \tag{2-18}$$

where the matrix $\left[\overline{B_b(x_b)}\right]$ is defined as below

$$[\overline{\overline{B_b(x_b)}}] = \begin{cases} \sum_{\substack{z=1 \\ z\neq i}}^{n} \frac{x_{b,z}}{\left(k_{i,z}(\overline{x_b})/_{\tau}\right)} & i = j \\ -\frac{x_{b,i}}{\left(k_{i,j}(\overline{x_b})/_{\tau}\right)} & i \neq j \end{cases} \tag{2-19}$$

Then, equation (2-18) will be replaced in equation (2-14) to complete the liquid bulk mass balance in the reactive chromatographic column.

To solve the mass balance equation (2-14), appropriate initial and boundary conditions have to be specified. As the initial condition for the liquid phase concentration, typically a constant value is assumed, because the column usually is initially equilibrated with the carrier.

Initial condition:

$$t = 0: \qquad C_{b,i} = C_{i,0} \qquad \text{for} \qquad i = 1 \cdots n \tag{2-20}$$

The standard Danckwerts boundary conditions are assumed:

$$z = 0 \qquad uC_{b,i} - \varepsilon_b D_{ax} \frac{\partial C_{b,i}}{\partial z}\bigg|_{z=0} = uC_{i,F} \tag{2-21}$$

$$z = L \qquad \frac{\partial C_{b,i}}{\partial z}\bigg|_{z=L} = 0 \tag{2-22}$$

The subscripts ***F*** and **0** refer to the feed and initial states, respectively.

2.1.1.2. Continuity Equation Inside of the Porous Solid Phase for FBCRs

Modeling of diffusion in adsorption and reaction process is usually started with the assumption that the solid phase is an unstructured homogeneous medium, that is, the solid characteristics are uniform throughout the solid volume. In chromatography, the porous particles in the column are spherical and of uniform diameter. The intraparticle diffusion process is usually simplified using linear driving force expressions or is characterized by a Fickian-like diffusion law with a parameter called the effective diffusivity. Complex

models, such as the one we propose, usually incorporate most or all possible phenomena occurring in the particle, and hence the solution gives greater details of the transport phenomena taking place as a function of the system parameters, but an extra computational effort is needed in the analysis.

In the work proposed, we will study the situation where the interaction between different species will occur during diffusion, adsorption, as well as reaction. Analysis of multicomponent systems will require the application of the Maxwell-Stefan approach to demonstrate the methodology as well as to show the essential features of how multiple species interact during the course of diffusion, adsorption, and reaction inside porous media.

Carrying out a mass balance over a thin shell within the particle, we obtain the following mass balance equation:

$$\boxed{\varepsilon_p \frac{\partial C_{p,i}}{\partial t} + \left(1-\varepsilon_p\right)\frac{\partial C_{q,i}}{\partial t} = -\frac{1}{r^2}\frac{\partial}{\partial r}\left\{r^2\left[\varepsilon_p \overline{N_p}\right]\right\} + \sum_{j=1}^{N_R} \nu_{i,j} r_j^{het}} \qquad (2\text{-}23)$$

where r is the radial coordinate of the particle, $\boldsymbol{C_{p,i}}$ and $\boldsymbol{C_{q,i}}$ are the concentration vectors in the void space and in the adsorbent phase, respectively, and the vector $\overline{N_p}$ is the flux in the void space. The flux in the void space is controlled by two transport mechanisms:

- **Free molecule (Knudsen):** This mode of diffusion was first described by Knudsen, who observed the transport of molecules as colliding and bouncing of molecules back from the wall of the porous medium (Figure 2.3). The driving force for this transport is the concentration gradient and the parameter characterizing this transport is called Knudsen diffusivity $\boldsymbol{D_{K,i}}$.

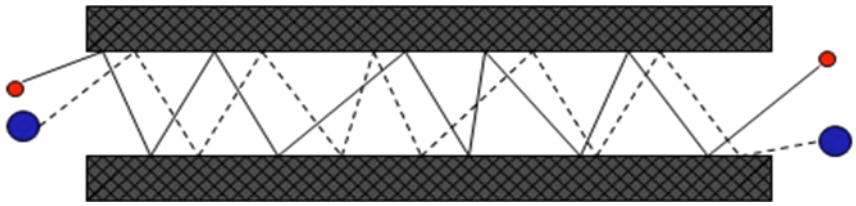

Figure 2.3 Knudsen diffusion mechanism.

- **Continuum diffusion:** this mode of diffusion is where the molecule-molecule collision is dominant over the collisions between molecules and the wall (Figure 2.4). In this mode of transport, different species move relative to each other. The parameter characterizing this relative motion between species of different type is the binary bulk diffusion coefficient, $\boldsymbol{D_{i,j}}$, where the subscripts ***i*** and ***j*** denote the species ***i*** and ***j***, respectively.

Figure 2.4 Continuum bulk diffusion mechanism.

When the mean free path of the molecules is much shorter than the pore dimension, bulk diffusion is the only diffusion mechanism. However, when the mean free path of the molecules is much greater than the pore dimension, which is usually the case for many practical applications in solids, the molecules will collide with the wall more frequently than between themselves. This is the basis of the Knudsen diffusion mechanism.

When the mean free path is comparable to the pore dimension, the overall transport of molecules is due to the reflection of molecules from the wall as well as to the collisions between the diffusing molecules. This is the case where the bulk diffusion and the Knudsen

diffusion will occur together. To combine these two modes of transport in a systematic way, we will use in this thesis a "dusty fluid model" proposed by Higler et al., 2000. In this model, the porous solid is modeled as a collection of stationary giant molecules (Figure 2.5). If we have ***n*** diffusing species in the liquid phase, the solid is treated as the $(n+1)$ species, uniformly distributed in space with a zero velocity. Now we apply the Maxwell-Stefan equation for the species ***i*** by balancing the force acting on a mole of species ***i*** with other species including the giant solid object, that is

$$-\frac{\partial \mu_i}{\partial r} = RTx_1\frac{(u_i-u_1)}{D_{i,1}} + RTx_2\frac{(u_i-u_2)}{D_{i,2}} + \cdots + RTx_n\frac{(u_i-u_n)}{D_{i,n}} + RTx_{n+1}\frac{(u_i-u_{n+1})}{D_{i,n+1}} \qquad (2\text{-}24)$$

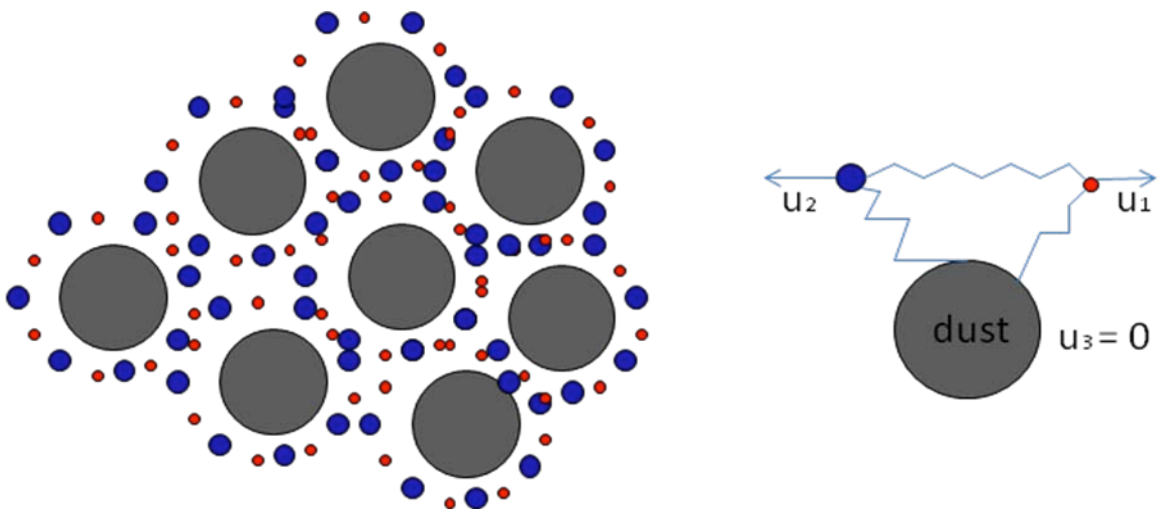

Figure 2.5 Schematic of the dusty fluid model.

But the giant molecule (that is, the solid) is assumed stationary $(u_{n+1} = 0)$, the above equation then becomes:

$$-\frac{\partial \mu_i}{\partial r} = RTx_1\frac{(u_i-u_1)}{D_{i,1}} + RTx_2\frac{(u_i-u_2)}{D_{i,2}} + \cdots + RTx_n\frac{(u_i-u_n)}{D_{i,n}} + RTx_{n+1}\frac{u_i}{D_{K,i}} \qquad (2\text{-}25)$$

where $\boldsymbol{D_{K,i}}$ is the Knudsen diffusivity defined as follows:

$$D_{K,i} = \frac{D_{i,n+1}}{x_{n+1}} \tag{2-26}$$

The constitutive flux equation written as in equation (2-25) is not useful for mass transfer calculation. Written in terms of the fluxes $(N_i = C_i u_i)$, the desired constitutive flux equations are:

$$\frac{x_{p,i}}{RT}\frac{\partial \mu_i^L}{\partial \eta} = \sum_{\substack{j=1 \\ j\neq i}}^{n} \frac{x_{p,i}N_{p,j} - x_{p,j}N_{p,i}}{C_{p,t}D_{i,j}} + \frac{N_{p,i}}{C_{p,t}D_{i,K}} \quad \text{for} \quad i = 1 \cdots n \tag{2-27}$$

Replacing equation (2-16) in (2-27) we have

$$\sum_{j=1}^{n} \Gamma_{i,j} \frac{\partial x_{p,i}}{\partial r} = \sum_{\substack{j=1 \\ j\neq i}}^{n} \frac{x_{p,i}N_{p,j} - x_{p,j}N_{p,i}}{C_{p,t}D_{i,j}} + \frac{N_{p,i}}{C_{p,t}D_{i,K}} \tag{2-28}$$

With ***n*** components in the mixture, the constitutive equation 2-28 can be conveniently cast into more compact form by using the vector-matrix format.

$$\boxed{\overline{N_p} = -\overline{\overline{\Gamma}}(\overline{x_p})\left[\overline{\overline{B_p}}(\overline{x_p})\right]^{-1}\frac{\partial \overline{C_p}}{\partial r}} \tag{2-29}$$

where the matrix $\left[\overline{\overline{B_p}}(\overline{x_p})\right]$is defined as below

$$\left[\overline{\overline{B_p}}(\overline{x_p})\right] = \begin{cases} \frac{1}{\left(D_{K,i}/\tau\right)} + \sum_{\substack{k=1 \\ k\neq i}}^{n} \frac{x_{p,k}}{\left(D_{i,k}(\overline{x_p})/\tau\right)} & i = j \\ -\frac{x_{p,i}}{\left(D_{i,j}(\overline{x_p})/\tau\right)} & i \neq j \end{cases} \tag{2-30}$$

Equation (2-30) is replaced in equation (2-23):

$$\varepsilon_p \frac{\partial C_{p,i}}{\partial t} + (1-\varepsilon_p)\frac{\partial C_{q,i}}{\partial t} = \frac{1}{r^2}\frac{\partial}{\partial r}\left\{r^2\left[\varepsilon_p \overline{\overline{\Gamma}}(\overline{x_p})\left[\overline{\overline{B_p}}(\overline{x_p})\right]^{-1}\frac{\partial \overline{C_p}}{\partial r}\right]\right\} + \sum_{j=1}^{N_R} \nu_{i,j} r_j^{het} \tag{2-31}$$

2.1.1.3. Adsorption Equilibrium Isotherms

Adsorption phenomena have been known for a very long time, and they are increasingly utilized to perform desired bulk separation or purification processes. The strength of an adsorption process is usually due to a porous solid medium. The advantage of

a porous solid is simply that it provides a very large surface area resulting in a high adsorption capacity. The adsorption separation is based on three distinct mechanisms: steric, equilibrium, and kinetic mechanisms. In the steric separation mechanism, the porous solid has pores having dimension such that it allows small molecules to enter while excluding large molecules from entry. The equilibrium mechanism is based on the solid having different abilities to accommodate different species, that is, the stronger adsorbing species is preferentially removed by the solid. The kinetic mechanism is based on the different rates of diffusion of different species into the pore, thus by controlling the time of exposure the faster diffusing species is preferentially removed by the solid.

The choice of porous solid used in a given adsorption process is a critical variable. The success or failure of the process depends on how the solid performs in both equilibria and kinetics. A solid with a good capacity but slow kinetics is not a good choice as it takes adsorbate molecules too long a time to reach the particle interior. This means long residence time in a column, hence a low throughput. On the other hand, a solid with fast kinetics but low capacity is not good either as a large amount of solid is required for a given throughput. Thus, a good solid is one that provides good adsorptive capacity as well as good kinetics. To satisfy these two requirements, the following aspects must be satisfied. The solid must have reasonably high surface area or micropore volume and large pore network for the transport of molecules to the interior. Most of the adsorbents commonly used in industry do satisfy these two criteria, with solids such as activated carbon, zeolite, alumina, silica gel, and Amberlyst ion exchange resin being the most popular.

Adsorption equilibrium data are the most important pieces of information in understanding an adsorption process. No matter how many components are present in the system, the adsorption equilibria of the pure components are the essential ingredients for understanding how many of those components can be accommodated by a solid adsorbent.

The adsorption isotherm is the equilibrium relationship between the concentration in the fluid and the concentration in the adsorbent particles at a given temperature and pressure. Here we will briefly discuss the concept of adsorption isotherms and its role in chromatography. Since chromatography is a separation method (Guiochon et al., 1994), we mostly consider mixtures of diluted species. In many cases, the mobile phase itself is not a pure solvent but a mixture and it may contain additives which themselves are more or less strongly adsorbed. The concentration of one of these components at equilibrium no longer depends only on its own concentration in the mobile phase. It also depends on the concentration of all the other components involved. At high concentrations, the molecules of the various components of the mobile phase and of the feed compete for their involvement in the retention mechanism, which has a limited capacity. In liquid-solid chromatography, the competition comes from the finite capacity of the adsorbent surface. An adsorption isotherm is a plot of the concentration or amount of a species on a solid surface as a function of the liquid concentration in the pores.

$$C_{q,i} = f\left(C_{p,1}, \ldots, C_{p,n}\right) \tag{2-32}$$

In the simplest form of chromatographic theory, it is assumed that the adsorption isotherm for the solute is linear, i.e.

$$C_{q,i} = K_i C_{p,i} \tag{2-33}$$

where $C_{q,i}$ and $C_{p,i}$ are the concentrations of the solute on the surface and in the mobile phase, respectively, and $\boldsymbol{K_i}$ is the adsorption constant of the solute on the stationary phase surface, also called the Henry constant. The linearity of the adsorption isotherm is, however, limited to a certain low concentration range. At higher concentrations the adsorption isotherm becomes non-linear. It is customary to describe this non-linearity with a Langmuir adsorption isotherm. The mathematical expression for this adsorption isotherm is:

$$C_{q,i} = \frac{K_i C_{p,i}}{1+\sum_{k=1}^{n} b_k C_{p,k}} \tag{2-34}$$

where b_k is called the affinity constant or Langmuir constant.

Replacing equation (2-33) in (2-31) for the linear case we have

$$\left(\varepsilon_p + (1-\varepsilon_p)K_i\right)\frac{\partial C_{p,i}}{\partial t} = \frac{1}{r^2}\frac{\partial}{\partial r}\left\{r^2\left[\varepsilon_p \bar{\bar{\Gamma}}(\overline{x_p})\left[\overline{\overline{B_p}}(\overline{x_p})\right]^{-1}\frac{\partial \overline{C_p}}{\partial r}\right]\right\} + \sum_{j=1}^{N_R} \nu_{i,j} r_j^{het} \tag{2-35}$$

and for the non-linear case, replacing equation (2-34) in (2-31) we have

$$\left(\varepsilon_p + (1-\varepsilon_p)\overline{\overline{J(C_{p,i})}}\right)\frac{\partial C_{p,i}}{\partial t} = \frac{1}{r^2}\frac{\partial}{\partial r}\left\{r^2\left[\varepsilon_p \bar{\bar{\Gamma}}(\overline{x_p})\left[\overline{\overline{B_p}}(\overline{C_p})\right]^{-1}\frac{\partial \overline{C_p}}{\partial r}\right]\right\} + \sum_{j=1}^{N_R} \nu_{i,j} r_j^{het} \tag{2-36}$$

where $J_i(C_{p,i})$ is the Jacobian of the equilibrium vector

$$\overline{\overline{J(C_{p,i})}} = \frac{\partial C_{q,i}}{\partial C_{p,i}} = \begin{bmatrix} \frac{\partial C_{q,1}}{\partial C_{p,1}} & \cdots & \frac{\partial C_{q,1}}{\partial C_{p,n}} \\ \vdots & \ddots & \vdots \\ \frac{\partial C_{q,n}}{\partial C_{p,1}} & \cdots & \frac{\partial C_{q,n}}{\partial C_{p,n}} \end{bmatrix} \tag{2-37}$$

To solve the mass balance equation (2-35) or (2-36), appropriate initial and boundary conditions have to be specified. As the initial condition for the liquid phase concentrations, typically a constant is assumed, due to the fact that the column is initially equilibrated with the carrier.

Initial condition:

$$t = 0: \qquad C_{p,i} = C_{i,0} \qquad \text{for} \qquad i = 1 \cdots n \tag{2-38}$$

Boundary conditions:

$$r = 0: \qquad \left.\frac{\partial C_{p,i}}{\partial r}\right|_{r=0} = 0 \tag{2-39}$$

$$r = {}^{d_p}/_{2}: \qquad \overline{N_{film}} = \overline{N_p} \tag{2-40}$$

Introducing the dimensionless variables:

Space (axial): $\xi = {}^{z}/_{L}$ (2-41)

Space (radial): $\Theta = {}^{r}/_{r_p}$ (2-42)

Time: $\theta = {}^{tu}/_{\varepsilon_b L}$ (2-43)

Peclet number: $$Pe = {uL}/{\varepsilon_b D_{ax}} \tag{2-44}$$

Damköehler number: $$Da = {\rho_b k_c \varepsilon_b L}/{(1-\varepsilon_b)u} \tag{2-45}$$

Mass transfer number: $$K_L = {3\varepsilon_b L K_t}\Big/{\left({d_p}/{2}\right)u} \tag{2-46}$$

Diffusivity number: $$D_L = {3\varepsilon_b \varepsilon_p L D_t}\Big/{\left({d_p}/{2}\right)^2 u} \tag{2-47}$$

Equations (2-35) or (2-36) and (2-14) can be written as follows:

$$\frac{\partial C_{b,i}}{\partial \theta} = \frac{1}{Pe}\frac{\partial^2 C_{b,i}}{\partial \xi^2} - \frac{\partial C_{b,i}}{\partial \xi} - K_L \frac{(1-\varepsilon_b)}{\varepsilon_b} N_{film,i}\Big|_{r={d_p}/{2}} + \sum_{j=1}^{N_R} \nu_{i,j} r_j^{hom} \quad i = 1 \cdots n \tag{2-48}$$

$$\left(\varepsilon_p + (1-\varepsilon_p)\overline{\overline{J(C_{p,i})}}\right)\frac{\partial \overline{C_p}}{\partial \theta} = D_L \frac{1}{\Theta^2}\frac{\partial}{\partial \Theta}\left\{\Theta^2\left[\overline{\overline{\Gamma}}(\overline{x_p})\left[\overline{\overline{B_p}}(\overline{C_p})\right]^{-1}\frac{\partial \overline{C_p}}{\partial \Theta}\right]\right\} + Da\sum_{j=1}^{N_R} \nu_{i,j} r_j^{het}$$

(2-49)

with initial and boundary conditions:

$$\theta = 0: \qquad C_{b,i} = C_{p,i} = C_{i,0} \tag{2-50}$$

$$\xi = 0 \qquad C_{b,i} - \frac{1}{Pe}\frac{\partial C_{b,i}}{\partial \xi}\Big|_{\xi=0} = C_{i,F} \tag{2-51}$$

$$\xi = 1 \qquad \left.\frac{\partial C_{b,i}}{\partial \xi}\right|_{\xi=1} = 0 \tag{2-52}$$

$$\Theta = 0: \qquad \left.\frac{\partial C_{p,i}}{\partial \Theta}\right|_{\Theta=0} = 0 \tag{2-53}$$

$$\Theta = 1 \qquad \overline{N_{film}} = \overline{N_p} \tag{2-54}$$

2.1.2 Model Solution

The numerical solution of the model described above can be obtained through a wide choice of numerical methods.

2.1.2.1. Numerical Solution

The model consists of a coupled PDE system with two sets of mass balance equations, one for the bulk-fluid and one for the particle phases for each component, respectively. The finite difference method is a simple numerical procedure that can be directly applied to solution of the entire model. This often requires a huge amount of computer memory during computation, and its efficiency and accuracy are not competitive compared with other more advanced numerical methods, such as the orthogonal collocation (OC), or the orthogonal collocation on finite element (OCFE) methods.

For the particle phase governing equation, the OC method is the choice. It is a very accurate, efficient and simple method for discretization. It has been widely used with success for many particle problems (Finlayson, 1980; Rice and Do, 1995; Do, 1998). Unfortunately, concentration gradients in the bulk-fluid phase can be very steep, thus the OC method is no longer a desirable choice, since global splines using high order polynomial are expensive (Finlayson, 1980) and sometimes unstable. The method of OCFE uses finite elements and

collocation points inside each element. This discretization method can be used for system with stiff gradients and is very powerful (Finlayson, 1980; Rice and Do, 1995).

2.1.2.2. Solution to the ODE System

If the OCFE method and the OC method are used for the discretization of the bulk-fluid phase PDE and for the discretization of the particle phase PDE, respectively, an ODE system is produced (Finlayson, 1980; Rice and Do, 1995). The ODE system with initial values can be readily solved using ODE solver subroutines such as "ODE15S" or "ODE113" of MATLAB® which is a variable-order solver based on the numerical differentiation formulas (NDFs). Optionally it uses the backward differentiation formulas, BDFs, (also known as Gear's method) that are usually less efficient (Mathworks, 2007). Figure 2.6 shows the strategy of numerical method used to solve the PDE system in the model.

2.1.2.3. OC Formulation of the Particle Phase Equation

The symmetry of equation (2-49) at $\Theta = 0$ suggests the following transformation of the independent variable (Finlayson, 1980; Rice and Do, 1995) $\Psi = \Theta^2$. With this new variable, equation (2-49) will become:

$$\left(\varepsilon_p + (1-\varepsilon_p)\overline{\overline{J(C_{p,i})}}\right)\frac{\partial \overline{C_p}}{\partial \theta} = D_L\left[\left[D_t\overline{\overline{B_p}}(\overline{C_p})\right]^{-1}\bar{\bar{\Gamma}}(\overline{x_p})\left\{4\Psi\frac{\partial^2\overline{C_p}}{\partial\Psi^2} + 6\frac{\partial\overline{C_p}}{\partial\Psi}\right\} + 4\Psi\bar{\bar{\Gamma}}(\overline{x_p})\frac{\partial\overline{C_p}}{\partial\Psi}\frac{\partial\left[D_t\overline{\overline{B_p}}(\overline{C_p})\right]^{-1}}{\partial\Psi} + 4\Psi\left[D_t\overline{\overline{B_p}}(\overline{C_p})\right]^{-1}\frac{\partial\overline{C_p}}{\partial\Psi}\frac{\partial\bar{\Gamma}(\overline{x_p})}{\partial\Psi}\right] + Da\sum_{j=1}^{N_R}\nu_{i,j}r_j^{het} \tag{2-55}$$

To apply the OC method, we choose N interior collocation points in the spatial domain Ψ, that is $0 < \Psi_1, \Psi_2 \cdots \Psi_N < 1$. These N interior points together with the point at the boundary

$\Psi = 1$ will form N+1 interpolation points. Evaluating equation (2-55) at the j-th interior collocation point, we get:

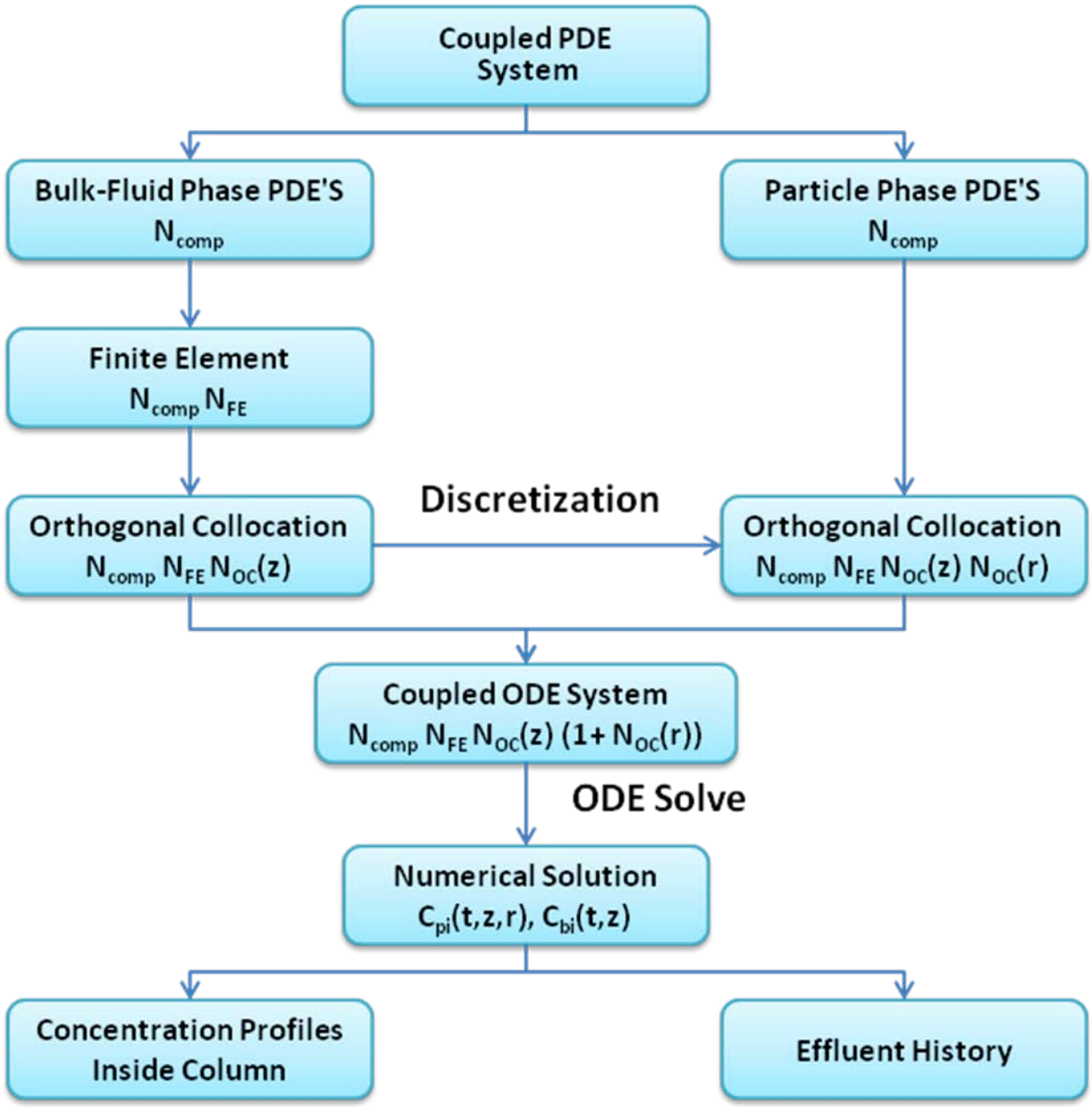

Figure 2.6 Solution strategy.

$$\left(\varepsilon_p + (1-\varepsilon_p)\overline{\overline{J\left(\overline{C_p}\right)}}\right)\frac{\partial \overline{C_p}_j}{\partial \theta} = D_L\left[\left[D_t\overline{\overline{B_p}}\left(\overline{C_p}_j\right)\right]^{-1}\overline{\overline{\Gamma}}\left(\overline{x_p}_j\right)\left\{4\Psi_j\frac{\partial^2\overline{C_p}}{\partial\Psi^2}\bigg|_{\Psi_j} + 6\frac{\partial\overline{C_p}}{\partial\Psi}\bigg|_{\Psi_j}\right\} + 4\Psi_j\overline{\overline{\Gamma}}\left(\overline{x_p}_j\right)\frac{\partial\overline{C_p}}{\partial\Psi}\bigg|_{\Psi_j}\frac{\partial\left[D_t\overline{\overline{B_p}}\left(\overline{C_p}_j\right)\right]^{-1}}{\partial\Psi}\bigg|_{\Psi_j} + 4\Psi_j\left[D_t\overline{\overline{B_p}}\left(\overline{C_p}_j\right)\right]^{-1}\frac{\partial\overline{C_p}}{\partial\Psi}\bigg|_{\Psi_j}\frac{\partial\overline{\Gamma}\left(\overline{x_p}_j\right)}{\partial\Psi}\bigg|_{\Psi_j}\right] + Da\sum_{d=1}^{N_R}\nu_{i,d}r_d^{het} \quad \text{for} \quad j = 1,2,3,\ldots,N \tag{2-56}$$

Here $\overline{C_p}_j$ is the value of $\overline{C_p}$ at the collocation point Ψ_j, or for the collocation point *j*. The first and second derivatives at any interpolation points can be expressed in terms of the dependent variables $\overline{C_p}$, as given below:

$$\frac{\partial\overline{C_p}_j}{\partial\Psi}\bigg|_{\Psi_j} = \sum_{k=1}^{N+1}A_{j,k}\overline{C_p}_k \tag{2-57a}$$

$$\frac{\partial^2\overline{C_p}_j}{\partial\Psi^2}\bigg|_{\Psi_j} = \sum_{k=1}^{N+1}B_{j,k}\overline{C_p}_k \tag{2-57b}$$

$$\frac{\partial\left[D_t\overline{\overline{B_p}}\left(\overline{C_p}_j\right)\right]^{-1}}{\partial\Psi}\bigg|_{\Psi_j} = \sum_{k=1}^{N+1}A_{j,k}\left[D_t\overline{\overline{B_p}}\left(\overline{C_p}_k\right)\right]^{-1} \tag{2-57c}$$

$$\frac{\partial\overline{\Gamma}\left(\overline{x_p}_j\right)}{\partial\Psi}\bigg|_{\Psi_j} = \sum_{k=1}^{N+1}A_{j,k}\overline{\overline{\Gamma}}\left(\overline{x_p}_k\right) \tag{2-57d}$$

where $\overline{\overline{A}}$ and $\overline{\overline{B}}$ are known constant matrices for a given set of *N+1* interpolation points (Finlayson, 1980; Rice and Do, 1995).

Substitution of equations (2-57) into equation (2-56) gives:

$$\left(\varepsilon_p + (1-\varepsilon_p)\overline{\overline{J\left(\overline{C_{p_j}}\right)}}\right)\frac{\partial \overline{C_{p_j}}}{\partial \theta} = D_L\left[\left[D_t\overline{\overline{B_p}}\left(\overline{C_{p_j}}\right)\right]^{-1}\overline{\overline{\Gamma}}\left(\overline{x_{p_j}}\right)\left\{4\Psi_j\sum_{k=1}^{N+1}B_{j,k}\,\overline{C_{p_k}} + 6\sum_{k=1}^{N+1}A_{j,k}\,\overline{C_{p_k}}\right\} + 4\Psi_j\overline{\overline{\Gamma}}\left(\overline{x_{p_j}}\right)\sum_{k=1}^{N+1}A_{j,k}\,\overline{C_{p_k}}\sum_{k=1}^{N+1}A_{j,k}\left[D_t\overline{\overline{B_p}}\left(\overline{C_{p_k}}\right)\right]^{-1} + 4\Psi_j\left[D_t\overline{\overline{B_p}}\left(\overline{C_{p_j}}\right)\right]^{-1}\sum_{k=1}^{N+1}A_{j,k}\,\overline{C_{p_k}}\sum_{k=1}^{N+1}A_{j,k}\,\overline{\overline{\Gamma}}\left(\overline{x_{p_k}}\right)\right] + Da\sum_{d=1}^{N_R}\nu_{i,d}r_d^{het} \quad \text{for} \quad j = 1, 2, 3, \ldots, N \tag{2-58}$$

Equation (2-58) is valid for N interior collocation points. The equation for the N+1 interpolation point is the following:

$$\Psi = 1 \qquad \overline{N_{film}} = \overline{N_p} \tag{2-59}$$

Equation (2-59) is a nonlinear algebraic equation for $\overline{C_{p_{N+1}}}$ expressed in terms of the concentrations at the N collocation points, $\overline{C_{p_j}}$.

2.1.2.4. OCFE Formulation for Bulk Fluid Phase Equation

The governing equations in the bulk fluid phase written in nondimensional form are (2-48), (2-50), (2-51), and (2-52). The first step to apply OCFE is to split the domain [0, 1] into many subdomains. In this work, we will use five, ten or twenty subdomains. For the sake of demonstration, we first use only two subdomains (Rice and Do, 1995). Let ***w*** be the point that splits the domain [0, 1] into two subdomains [0, w] and [w, 1]. Next, we denote C_{b1} and C_{b2} to describe C_b in the first and second subdomain, respectively. C_{b1} and C_{b2} must satisfy the equation 2-48, which is valid at all points within the domain [0, 1]. Before applying the OC in each subdomain, we must normalize the domains to have a range of [0, 1]. This can be achieved by denoting a new coordinate for the subdomain 1 as φ_1 defined as

$$\varphi_1 = \frac{\xi}{w} \tag{2-60}$$

Similarly, we denote a new coordinate for the subdomain 2 as φ_2 and it is defined as

$$\varphi_2 = \frac{\xi - w}{1 - w} \tag{2-61}$$

Thus, we see immediately that φ_1 and φ_2 range is between 0 and 1 in their respective domains as shows the Figure 2.7.

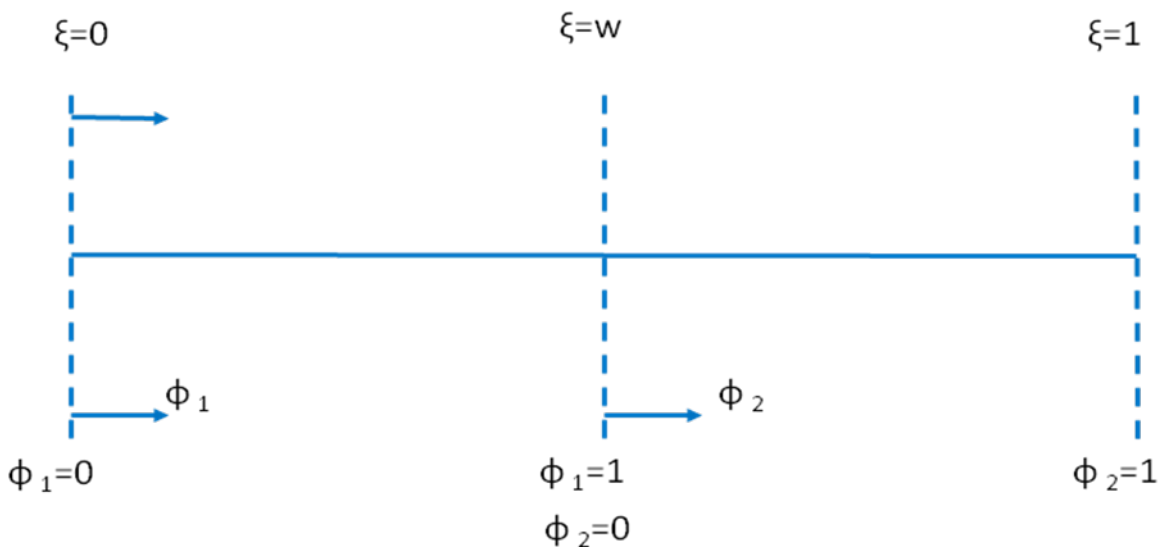

Figure 2.7 Two elements in the domain [0, 1].

Differentiating equations (2-60) and (2-61) we have:

$$\frac{\partial \varphi_1}{\partial \xi} = \frac{1}{w} \qquad \text{and} \qquad \frac{\partial \varphi_2}{\partial \xi} = \frac{1}{(1-w)} \tag{2-62}$$

Applying the chain rule and using equation (2-62) we have:

$$\frac{\partial \overline{C_{b1}}}{\partial \xi} = \frac{\partial \overline{C_{b1}}}{\partial \varphi_1}\frac{\partial \varphi_1}{\partial \xi} = \frac{1}{w}\frac{\partial \overline{C_{b1}}}{\partial \varphi_1} \tag{2-63}$$

$$\frac{\partial^2 \overline{C_{b1}}}{\partial \xi^2} = \frac{\partial}{\partial \xi}\left[\frac{1}{w}\frac{\partial \overline{C_{b1}}}{\partial \varphi_1}\right] = \frac{\partial}{\partial \varphi_1}\left[\frac{1}{w}\frac{\partial \overline{C_{b1}}}{\partial \varphi_1}\right]\frac{\partial \varphi_1}{\partial \xi} = \frac{1}{w^2}\frac{\partial^2 \overline{C_{b1}}}{\partial {\varphi_1}^2} \tag{2-64}$$

Substituting equations (2-63) and (2-64) in equations (2-48) and (2-51) we have

$$\frac{\partial \overline{C_{b1}}}{\partial \theta} = \frac{1}{w^2 Pe} \frac{\partial^2 \overline{C_{b1}}}{\partial {\varphi_1}^2} - \frac{1}{w} \frac{\partial \overline{C_{b1}}}{\partial \varphi_1} - K_L \frac{(1-\varepsilon_b)}{\varepsilon_b} N_{film}\Big|_{r={}^{d_p}/_2} \tag{2-65}$$

$$\varphi_1 = 0 \qquad \overline{C_{b1}} - \frac{1}{wPe} \frac{\partial \overline{C_{b1}}}{\partial \varphi_1}\Bigg|_{\varphi_1=0} = \bar{C}_F \tag{2-66}$$

Similarly, for the second subdomain we have:

$$\frac{\partial \overline{C_{b2}}}{\partial \theta} = \frac{1}{(1-w)^2 Pe} \frac{\partial^2 \overline{C_{b2}}}{\partial {\varphi_2}^2} - \frac{1}{(1-w)} \frac{\partial \overline{C_{b2}}}{\partial \varphi_2} - K_L \frac{(1-\varepsilon_b)}{\varepsilon_b} N_{film}\Big|_{r={}^{d_p}/_2} \tag{2-67}$$

$$\varphi_2 = 1 \qquad \frac{\partial \overline{C_{b2}}}{\partial \varphi_2}\Bigg|_{\varphi_2=1} = 0 \tag{2-68}$$

Equations (2-65) and (2-67) are two second order differential equations, and therefore for the complete formulation we must have four conditions. Equations (2-66) and (2-68) provide two, and hence, we require two more conditions. These are obtained by the continuity of concentration and mass flux at the junction of the two subdomains, that is,

$$\overline{C_{b1}}\Big|_{\varphi_1=1} = \overline{C_{b2}}\Big|_{\varphi_2=0} \tag{2-69}$$

and

$$\frac{1}{w}\left[\frac{\partial \overline{C_{b1}}}{\partial \varphi_1}\right]_{\varphi_1=1} = \frac{1}{(1-w)}\left[\frac{\partial \overline{C_{b2}}}{\partial \varphi_2}\right]_{\varphi_2=0} \tag{2-70}$$

We are ready now to apply the OC to each subdomain. We now use *N* interior collocation points in the φ_1 domain, and together with the two boundary points ($\varphi_1 = 0$ and $\varphi_1 = 1$) we have *N*+2 interpolation points. The derivatives in equation (2-65) at the *j*-th interpolation point are given by:

$$\frac{\partial \overline{C_{b1}}}{\partial \varphi_1}\Big|_j = \sum_{k=1}^{N+2} A1_{j,k}\, \overline{C_{b1}}_k \tag{2-71}$$

$$\frac{\partial^2 \overline{C_{b1}}}{\partial {\varphi_1}^2}\Big|_j = \sum_{k=1}^{N+2} B1_{j,k}\, \overline{C_{b1}}_k \tag{2-72}$$

Substituting equations (2-71) and (2-72) in equations (2-63) and (2-64) we have

$$\frac{\partial \overline{C_{b1_j}}}{\partial \theta} = \frac{1}{w^2 Pe}\sum_{k=1}^{N+2} B1_{j,k}\,\overline{C_{b1_k}} - \frac{1}{w}\sum_{k=1}^{N+2} A1_{j,k}\,\overline{C_{b1_k}} - K_L\frac{(1-\varepsilon_b)}{\varepsilon_b} N_{film,j}\Big|_{r={}^{d_p}/_2}$$

$$j = 2 \cdots N+1 \qquad (2\text{-}73)$$

$$j = 1 \qquad \overline{C_{b1_1}} - \frac{1}{wPe}\sum_{k=1}^{N+2} A1_{1,k}\,\overline{C_{b1_k}} = \bar{C}_F \qquad (2\text{-}73a)$$

Similarly, we now use M interior collocation points in the φ_2 domain, and together with the two boundary points $(\varphi_2 = 0 \text{ and } \varphi_2 = 1)$ we have M+2 interpolation points. The derivatives in equation (2-60) at the j-th interpolation point are given by:

$$\frac{\partial \overline{C_{b2}}}{\partial \varphi_2}\Big|_j = \sum_{k=1}^{M+2} A2_{j,k}\,\overline{C_{b2_k}} \qquad (2\text{-}74)$$

$$\frac{\partial^2 \overline{C_{b2}}}{\partial {\varphi_2}^2}\Big|_j = \sum_{k=1}^{M+2} B2_{j,k}\,\overline{C_{b2_k}} \qquad (2\text{-}75)$$

Substituting equations (2-74) and (2-75) in equations (2-72) and (2-73) we have

$$\frac{\partial \overline{C_{b2_k}}}{\partial \theta} = \frac{1}{(1-w)^2 Pe}\sum_{k=1}^{M+2} B2_{j,k}\,\overline{C_{b2_k}} - \frac{1}{(1-w)}\sum_{k=1}^{M+2} A2_{j,k}\,\overline{C_{b2_k}} - K_L\frac{(1-\varepsilon_b)}{\varepsilon_b} N_{film,j}\Big|_{r={}^{d_p}/_2} + \sum_{d=1}^{N_R} \nu_{i,d} r_d^{hom} \quad j = 2 \cdots M+1$$

(2-76)

$$j = M+2 \qquad \sum_{k=1}^{M+2} A2_{M+2,k}\,\overline{C_{b2_k}} = 0 \qquad (2\text{-}77)$$

Applying equations (2-74) and (2-75) at the junction of the two subdomains, equations (2-69) and (2-70) become:

$$\overline{C_{b1_{N+2}}} = \overline{C_{b2_1}} \qquad (2\text{-}78)$$

and

$$\frac{1}{w}\sum_{k=1}^{N+2} A1_{N+2,k}\,\overline{C_{b2_k}} = \frac{1}{(1-w)}\sum_{k=1}^{M+2} A2_{1,k}\,\overline{C_{b2_k}} \qquad (2\text{-}79)$$

where *A1*, *A2*, *B1*, and *B2* are the first and second order derivative matrices of OC for each one of the subdomains, respectively. Thus, we have completed the orthogonal collocation treatment on finite elements. We have an equal number of equations and unknown variables.

2.1.3 Parameters Estimation

The multicomponent activity coefficients will be evaluated using the UNIFAC method (Fredenslund et al., 1977). This method for estimation of activity coefficients depends on the concept that the liquid mixture may be considered a solution of the structural units from which the molecules are formed rather than a solution of the molecules themselves. The fundamental idea of a solution of group model is to utilize existing phase equilibrium data for predicting phase equilibria of systems for which no experimental data are available. In UNIFAC, the molecular activity coefficient is separated into two parts: one part provides the contribution due to differences in molecular size and shape, and the other provides the contribution due to molecular interactions (Poling et al., 2001).

The Wilke-Chang equation (Poling et al., 2001 and Benitez, 2002) will be used to predict the molecular diffusion coefficient in an infinitely dilute solution:

$$D_{i,j}^{\circ} = 7.4 * 10^{-8} \frac{(\Phi_j M_j)^{1/2} T}{\eta_j V_i^{0.6}} \qquad (2\text{-}80)$$

where $D_{i,j}^{\circ}$ is the diffusivity of *i* in very dilute solution in solvent *j*, M_j is the molecular weight of solvent *j*, *T* is the temperature, η_j is the viscosity of the solvent *j*, V_i is solute molar volume at its normal boiling point, and Φ_j is the association factor of solvent *j*.

The Taylor and Krishna equation (Taylor and Krishna, 1993) will be used to predict Maxwell-Stefan diffusion coefficients for multicomponent concentrated liquid mixtures:

$$Đ_{i,j} = \left(D^{\circ}_{i,j}\right)^{(1+x_j-x_i)/2}\left(D^{\circ}_{j,i}\right)^{(1+x_i-x_j)/2} \tag{2-81}$$

The binary pair Maxwell-Stefan diffusion coefficients are related to the free diffusion binary pair Maxwell-Stefan diffusion coefficients by:

$$D_{i,j} = \frac{\varepsilon_p}{\tau} Đ_{i,j} \tag{2-82}$$

where τ is the tortuosity factor and can be estimated by the following equation (Akanni et al., 1987):

$$\tau = 1 + \frac{1}{2}\left(1 - \varepsilon_p\right) \tag{2-83}$$

The film mass transfer coefficients $k_{i,j}$, will be estimated with the correlation proposed by Wilson and Geankoplis (Ruthven, 1984)

$$Sh_p = \frac{1.09}{\varepsilon_p}\left(Re_p Sc\right)^{0.33} \qquad 0.0015 < Re_p < 55 \tag{2-84}$$

where Sh_p, Re_p, and Sc are the Sherwood, Reynolds, and Schmidt numbers, respectively, relative to particle size

$$Sh_p = \frac{k_{i,j} d_p}{D_{i,j}} \tag{2-85}$$

$$Re_p = \frac{\rho d_p u}{\eta_m} \tag{2-86}$$

$$Sc = \frac{\eta_m}{\rho D_{i,j}} \tag{2-87}$$

The mixture viscosity η_m is predicted by the generalized corresponding states method proposed by Teja and Rice (1981).

2.2 FBCR Simulation with Maxwell-Stefan Approach

In this section, the use of the Maxwell-Stefan approach model for FBCR is illustrated by means of two application examples. The first describes a process for the production of acetal. This process has been the subject of several studies (Silva and Rodrigues 2001, 2002, and 2005), They employ a linear driving force model (LDF) in the description of mass transfer effects in the column. The results of our simulations will be compared to some experimental data presented by Silva and Rodrigues (2002 and 2005).

In a second application example, a process for the production of triacetin is studied. Gelosa et al., (2003) studied this process employing also a LDF model in the description of mass transfer effects in the column. The simulation of this process is very complex because it involves several steps of reaction limited by equilibrium, separation, and purification.

2.2.1 Application 1: Diethylacetal Synthesis

Acetals (acetaldehyde diethylacetal) are oxygenated organic compounds used as starting materials for perfumes, agricultural chemicals, and pharmaceuticals (Iwasaki et al., 1996), and they are represented by the following structure:

$$R_1 - O - C\ (R_2)\ (R_3) - O - R_1$$

where R_1 is an alkyl group, and R_2 and R_3 each represent a hydrogen atom or an alkyl group. Acetal is an important raw material for fragrances and pharmaceutical products (Kaufhold and El-Chabawi, 1996) and is used in the flavoring of alcoholic drinks (Kelly et al., 1999). In perfumery, acetal is used for the design of synthetic perfumes to increase the resistance to

oxidation and therefore the lifetime of perfumes. Acetal is also widely used as an intermediate for the synthesis of various industrial chemicals, especially alkyl vinyl ethers and polyacetal resins (AIzawa et al., 1994).

Apart from the above uses, acetals can be used as oxygenates for high-volume fuels in order to increase the cetane number of diesel fuel. The cetane number is one of the most important properties of a diesel fuel, and it is used to describe its ignition quality. Many attempts have been made to improve the cetane number of diesel engine fuels in order to suppress the emissions of soot and smoke. A higher cetane number indicates the ability of a diesel engine fuel to ignite quickly after being injected into the combustion cylinder (Waller et al., 1999).

The main process for the manufacture of acetals is the reversible reaction of an aldehyde with excess alcohol in acid medium according to:

$$2\ Alcohol\ (A) + Aldehyde\ (B) \leftrightarrow Acetal(C) + Water\ (D)$$

where the alcohol could be methanol or ethanol, and the aldehyde could be acetaldehyde, vinyl ether, acetylene, or ethylene (Kohlpaintner et al., 1999). The advantage of using ethanol and acetaldehydes as reactants is that ethanol is produced from renewable sources (mainly from the sugarcane industry) and acetaldehyde could be produced from dehydrogenation of ethanol or direct ethylene oxidation.

Traditionally, the reaction is catalyzed by mineral or carboxylic acids (Morrison, 1983). The disadvantage of using soluble catalysts is that they must be neutralized after the reaction and separated from the product. Therefore, heterogeneous catalysts such as ion-exchange resins (acid type) or zeolites are used, which have the advantages of being easily separated from the reaction product and having a long lifetime. Acid resins are interesting because they

serve as catalysts for the acetalization reaction and selective adsorbents for the species involved in the process. Ion-exchange resins (Amberlyst® 15) conventionally used to catalyze etherification and esterification reactions can be used (Mazzotti et al., 1996; Mazzotti et al., 1997).

With ordinary distillation, dimethylacetal cannot be separated from the reaction mixture due to the close boiling temperatures of methanol and acetal: 64.5 and 64.3°C, respectively (Perry's Handbook, 1984). In this work, an adsorptive/chromatographic reaction process for the production of acetal is considered for validation of the model proposed.

- **Diethylacetal Synthesis Using Ethanol**

The first example under consideration is a reactive system utilized by Silva and Rodrigues (2002). The reaction is:

$$2\ Ethanol\ (A) + Acetaldehyde\ (B) \leftrightarrow Acetal(C) + Water\ (D) \qquad (2\text{-}88)$$

The reaction is reversible and the reaction rate equation proposed by the authors is given by:

$$\mathcal{R} = k_c \frac{a_A a_B - \frac{a_C a_D}{K_{eq} a_A}}{\left(1 + {}^{K_I a_C}/_{a_A}\right)^2} \qquad (2\text{-}89)$$

and the parameters are listed in Table 2.1

Table 2.1 Reaction equilibrium constant and kinetic parameters.

T (K)	K_{eq}	K_C	K_I
283	1.39	2.83	2.34
288	1.29	4.05	2.68

The activity coefficients of compounds were computed by the UNIFAC method. The parameters needed for its use (relative molecular volume and surface area of pure species and the interaction parameters) are presented in Tables 2.2 and 2.3 (Poling et al., 2001).

Table 2.2 Relative molecular volume and surface area of pure species parameters.

Molecule (i)	Group Identification			ν_K^i	R_K	Q_K
	Name	No. Main	No. Section			
1: ethanol	CH_3	1	1	1	0.9011	0.848
	CH_2	1	2	1	0.6744	0.540
	OH	5	15	1	1.0000	1.200
2: acetaldehyde	CH_3	1	1	1	0.9011	0.848
	CHO	10	21	1	0.9980	0.948
3: acetal	CH_3	1	1	3	0.9011	0.848
	CH	1	3	1	0.4469	0.228
	CH_2O	13	26	2	0.9183	0.780
4: water	H_2O	7	17	1	0.9200	1.400

Table 2.3 Interaction parameters.

$a_{m,n}$	1	5	7	10	13
1	0	986.5	1318	677	251.5
5	156.4	0	353.5	-203.6	28.06
7	300	-229.1	0	-116	540.5
10	505.7	529	480.8	0	304.1
13	83.36	237.7	-314.7	-7.838	0

The characteristics of the FBCR column used in the simulations are presented in Table 2.4 (Silva and Rodrigues, 2002).

The adsorption isotherm is the equilibrium relationship between the concentration in the fluid and the concentration in the adsorbent particles at a given temperature and pressure. The concentration of the adsorbate on the solid is given as the number of moles or the mass adsorbed per unit mass or unit volume of adsorbent (solid phase). For this case, it was shown to follow the Langmuir isotherm model for multicomponent adsorption, equation (2-34), and the parameters are presented in Table 2.5 (Silva and Rodrigues 2002; Poling et al., 2001).

Table 2.4 Characteristics of FBCR column.

Length (L)	28 cm
Internal diameter (D)	2.2 cm
Temperture (T)	288 K
Radius of the particle (r_p)	239 µm
External void fraction (ε_b)	0.40
Internal void fraction (ε_p)	0.40
Tortuosity (τ)	1.3
Peclet number (Pe)	300
Bulk density (ρ_b)	390 kg/m^3
Resin	Amberlyst 15

Table 2.5 Adsorption equilibrium isotherms and component parameters at 288 K.

Components	Q (mol/L$_r$)	b (L/mol)	density (kg/m^3)	η (Cp)	Φ	$\bar{V}$ (cm^3/mol)	T_b K	T_c K	P_c bar
Ethanol (A)	25.9	195	795	1.342	1.5	58.165	351.8	513.9	61.48
Acetaldehyde	35.4	173	785	0.296	1	50.789	293.3	454.7	55.5
Acetal (C)	15.9	71	852	0.354	1	136.94	375.4	527	30.1
Water (D)	60.7	310	1003	1.139	2.6	16.649	373.1	647.1	220.6

- **Model Validation**

The test case for the simulation is a typical reaction with a mixture of ethanol and acetaldehyde, which is continuously fed to the chromatographic reactor with the

characteristics of Table 2.4 and that initially is saturated with ethanol. The conditions for the first simulation are a constant flow rate of 14.5 mL/min and the feed composition of ethanol and acetaldehyde with a concentration of 11.7 kmol/m^3 and 6.3 kmol/m^3, respectively. Our proposed model, based on the Maxwell-Stefan approach, is validated when the experimental results obtained by Silva and Rodrigues (2002) are compared with our simulation results as shown in Figure 2.8 for the production step. It is observed that our model predicts very well the experimental results shown in that figure. The breakthrough times of the different transitions, as well as the shape of the concentration peaks and the steady state effluent concentrations are well predicted. Similar results were obtained by Silva and Rodrigues (2002) using a model with the LDF approximation as shown in Figure 2.9. The fact that there is no significant difference between the results obtained by the two models presented, one using the LDF approximation and the other using the more rigorous Maxwell-Stefan approach, suggests that the effects of mass transfer on the kinetics of the process are not significant in this case.

Recently, Silva and Rodrigues (2005) analyzed the same reaction under different conditions. In this case the column was packed with Amberlyst 15 resin with a particle diameter of 700 μm and the length of column was 86 cm, at 15°C. The other characteristics of the column are similar to those presented in Table 2.4. They carried out kinetic experiments in the temperature range 16–26°C and proposed a modified reaction rate law given by:

$$\mathcal{R} = k_c \frac{a_A a_B - \frac{a_C a_D}{K_{eq} a_A}}{(1 + K_D a_D)^2} \tag{2-90}$$

with parameters given by:

$$\ln K_{eq} = \frac{1270}{T} - 3.07 \tag{2-91}$$

$$k_c = 3.3 \times 10^{11} exp\left[\frac{-7824}{T}\right] \quad (2\text{-}92)$$

$$K_D = 6.4 \times 10^{5} exp\left[\frac{-4003}{T}\right] \quad (2\text{-}93)$$

In this case, the simulation is with the same reaction as before but, with a mixture of ethanol, acetaldehyde, and water, which is continuously fed to the chromatographic reactor. The reactor is initially equilibrated with ethanol and water. The conditions for this simulation are a constant flow rate of 9.2 mL/min and a feed composition of ethanol, acetaldehyde, and water of 10.6 kmol/m^3, 5.2 kmol/m^3, and 5.2 kmol/m^3, respectively.

The proposed model based on the Maxwell-Stefan approach is validated again, when compared to the experimental results obtained by Silva and Rodrigues (2005) as shown in Figure 2.10 for the production step. It is observed that our model accurately predicts the experimental results shown in Figure 2.10. The breakthrough times of the different transitions, as well as the shape of the concentration peaks and the steady state effluent concentrations are well predicted. Similar results were obtained by Silva and Rodrigues (2005) using a model with the LDF approximation as is shown in Figure 2.11.

2.2.2 Application 2: Production of Triacetin

In this case we analyze the synthesis of glycerol triacetate (triacetine) by the esterification of glycerol with acetic acid (Gelosa et al., 2003). This requires a series of three esterification steps, each producing a molecule of water, with glycerol monoacetate (monoacetine) and glycerol diacetate (diacetine) as intermediate products, according to the following kinetic scheme

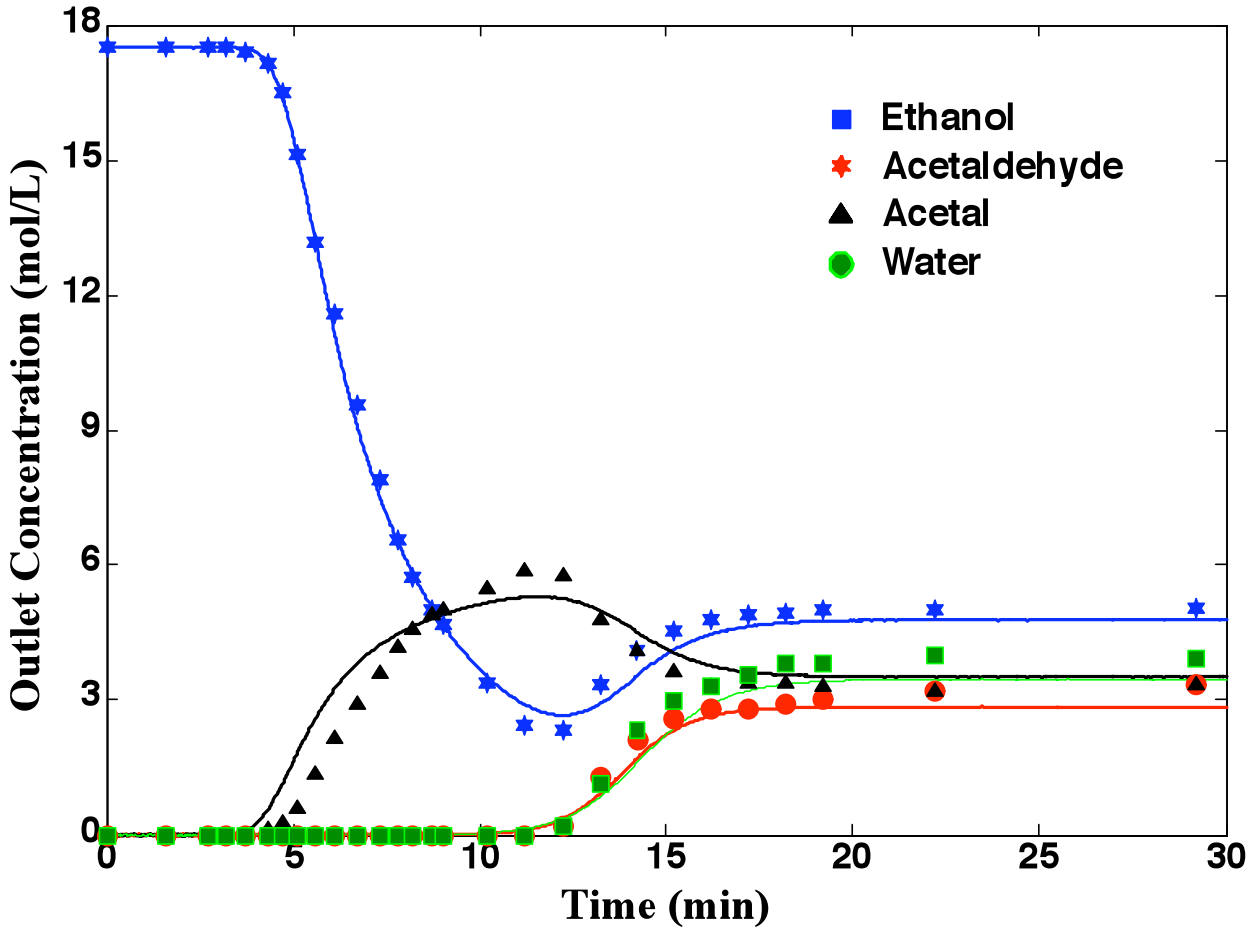

Figure 2.8 Production step in a FBCR modeled with the Maxwell-Stefan approach. Experimental data are from Silva and Rodrigues (2002).

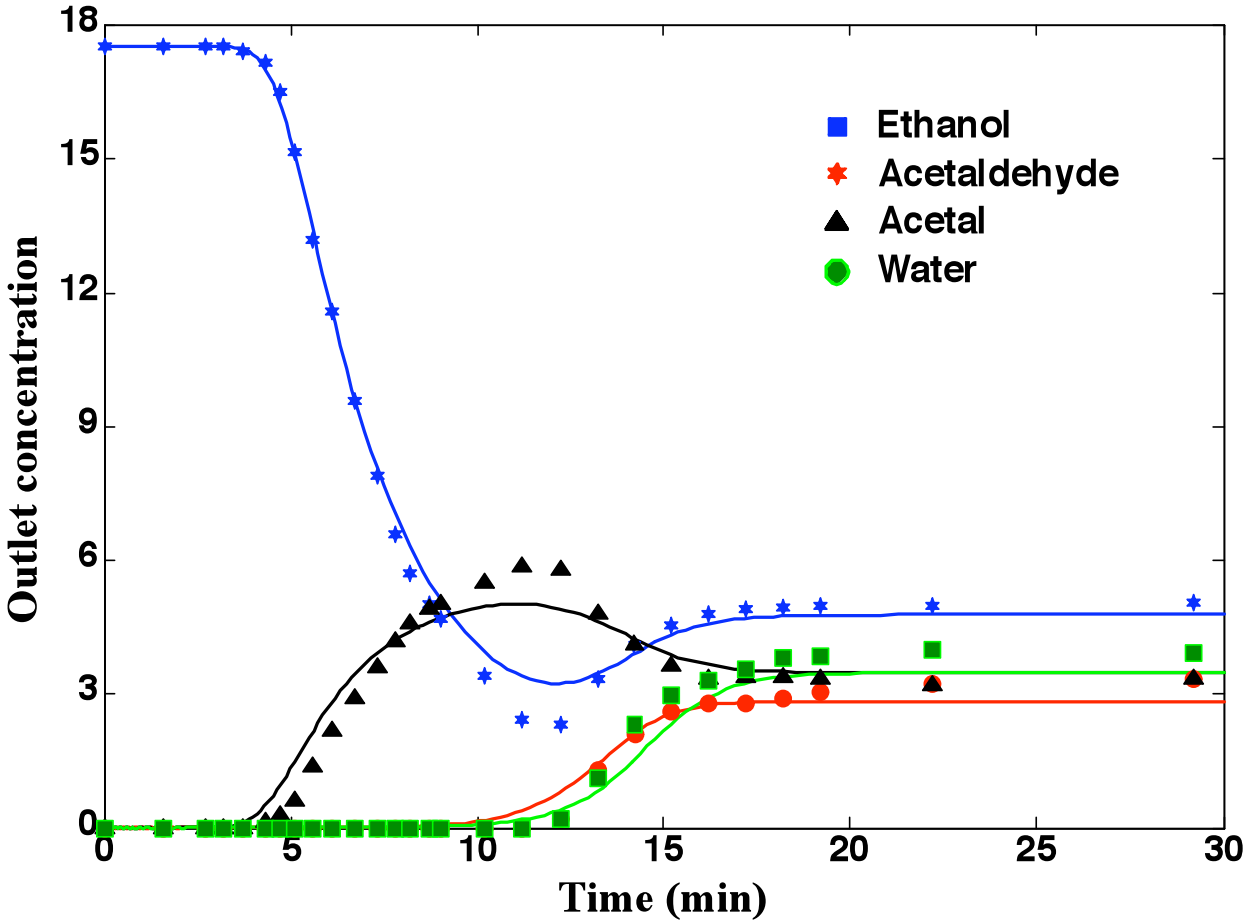

Figure 2.9 Production step in a FBCR modeled with the LDF approximation. Experimental data are from Silva and Rodrigues (2002).

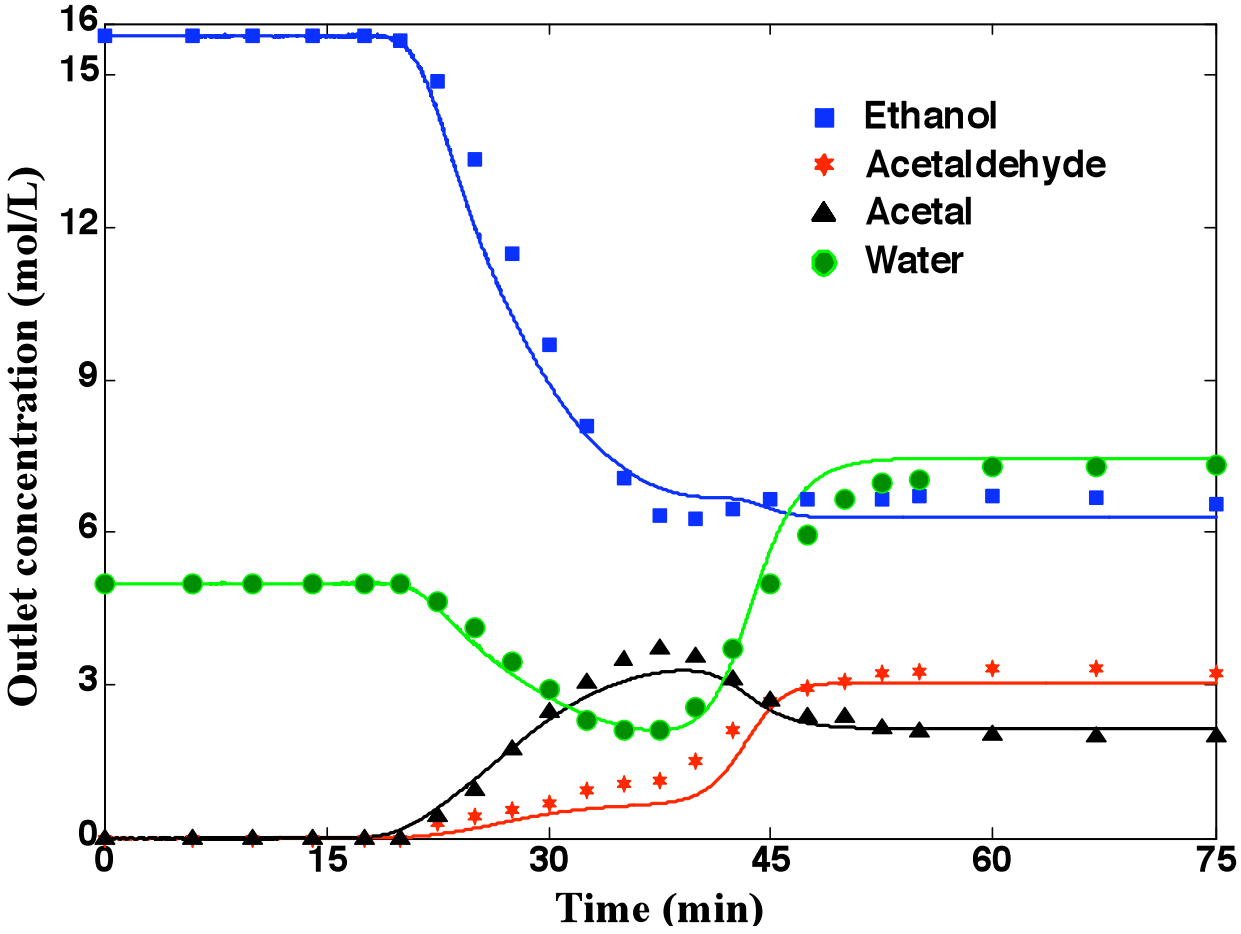

Figure 2.10 Production step in a FBCR modeled with the Maxwell-Stefan approach. Experimental data are from Silva and Rodrigues (2005).

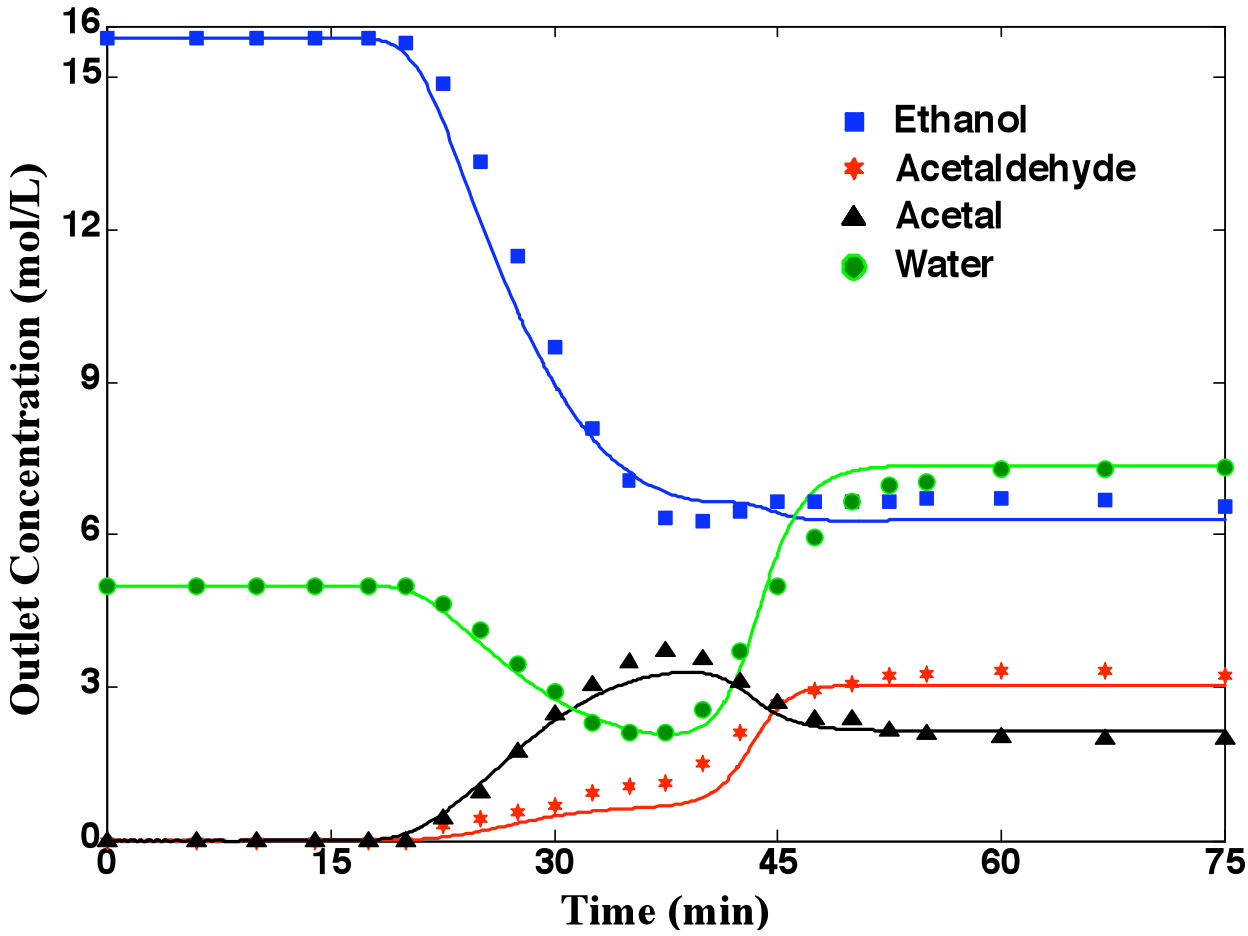

Figure 2.11 Production step in a FBCR modeled with the LDF approximation. Experimental data are from Silva and Rodrigues (2005).

Glycerol (A) + acetic acid (B) ⇔ monoacetine (C) + water (F)

Monoacetine (C) + acetic acid (B) ⇔ diacetine (D) + water (F)

Diacetine (D) + acetic acid (B) ⇔ triacetine (E) + water (F)

This process is strongly limited by equilibrium considerations, which starting with the stoichiometric composition at 80°C leads to a mass fraction of triacetine of about 5.5%. The triglyceride 1,2,3-triacetoxypropane is more generally known as triacetine.

Triacetine is an artificial chemical compound, commonly used as a food additive, which is required to be food grade. This imposes severe specifications that the current technology satisfies through a rather complex process involving several steps of reaction, separation, and purification. Therefore, producing food-grade triacetine directly in a single unit overcoming equilibrium limitations is particularly attractive. In addition, the use of a chromatographic reactor might allow the production of significantly pure quantities of monoacetine and diacetine to stimulate new applications.

The parameters of adsorption equilibria and reaction kinetics of the multicomponent mixture investigated by Gelosa et al. (2003) are introduced into our mathematical model to predict the behavior of the chromatographic reactor. The reliability of our model will be assessed by comparison with the experimental results of Gelosa et al. (2003), involving both the production and regeneration steps in a FBCR. Gelosa et al. (2003) also investigated experimentally the effect of intraparticle mass transport, and concluded that intraparticle mass transport resistances might significantly affect the kinetics of the process. Knowing that the effects of intraparticle mass-transfer resistance in this process are significant, this case will be a good standard to compare our model with the two models most often used in the reactive chromatography literature.

The reactions are reversible and the reaction rate equations are given by:

$$\mathcal{R}_1 = k_{c_1} C_{q_A} C_{q_B} \left[1 - \prod_{i=1}^{N} \left(C_{q_i} \right)^{\nu_{i1}} \Big/ K_{eq_1} \right] \tag{2-94}$$

$$\mathcal{R}_2 = k_{c_2} C_{q_C} C_{q_B} \left[1 - \prod_{i=1}^{N} \left(C_{q_i} \right)^{\nu_{i,2}} \Big/ K_{eq_2} \right] \tag{2-95}$$

$$\mathcal{R}_3 = k_{c_3} C_{q_D} C_{q_B} \left[1 - \prod_{i=1}^{N} \left(C_{q_i} \right)^{\nu_{i,3}} \Big/ K_{eq_3} \right] \tag{2-96}$$

and the parameters are listed in Table 2.6

Table 2.6 Reaction equilibrium constant and kinetic parameters at 353 K (Gelosa et al., 2003).

k_{c1} mol^{-1}s^{-1}	k_{c2} mol^{-1}s^{-1}	k_{c3} mol^{-1}s^{-1}	K_{eq1}	K_{eq2}	K_{eq3}
2740	995	462	23.3	2.89	0.12

The activity coefficients of compounds were computed by the UNIQAC method. The parameters needed for its use are presented in Tables 2.7 and 2.8 (Poling et al., 2001). The characteristics of the FBCR column used in the simulations are presented in Table 2.9.

The adsorption isotherm is of the Langmuir type for multicomponent adsorption that can be expressed by equation (2-34) and the parameters are presented in Table 2.10 (Gelosa et al., 2003; Poling et al., 2001).

Table 2.7 Relative molecular volume and surface area of pure species parameters.

	Glycerol	Acetic Acid	Monoacetine	Water	Diacetine	Triacetine
R	4.908	2.072	5.756	1	6.604	7.452
Q	4.7957	2.2024	6.0768	0.92	7.3579	8.639

Table 2.8 Interaction parameters.

$a_{m,n}$	Glycerol	Acetic Acid	Monoacetine	Water	Diacetine	Triacetine
Glycerol	0	114.429	6.336	340.893	4.19	9.597
Acetic Acid	-86.306	0	-173.26	156.48	-207.51	-254.92
Monoacetine	31.687	173.26	0	205.32	0	0
Water	91.09	269	123.321	0	134.972	161.327
Diacetine	91.09	269	0	341.393	0	0
Triacetine	164.82	489.721	0	559.906	0	0

Table 2.9 Characteristics of FBCR column (Gelosa et al., 2003).

Length (L)	44 cm
Internal diameter (D)	1.72 cm
Temperture (T)	353 K
Radius of the particle (r_p)	239 µm
External void fraction (ε_b)	0.42
Internal void fraction (ε_p)	0.36
Tortuosity (τ)	1.3
Peclet number (Pe)	361
Resin density (ρ)	1400 kg/m^3
Resin	Amberlyst 15

Table 2.10 Adsorption isotherms parameters at 353 K (Gelosa et al., 2003).

Components	Q (mol/cm^3)	b (mmol/g)	Density (kg/cm^3)	η (Cp)	Φ	$\bar{V}$ (cm^3/mol)
Glycerol (A)	714	5.32	1.261	31.9	1	98
Acetic Acid	564	4.22	1.049	0.561	1	62.38
Monoacetine(F)	512	3.95	1.21	11.42	1	140
Water (D)	965	22.1	0.92	0.355	2.3	55.95
Diacetate (D)	310	2.57	1.1875	4.036	1	182
Triacetate (E)	107	1.2	1.155	1.355	1	224

- **Modeling with LDF utilized by Gelosa et al. (2003)**

This model assumes that intraparticle mass transfer is described in terms of a simple linear driving force (LDF) approximation. This means that equation (2-29) is simplified to the following expression

$$\boxed{N_{p_i} = -\frac{3\varepsilon_p k_i}{r_p}\left(C_{b_i} - \overline{C_{p_i}}\right)} \qquad \text{for} \quad i = 1,2\cdots n \tag{2-97}$$

where $\overline{C_{p_i}}$ is the average concentration of the *i*th component inside the particle pores. The results of this model are presented in Figure 2-12. This figure clearly shows that the model proposed by Gelosa et al. (2003) does not agree with the experimental data. There is a time lag of approximately 75 minutes between the experimental results and the model predictions. This time lag probably occurs because to use equation (2.97) implies that:

1. The solutions are dilute.
2. The interactions between the mass transfer coefficients for the different species are negligible.
3. There is no concentration profile inside the particle pores.

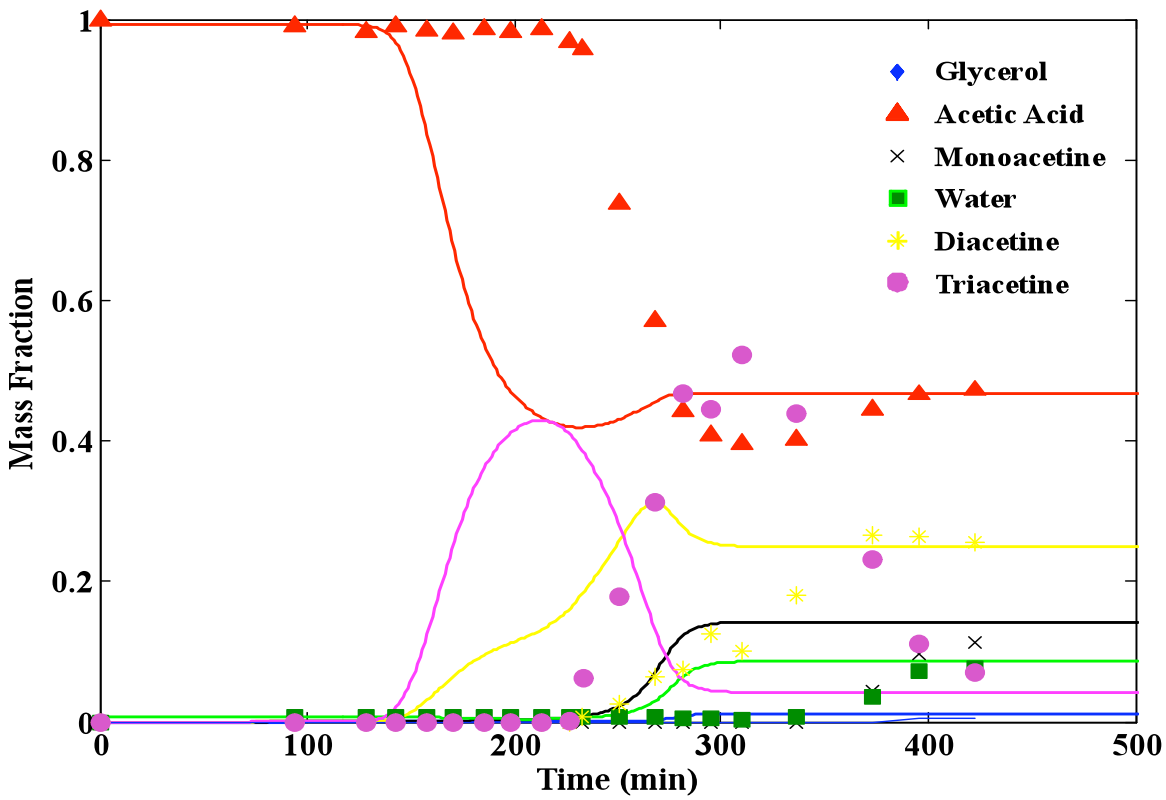

Figure 2.12 Production step in a FBCR modeled with the LDF approximation. Experimental data are from Gelosa et al. (2003).

These results demonstrate that this type of simplifications may be used only when the intraparticle mass-transfer resistance effects are not significant. It must be remembered that the models most often used for reactive chromatography are the same models used for chromatographic separations, but including the reaction. Normally, chromatographic separation is used to separate binary mixtures, under conditions such that equation (2.97) applies without restriction. On the other hand, reactive chromatography normally deals with multicomponent mixtures.

- **Modeling with Fick's Law (Fickian Diffusion)**

This model assumes that intraparticle mass transfer is described in terms of a Fickian diffusivity approximation. This means that equation (2-29) is simplified to the following expression

$$\boxed{N_{p_i} = -\varepsilon_p D_{p_i} \frac{\partial c_{p_i}}{\partial r}} \qquad \text{for} \quad i = 1,2 \cdots n \tag{2-98}$$

where D_{p_i} is the effective diffusivity coefficient of species *i*th in the mixture. The results of this model are presented in Figure 2-13. This figure shows that the model proposed using Fickian diffusivity represents the experimental data better than the model based on the LDF approach, but it still has a time lag of approximately 40 minutes.

- **Modeling with Maxwell-Stefan Approach**

This model assumes that intraparticle mass transfer is described in terms of the Maxwell-Stefan approach. It employs equation (2-29); and, as this equation shows explicitly, the matrix B_p and the diffusivities in a liquid mixture D_{ij} are functions of composition. In addition, it considers the non idealities utilizing the thermodynamic correction factor which is also function of concentration. As can be seen from Figure 2.14, our model predicts with excellent accuracy the experimental data composition profiles at the reactor outlet. The breakthrough times of the different transitions, as well as the shape of the concentration peaks and the steady state effluent concentrations are very well predicted.

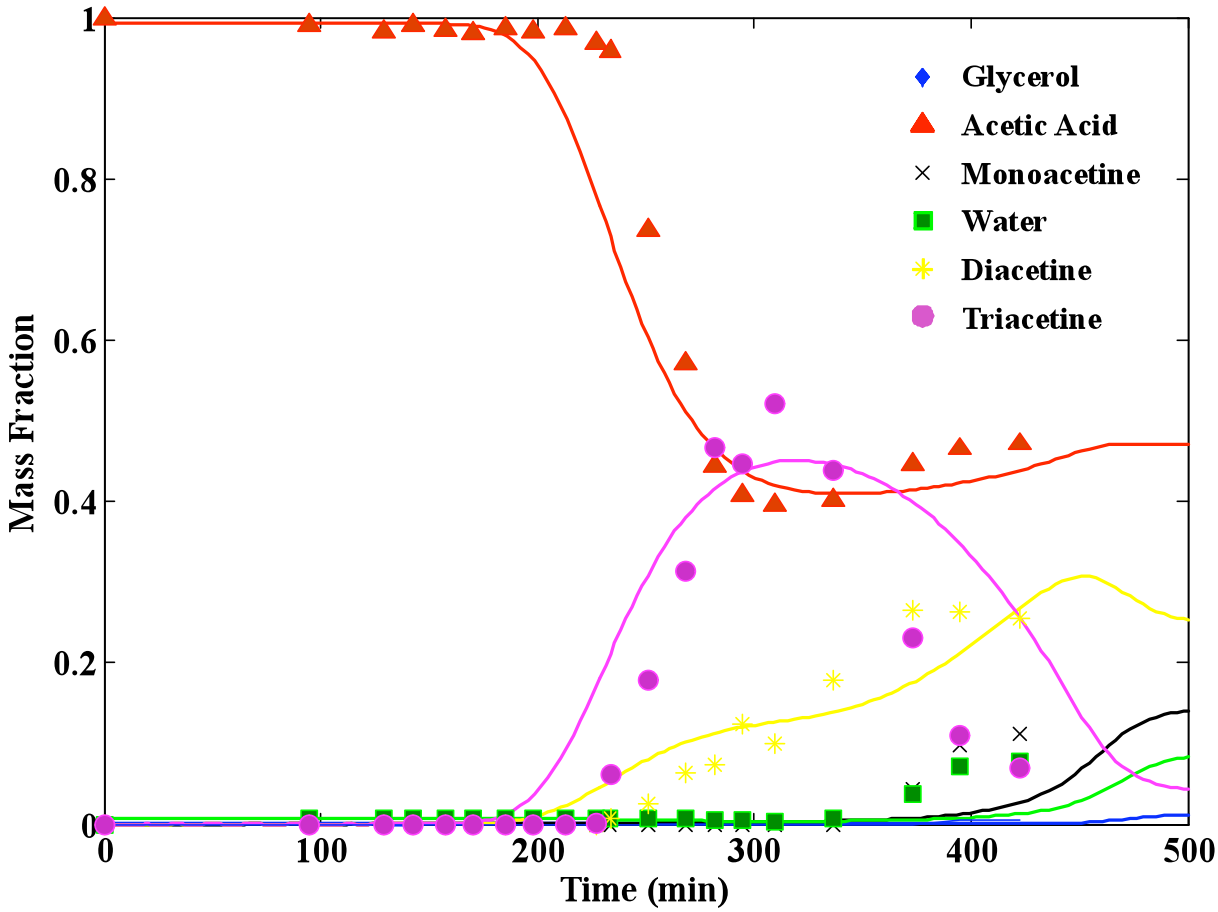

Figure 2.13 Production step in a FBCR modeled with a Fickian diffusion approximation. Experimental data are from Gelosa et al. (2003).

The regeneration step has also been simulated. Starting from the steady-state reached for the simulation presented in Figure 2.14, the reactor is fed with pure dry acetic acid at a constant flow rate of 1.5 cm^3/min. The results of the simulation of the regeneration step are displayed in Figure 2.15 and, again, the simulation results show excellent agreement with the experimental data from Gelosa et al. (2003).

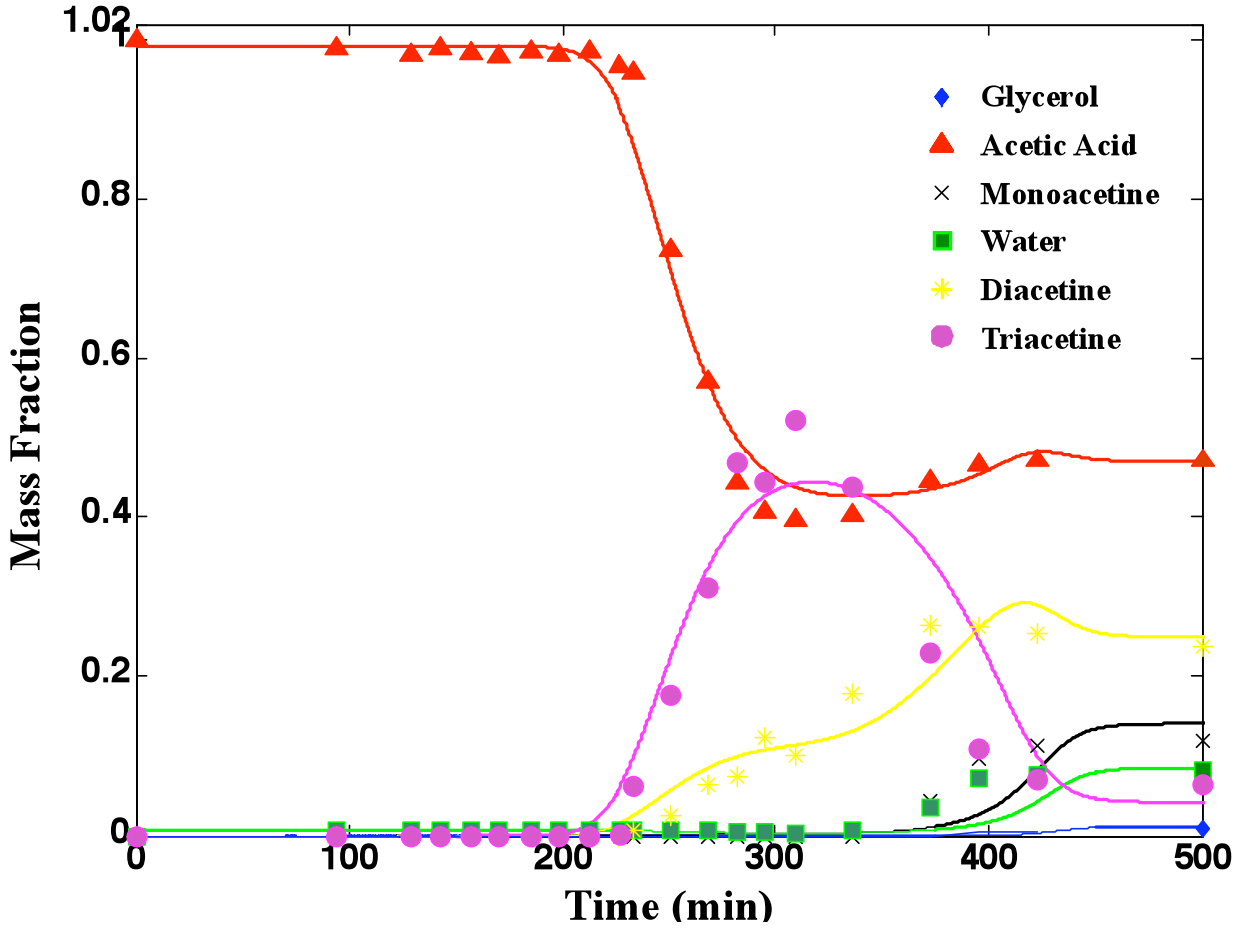

Figure 2.14 Production step in a FBCR modeled with the Maxwell-Stefan approach. The experimental data are from Gelosa et al. (2003).

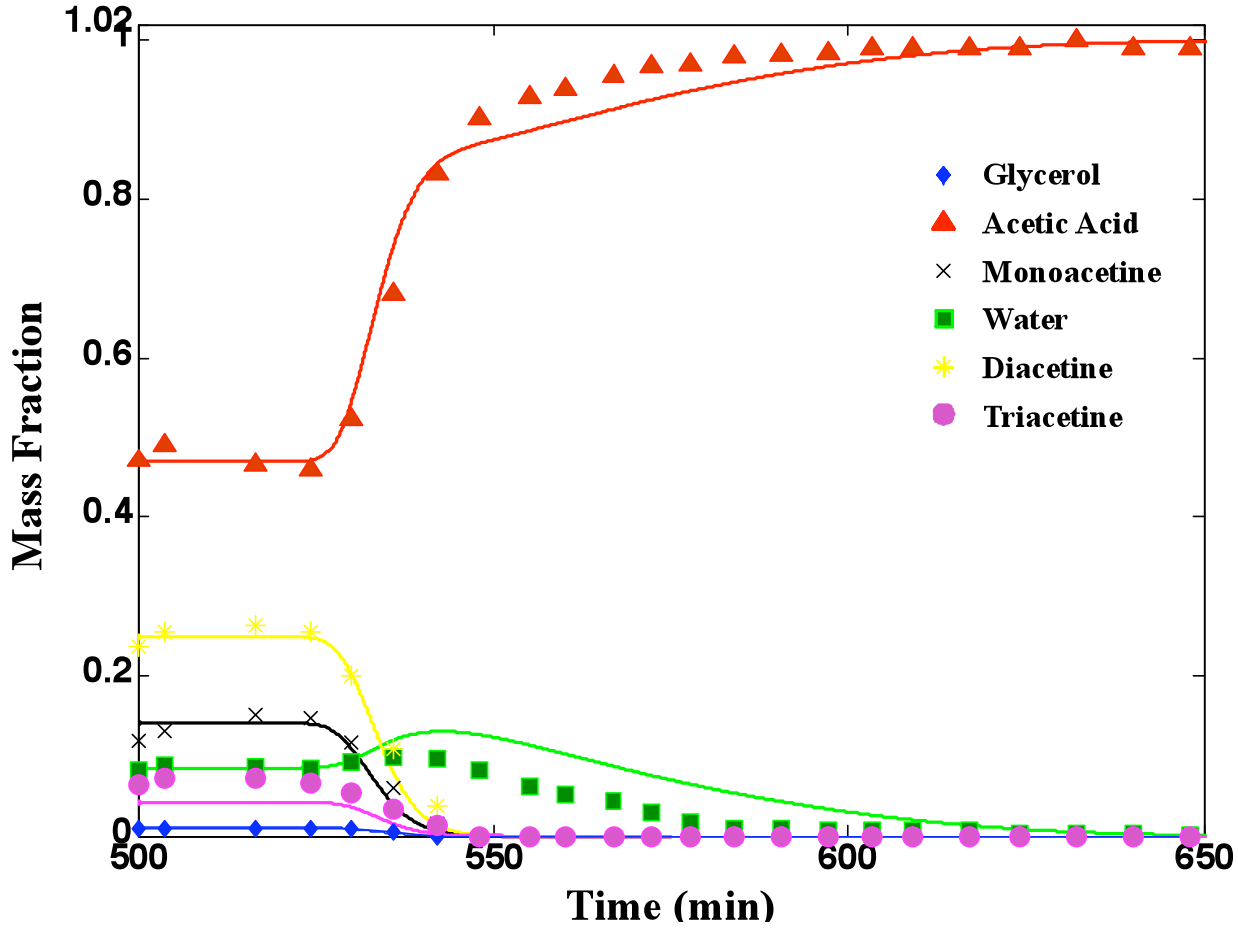

Figure 2.15 Regeneration step in a FBCR modeled with the Maxwell-Stefan approach. The experimental data are from Gelosa et al. (2003).

Finally, starting from the regenerated steady-state reached for the simulation presented in Figure 2.15, the reactor now is fed with pure acetic acid and glycerol in the same ratio used for the simulation results shown in Figure 2.14, with a constant flow rate of 0.3 cm^3/min. The results are displayed in Figure 2.16, showing again good agreement with the experimental results of Gelosa et al. (2003). Figure 2.16 also shows that if the column is regenerated with dry acetic acid, a better separation between triacetine and diacetine is achieved, demonstrating the detrimental effect of residual water in the process performance.

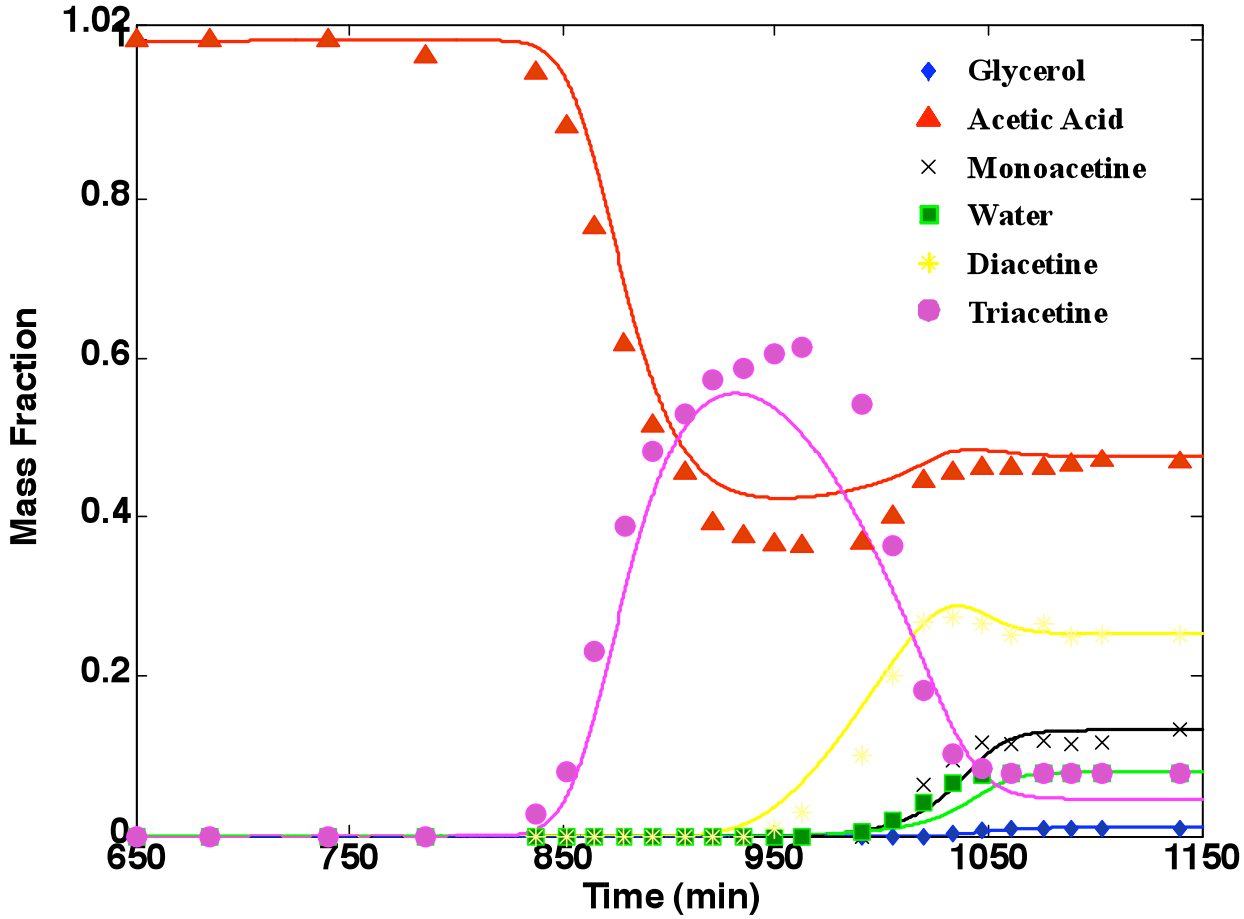

Figure 2.16 Production step in a previously regenerated FBCR modeled with the Maxwell-Stefan approach. The experimental data are from Gelosa et al. (2003).

2.3 Conclusions

Three different modeling and simulation approaches for chromatographic reaction processes have been presented and analyzed, starting with the rigorous model based on the Maxwell-Stefan approach for multicomponent mass transfer effects. Two simplified modeling approaches to describe the mass transfer effects have also been presented, the first based on the Fickian diffusivity concept, and the second based on the LDF approximation.

The suitable modeling and simulation approach has to be chosen depending on the specific application.

The capabilities of the proposed model have been illustrated using two different case studies taken from the literature on FBCR systems. The first system is for the production of diethylacetal (acetal) from the reversible reaction between ethanol and acetaldehyde catalyzed by the acid resin Amberlyst 15 and 18 with nonlinear multicomponent adsorption isotherms. The second system is the production of triacetine from the reversible reactions, starting from glycerol and acetic acid catalyzed by the acid resin Amberlyst 15 with nonlinear multicomponent adsorption isotherms. In both cases, our model proved to be robust and in all cases accurately predicted the experimental data.

In the acetal process, the intraparticle effects apparently had little effect on the process kinetics because the LDF model represented the experimental data almost as well as the rigorous Maxwell-Stefan model. In the triacetine process, however, the intraparticle effects are highly significant and neither one of the simplified models represented the experimental data nearly as well as the rigorous model proposed in this work.

The MATLAB®7 programming environment based on matrices proved to be very good for applications of this type. Using MATLAB®7 matrix notation and matrix processing routines it is possible to write a very compact code easy to understand, debug, and modify.

The Maxwell-Stefan approach can provide a useful tool for the exploration of the possible performance of more efficient continuous units, such as annular chromatography reactors or simulated moving bed reactors, and for their scale-up, which is needed to assess the economic performance that can be expected from these processes. In the proposed work, we will utilize this approach to simulate the TMBCR and SMBCR configurations.

C H A P T E R 3

3. Maxwell-Stefan in Continuous Reactive Chromatography: Simulated Moving Bed Chromatographic Reactor

3.1 Introduction

In Chapter 2, modeling with the Maxwell-Stefan approach quantitatively described the experimental data on the dynamic behavior of fixed bed chromatographic reactors (FBCR) obtained in three different experiments. However, the FBCR is not the most efficient technology and in the last 30 years the concept has been extended to continuous processes to improve productivity and decrease solvent consumption (Lode et al, 2003). The counter current moving bed technology is such a continuous process, also known as true moving bed (TMB). This technology presents some technical implementation difficulties concerning the solid flow. At this time, as far as we know, there is no publication on the actual implementation of this technology.

The TMB technology has been replaced by the simulated moving bed (SMB) approach. This technology simulates the true counter current system using a series of columns where the inlet and outlet ports are synchronously shifted in the direction of the fluid flow. The simulated moving bed chromatographic reactor (SMBCR) consists of set of interconnected columns packed with a solid, which acts as adsorbent and catalyst at the same time. Figure 3.1 shows schematically the operation of a SMBCR, explained in detail in Chapter 1.

The SMBCR approach examines each bed or subsection individually. In each switching time, the boundary conditions in all columns must be updated and the steady state is not

strictly reached. Instead, an axial motion of the band profiles occur in a steady periodic fashion repeated at every period as shown in Figure 3.1. The transient response of a SMBCR system, before steady state is achieved, may take as long as 20 cycles.

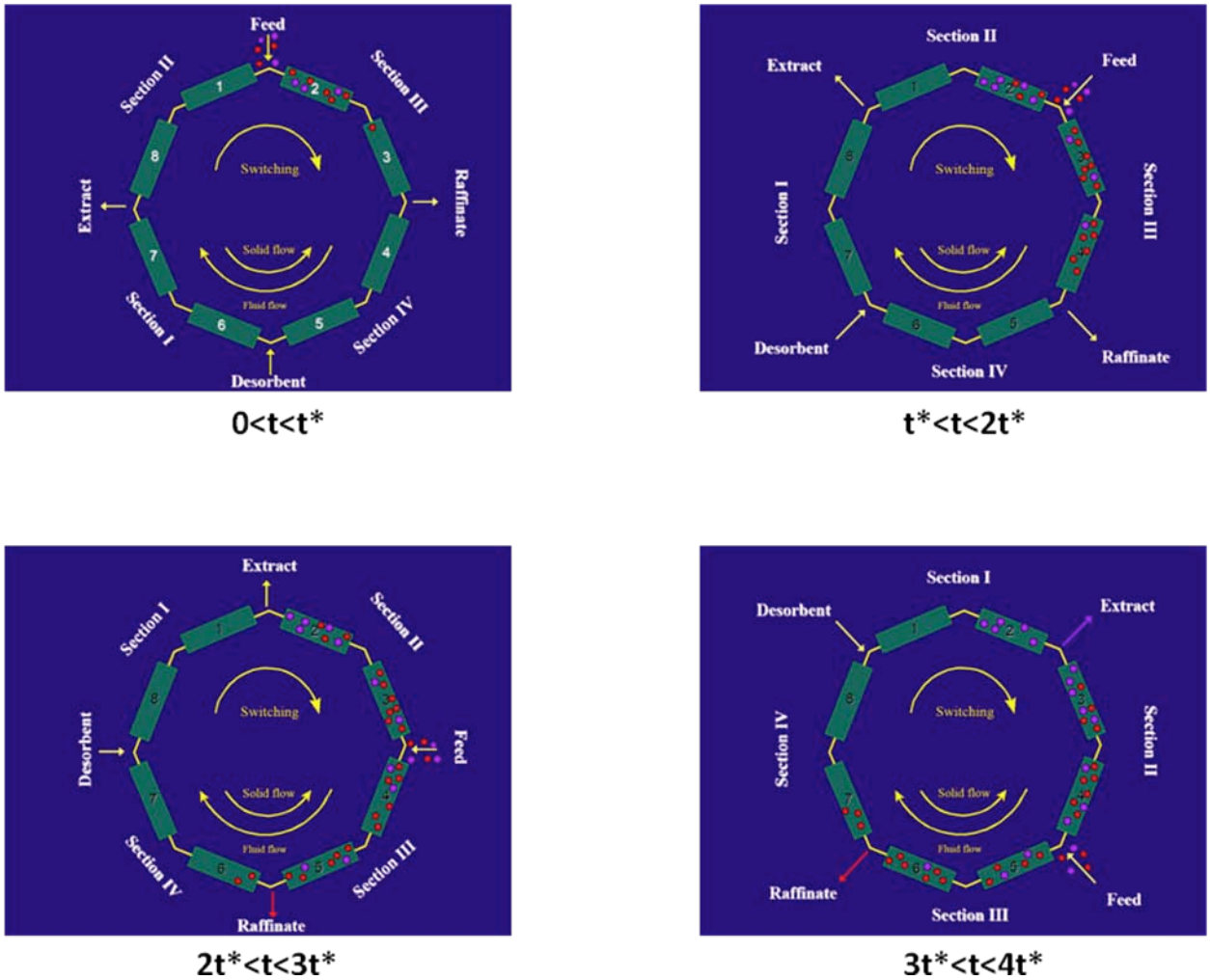

Figure 3.1 Schematic diagram of an eight-columns SMBCR; t is the time variable and t* is the switching time of the SMBCR ports.

3.2 Modeling Strategies for the SMBCR Process

Several authors have developed models to predict the performance of an SMBCR process with reasonable agreement with experimental results (Dünnebier et al., 2000, Lode et al., 2001).

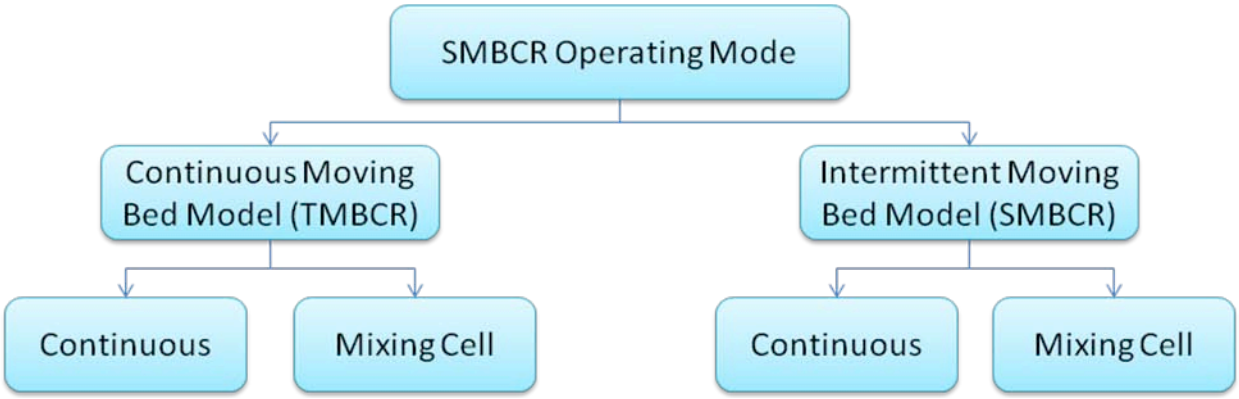

Figure 3.2 Classification of models for SMBCR analysis.

There are two main strategies of modeling an SMBCR process (Dünnebier et al., 2000, Lode et al., 2003, Silva and Rodrigues, 2005):

1. The first method, known as the moving-bed approach, treats the simulated counter current process as equivalent to a true countercurrent system
2. The second technique, known as the fixed bed approach, considers the simulated countercurrent process as a series of fixed beds and incorporates the actual flow switching of the process at fixed time intervals

The approach can also be classified as to whether the bed elements are represented by a continuous flow model (plug flow or axial dispersed plug flow) or as a cascade or mixing cells.

Each of these four models (Figure 3.2) may be treated either according to equilibrium theory or by including an appropriate rate expression to account for mass transfer resistance, generally in terms of a linear driving force model.

Another issue involved in the correct choice of a modeling approach is whether the TMBCR analysis represents accurately the performance of real SMBCR equipment. Liapis and Rippin (1979) reported a comparison between a TMB chromatograph and a corresponding SMB chromatograph and concluded that, by increasing the degree of subdivision of the SMB, its performance approaches that of the TMB. Pais et al. (1998) showed that the TMB chromatography approach may safely be used to predict the performance of SMB chromatography operation for a minimum subdivision of two columns per section. However, small deviations do appear between strategies especially when assessing the transient concentration profiles and if the number of columns is small (one per section). The eventual discrepancies observed between experimental results obtained at steady state and simulations from the TMBCR approach usually occur in sections II and III (Azevedo and Rodrigues, 2001). They have been attributed mainly to omission of the equipment dead zones in the model and to the over simplified description of film and intraparticle mass transfer brought by the linear driving force approximation.

3.2.1 Model Equations Using a SMBCR Strategy

In previous chapters, we described the modeling procedure needed to quantitatively describe the dynamic behavior of a single reactive chromatographic column. With a SMBCR being simply a specific assembly of a number of these units, no additional information regarding the phenomena involved is necessary when analyzing a SMBCR unit.

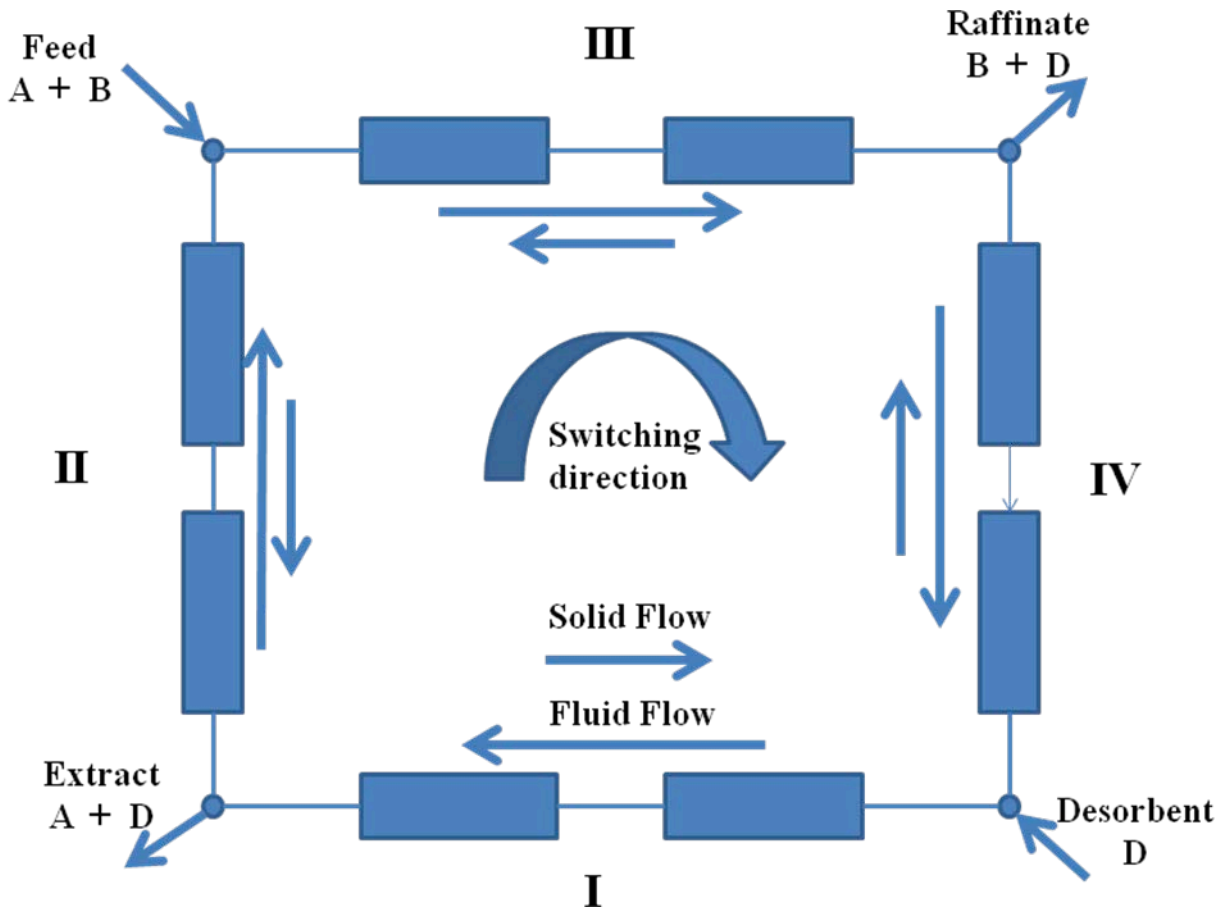

Figure 3.3 Schematic diagram of an eight-column SMBC.

Accordingly, the mathematical model describing the single chromatographic column can be extended in order to simulate the SMBCR unit by imposing the outlet concentration of one column as the inlet condition for the next column downstream, while properly accounting for additional feed or withdrawal streams. Column movement is then simulated by shifting all internal column profiles by one-column length against the direction of fluid flow at the end of a switch period (Storti et al., 1988). The process can be operated with varying numbers of columns. Figure 3.3 shows a SMBC with eight columns which can be divided into four sections of two columns each. Units with different number of columns per each section are also possible.

The following partial differential equations are proposed to represent the mass balance of species *i* in column *k* and section *j*:

Mass balance in the bulk phase:

$$\varepsilon_b \frac{\partial C_{b_{i,k}}}{\partial t} = \varepsilon_b D_{ax_j} \frac{\partial^2 C_{b_{i,k}}}{\partial z^2} - \varepsilon_b u_j \frac{\partial C_{b_{i,k}}}{\partial z} - (1-\varepsilon_b) N_{film_{i,k}}\Big|_{r=r_p} \qquad i = 1 \cdots n \tag{3-1}$$

Mass balance in the particle:

$$\varepsilon_p \frac{\partial C_{p_{i,k}}}{\partial t} + (1-\varepsilon_p) \frac{\partial C_{q_{i,k}}}{\partial t} = \frac{1}{r^2}\frac{\partial}{\partial r}\left\{r^2 \left[\varepsilon_p \left[\Gamma\left(x_{p_{i,k}}\right)\right]\left[B_p\left(x_{p_{i,k}}\right)\right]^{-1} \frac{\partial C_{p_{i,k}}}{\partial r}\right]\right\} + \sum_{j=1}^{N_R} \nu_{i,j} r_j^{het} \tag{3-2}$$

Initial conditions:

$$t = 0: \qquad C_{b_{i,k}} = C_{i,0} \quad \text{for} \quad i = 1 \cdots n \tag{3-3}$$

$$C_{p_{i,k}} = C_{i,0} \quad \text{for} \quad i = 1 \cdots n \tag{3-4}$$

The standard Danckwerts boundary conditions:

$$z = 0 \qquad u_j C_{b_{i,k}} - \varepsilon_b D_{ax_j} \frac{\partial C_{b_{i,k}}}{\partial z}\Big|_{z=0} = u_j C_{i,F} \tag{3-5}$$

$$z = L \qquad \frac{\partial C_{b_{i,k}}}{\partial z}\Big|_{z=L} = 0 \tag{3-6}$$

$$r = 0: \qquad \frac{\partial C_{p_{i,k}}}{\partial r}\Big|_{r=0} = 0 \tag{3-7}$$

$$r = r_p: \qquad N_{film_{i,k}} = N_{p_{i,k}} \tag{3-8}$$

Introducing the dimensionless variables:

$$\text{Space (axial):} \qquad \xi = {}^{z}/_{L} \tag{3-9}$$

Space (radial): $\Theta = {}^{r}/_{r_p}$ (3-10)

Time: $\theta = {}^{t}/_{t_c}$ (3-11)

Velocity ratio: $\varphi_j = {}^{u_j}/_{u_s}$ (3-12)

Peclet number: $Pe_j = {}^{u_j L}/_{\varepsilon_b D_{ax_j}}$ (3-13)

Damköehler number: $Da_j = {}^{\rho_b k_c L}/_{(1-\varepsilon_b)u_j}$ (3-14)

Mass transfer number: $K_{L_j} = {}^{3LK_t}/_{r_p u_j}$ (3-15)

Diffusivity number: $D_{L_j} = {}^{3\varepsilon_p L D_t}/_{(r_p)^2 u_j}$ (3-16)

where t_c is the switch time. Equations 3-1 and 3-2 can be written as follows:

$$\frac{\partial C_{b\,i,k}}{\partial \theta} = \varphi_j \left[\frac{1}{Pe_j}\frac{\partial^2 C_{b\,i,k}}{\partial \xi^2} - \frac{\partial C_{b\,i,k}}{\partial \xi} - K_{L_j}\frac{(1-\varepsilon_b)}{\varepsilon_b} N_{film,i}\Big|_{r=r_p}\right] \quad i = 1 \cdots n \tag{3-17}$$

$$\left(\varepsilon_p + (1-\varepsilon_p)J\left(C_{p_{i,k}}\right)\right)\frac{\partial C_{p_{i,k}}}{\partial \theta} = \varphi_j \left[D_{L_j}\frac{1}{\Theta^2}\frac{\partial}{\partial \Theta}\left\{\Theta^2\left[\varepsilon_p\left[\Gamma\left(x_{p_{i,k}}\right)\right]\left[D_t B_p\left(x_{p_{i,k}}\right)\right]^{-1}\frac{\partial C_{p_{i,k}}}{\partial \Theta}\right]\right\} + Da_j \sum_{d=1}^{N_R} \nu_{i,d} r_d^{het}\right]$$

(3-18)

with initial and boundary conditions:

$$\theta = 0: \qquad C_{b_{i,k}} = C_{p_{i,k}} = C_{i,0} \tag{3-19}$$

$$\xi = 0 \qquad C_{b_{i,k}} - \frac{1}{Pe_j}\frac{\partial C_{b_{i,k}}}{\partial \xi}\bigg|_{\xi=0} = C^F_{i,k} \tag{3-20}$$

$$\xi = 1 \qquad \frac{\partial C_{b_{i,k}}}{\partial \xi}\bigg|_{\xi=1} = 0 \tag{3-21}$$

$$\Theta = 0: \qquad \frac{\partial C_{p_{i,k}}}{\partial \Theta}\bigg|_{\Theta=0} = 0 \tag{3-22}$$

$$\Theta = 1 \qquad N_{film_{i,k}} = N_{p_{i,k}} \tag{3-23}$$

Mass balance at the nodes of the inlet and outlet lines of the SMBCR:

Desorbent node:

$$C_{b_{i,(j=4,z=L)}} = \frac{u_1}{u_4} C_{b_{i,(j=1,z=0)}} + \frac{u_D}{u_4} C_D \tag{3-24}$$

$$u_1 = u_4 + u_D \tag{3-25}$$

Extract node:

$$C_{b_{i,(j=1,z=L)}} = C_{b_{i,(j=2,z=0)}} = C_X \tag{3-26}$$

$$u_2 = u_1 - u_X \tag{3-27}$$

Feed node:

$$C_{b_{i,(j=2,z=L)}} = \frac{u_3}{u_2} C_{b_{i,(j=3,z=0)}} - \frac{u_F}{u_2} C_F \tag{3-28}$$

$$u_3 = u_2 + u_F \tag{3-29}$$

Raffinate node:

$$C_{b_{i,(j=3,z=L)}} = C_{b_{i,(j=4,z=0)}} = C_R \tag{3-30}$$

$$u_4 = u_3 - u_R \tag{3-31}$$

3.2 Numerical Solution

The numerical solution to the SMBCR model consist in applying at each column the numerical solution described in Chapter 2, Section 2.1.2, taking into account the mass balance at the nodes of the inlet and outlet of the SMBCR. Figure 3.4 shows the strategy of numerical method used to solve the PDE system in the model.

3.3 SMBCR Simulation with Maxwell-Stefan Approach

In this section, the use of Maxwell-Stefan approach model for SMBCR is illustrated by means two application examples. The first describes a process for production of dimethylacetal. This process has been the subject of several studies (Gandi et al, 2005, 2008 and Pereira et al, 2008), They employ a linear driving force model (LDF) in the description of mass transfer effects in the columns. The result of our simulation will be compared to some experimental data and with the model presented by Pereira et al. (2008).

In the second application example, a process for the synthesis of ethyl lactate was studied by Pereira et al. (2008 and 2009). They also studied this process employing a LDF model in the description of mass transfer effects in the columns.

3.3.1 Application 1: Dimethylacetal Synthesis

The synthesis of diethylacetal was modeled with the Maxwell-Stefan equations in a fixed bed chromatographic reactor described in Chapter 2, Section 2.2.1, using ethanol as alcohol. Now, the synthesis of dimethylacetal will be studied with Maxwell-Stefan equations in a FBCR, as well as in a SMBCR, using methanol as alcohol.

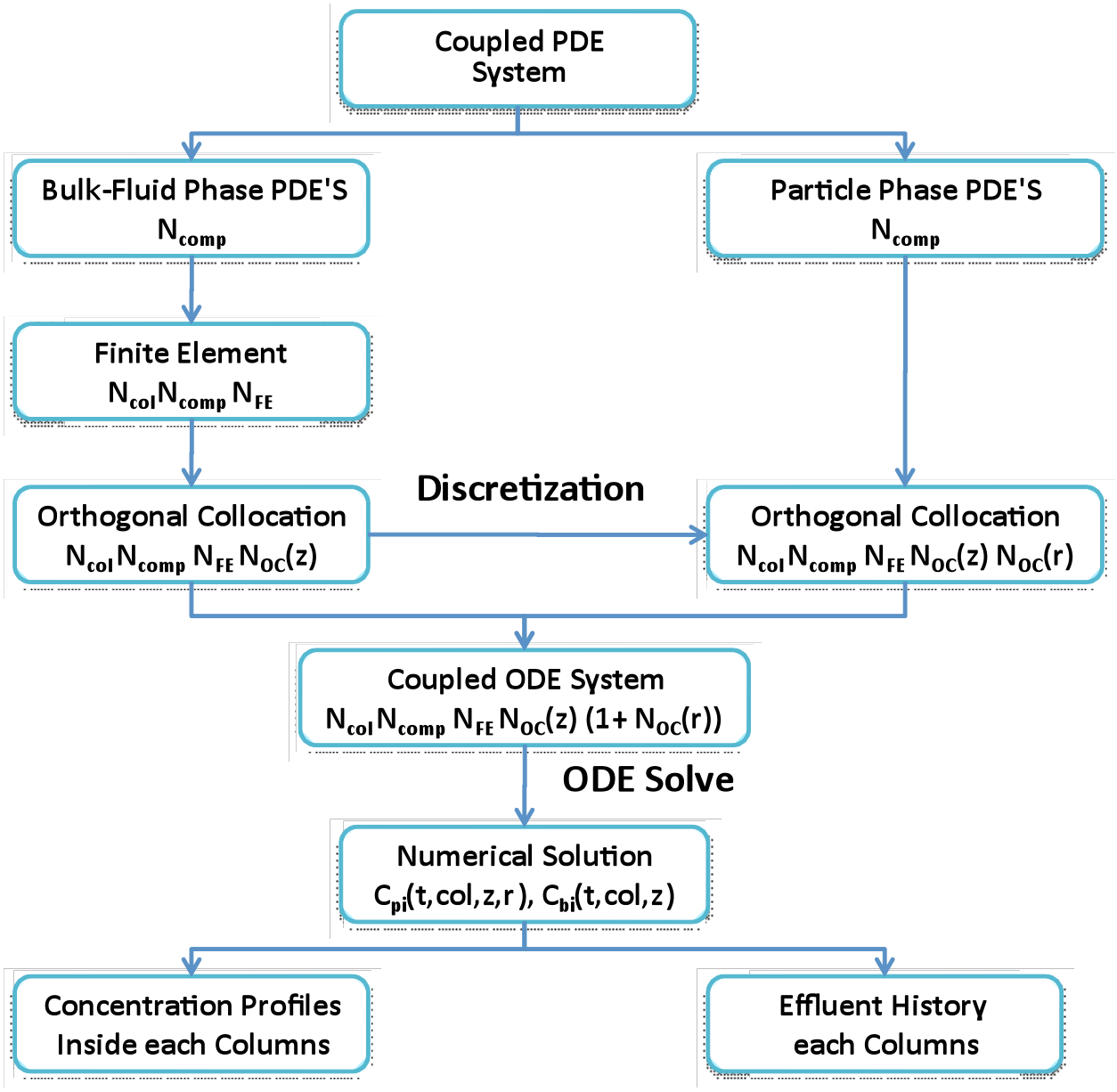

Figure 3.4 Solution strategy of the SMBCR.

3.3.1.1 Dimethylacetal Synthesis Using Methanol

The first example under consideration is a reactive system utilized by Gandi et al, (2005 and 2008). The reaction is:

$$2\ Methanol(A) + Acetaldehyde\ (B) \leftrightarrow Acetal(C) + Water\ (D) \tag{3-32}$$

The synthesis of diethyacetal was validated with Maxwell-Stefan equations in a fixed bed chromatographic reactor described in Chapter 2, section 2.21 using ethanol as alcohol. Now, the synthesis of dimethyacetal will be validated with Maxwell-Stefan equations in a FBCR as well as in a SMBCR using methanol.

The reaction is reversible and the reaction rate equation proposed by the authors is given by:

$$\mathcal{R} = k_c \frac{a_A a_B - \frac{a_C a_D}{K_{eq} a_A}}{(1 + K_D a_D)^2}$$

with parameters given by:

$$\ln K_{eq} = \frac{2142.5}{T} - 4.2475 \tag{3-33}$$

$$k_c = 6.91 \times 10^{13} exp\left[\frac{-8702.6}{T}\right] (mol\ g^{-1} min^{-1}) \tag{3-34}$$

$$K_D = 2.32 \times 10^{32} exp\left[\frac{-22713}{T}\right] \tag{3-35}$$

And the relation between the effectiveness factor (η) and Thiele modulus (φ) at 20˚C for the linear region (φ ≧10) is given by:

$$\ln \eta = -1.048\varphi_T + 1.706 \tag{3-36}$$

In the FBCR, the authors assumed that the effectiveness factor is constant and equal to 0.4. The activity coefficients of the various compounds were computed by the UNIFAC method. The parameters needed for its use (relative molecular volume and surface area of

pure species and the interaction parameters) are presented in Tables 3.1 and 3.2 (Poling et al, 2001).

Table 3.1 Relative molecular volume and surface area of pure species parameters.

Molecule (i)	Group Identification					
	Name	No. Main	No. Section	ν_K^i	R_K	Q_K
1: methanol	CH_3OH	6	16	1	1.4311	1.432
2: acetaldehyde	CH_3	1	1	1	0.9011	0.848
	CHO	10	21	1	0.9980	0.948
3: acetal (DME)	CH_3	1	1	1	0.9011	0.848
	CH	1	3	1	0.4469	0.228
	CH_3O	13	25	2	1.1450	1.088
4: water	H_2O	7	17	1	0.9200	1.400

Table 3.2 Interaction parameters.

$a_{m,n}$	1	6	7	10	13
1	0	697.2	1318	677	251.5
6	16.51	0	-181	306.4	-128.6
7	300	289.6	0	-257.3	540.5
10	505.7	-340.2	232.7	0	304.1
13	83.36	238.4	-314.7	-7.838	0

The characteristics of the FBCR column used in the simulations are presented in Table 3.3 (Gandi et al., 2008).

The adsorption isotherm is the equilibrium relationship between the concentration in the fluid and the concentration in the adsorbent particles at a given temperature and pressure.

The concentration of the adsorbate on the solid is given as the number of moles or the mass adsorbed per unit mass or unit volume of adsorbent (solid phase). For this case, it was shown that the isotherm follows the Langmuir model for multicomponent adsorption, equation (2-34), and the parameters are presented in Table 3.4 (Silva and Rodrigues 2002; Poling et al, 2001).

Table 3.3 Characteristics of FBCR Column.

Length (L)	86 cm
Internal diameter (D)	2.6 cm
Temperture (T)	293.15 K
Radius of the particle (r_p)	150-600 µm
External void fraction (ε_b)	0.40
Internal void fraction (ε_p)	0.36
Tortuosity (τ)	1.3
Peclet number (Pe)	300
Bulk density (ρ_b)	792 kg/m^3
Resin	Amberlyst 15

Table 3.4 Adsorption equilibrium isotherms and component parameters at 288 K.

Components	Q (mol/L$_r$)	b (L/mol)	density (kg/m^3)	η (Cp)	Φ	$\bar{V}$ (cm^3/mol)	T_b K	T_c K	P_c bar
Methanol (A)	14.52	600	791	1.342	1.5	40.52	337.7	512.6	61.48
Acetaldehyde	18.65	380	785	0.296	1	56.21	293.3	454.7	55.5
DME (C)	7.67	320	852	0.354	1	105.8	358.2	527	30.1
Water (D)	28.49	1150	1003	1.139	2.6	17.96	373.1	647.1	220.6

3.3.1.2 Model Validation for SMBCR

The dynamic behaviors of a FBCR for synthesis of diethyalacetal and triacetine were predicted by our proposed model, based on the Maxwell-Stefan approach. Our model was able to predict the response of chromatographic reactor with different column lengths and

different initial feed compositions. Based on the excellent results obtained modeling the FBCR, it was decided to go to the next step, which is to apply the Maxwell-Stefan approach to the SMBCR. The first case study is a reactive chromatographic system based on the synthesis of dimethylacetal presented by Gandi et al, (2008).

The dimethylacetal synthesis will be simulated at 20°C in a SMBCR unit with a three-columns-per-section configuration. The feed composition will be a mixture of methanol ($C_{A,F}$ = 8.03 mol/L) and acetaldehyde ($C_{B,F}$ = 12.05 mol/L), and the desorbent to be used is pure methanol. Table 3.5 shows the operating conditions and characteristics of the columns used for the SMBCR.

- **Modeling of SMBCR with the LDF model (Gandi et al, 2008).**

This model assumes that intraparticle mass transfer is described in terms of a simple linear driving force (LDF) approximation. This means that equation (2-29) is simplified by the following expression

$$N_{P_i} = \frac{3\varepsilon_P k_i}{r_P}\left(C_{b_i} - \overline{C_{P_i}}\right) \text{ for } i = 1,2\cdots n \qquad (3\text{-}37)$$

where $\overline{C_{p_i}}$ is the average concentration of the *i*th component into of particle pores. The results of bulk concentration profile during the fifth and eighth cycle with this model, the LDF approach, are presented in Figure 3.5. This figure shows that the model proposed predicted the bulk concentration profile with reasonable accuracy, except in the second section where significant differences with the experimental data are observed. This difference probably occurs because to use equation (3-37) it is assumed that there is no concentration gradient inside the particle pores. However, Gandi et al, (2005) concluded that, in this case, pore

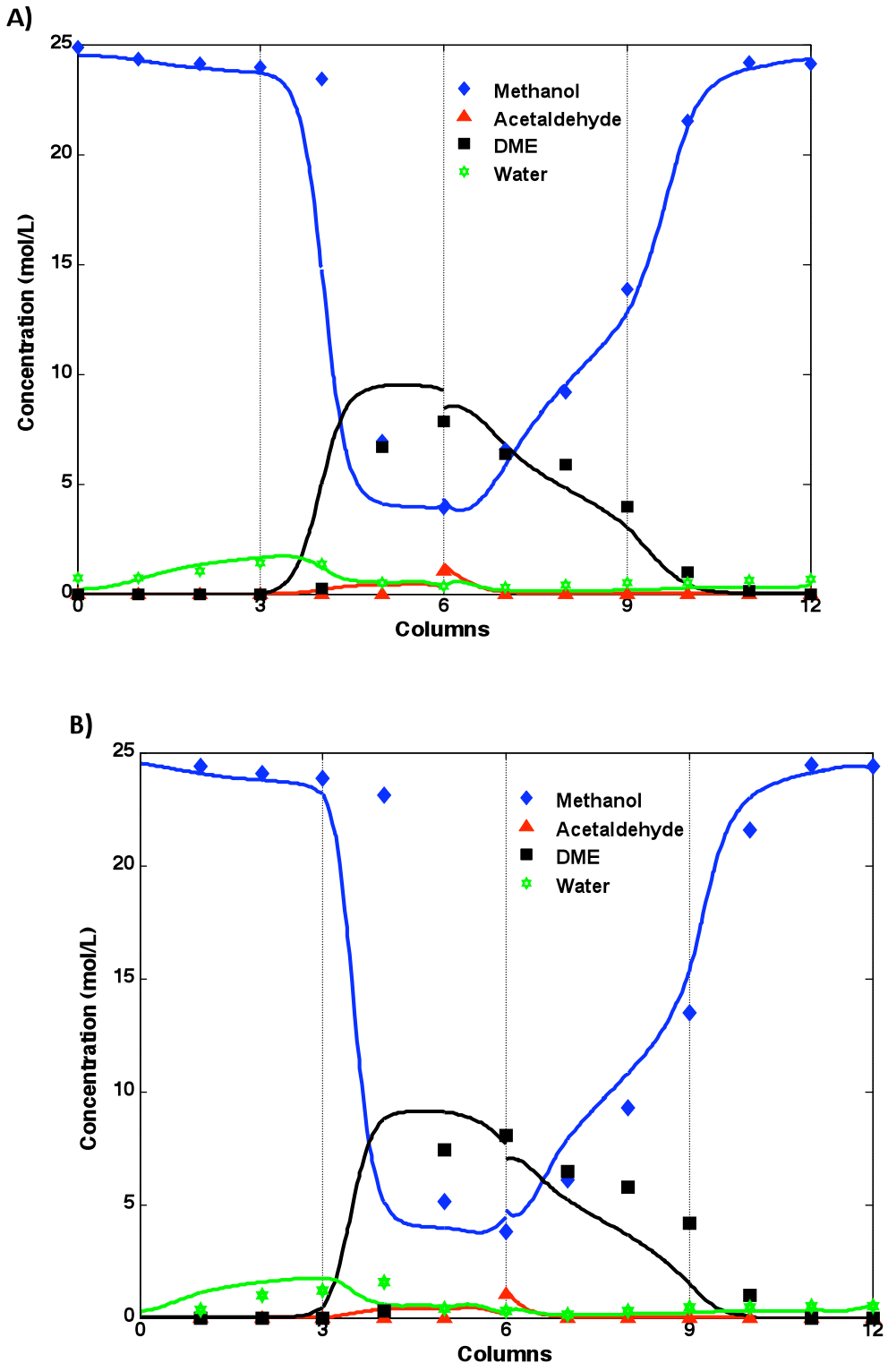

Figure 3.5 Bulk concentration profile during (A) the fifth and (B) the eighth cycles in a SMBCR modeled with the LDF approach. Experimental data are from Gandi et al, (2008).

diffusion is the controlling mass transfer effect. They proposed to use an effectiveness factor for correcting this deficiency of the LDF model, but evidently without good results.

Table 3.5 Operating conditions and characteristics of the SMBCR (Gandi et al., 2008).

Parameter	**Value**
Feed Flow Rate	3 mL/min
Raffinate Flow Rate	8 mL/min
Desorbent Flow Rate	25 mL/min
Recycle Flow Rate	25 mL/min
Switching Time (t_C)	3 min
Configuration	3-3-3-3
Feed Concentration C_{AF} C_{BF}	 8.03 mol/L 12.05 mol/L
Length of the packed bed (L)	0.23 m
Internal diameter of the columns (D)	0.026 m
Radius of the particles (r_P)	400µm
External void fraction (ε_b)	0.4
Internal void fraction (ε_P)	0.4
Peclet number ($u_j L/D_{ax,j}$)	300
Bulk density (ρ_b)	390kg/m^3
Solid Velocity (u_s)	L/t_C = 0.07667 m/min
Temperature	20˚C

- **Modeling of SMBCR with the Maxwell-Stefan Approach.**

Gandi et al. (2008) suggested that the deviations that they observed can be due to the use of a simple model (LDF) which assumes a constant global mass transfer coefficient and at the

same time an effectiveness factor based on the particle steady state profile, which does not take into account the reaction contribution (Silva and Rodrigues, 2005). The model that we propose, on the other hand, assumes that interparticle and intraparticle mass-transfer effects are described in terms of the rigorous Maxwell-Stefan approach. This model utilizes equation (2-29) which shows that the matrix B_p and the diffusivities in a liquid mixture D_{ij} are functions of composition. In addition, it takes into account the solutions' non idealities introducing the thermodynamic factors that are also functions of concentration.

As can be seen from Figure 3.6, the Maxwell-Stefan model predicts with excellent results the experimental data composition profiles at the SMBCR. The breakthroughs of the different transitions, as well as the shape of the concentration peaks are very well predicted. It is possible to conclude, then, that to model the synthesis of methylacetal in a SMBCR it is necessary to use a strategy that describes rigorously the mass transfer effects in the system.

3.3.2 Application 2: Ethyl Lactate Synthesis

Ethyl lactate is an important organic ester, which is biodegradable and can be used as food additive, in perfumery, to flavor chemicals, and as a solvent replacing a range of environment-damaging halogenated and toxic petroleum-derived solvents (Tanaka et al., 2002). However, for all these uses, it must be produced in a highly pure state. Ethyl lactate is produced by renewable resources, in acidic medium, according to the reaction:

$$ethanol(A) + lactic\ acid(B) \overset{H^+}{\leftrightarrow} ethyl\ lactate(C) + water(D)$$

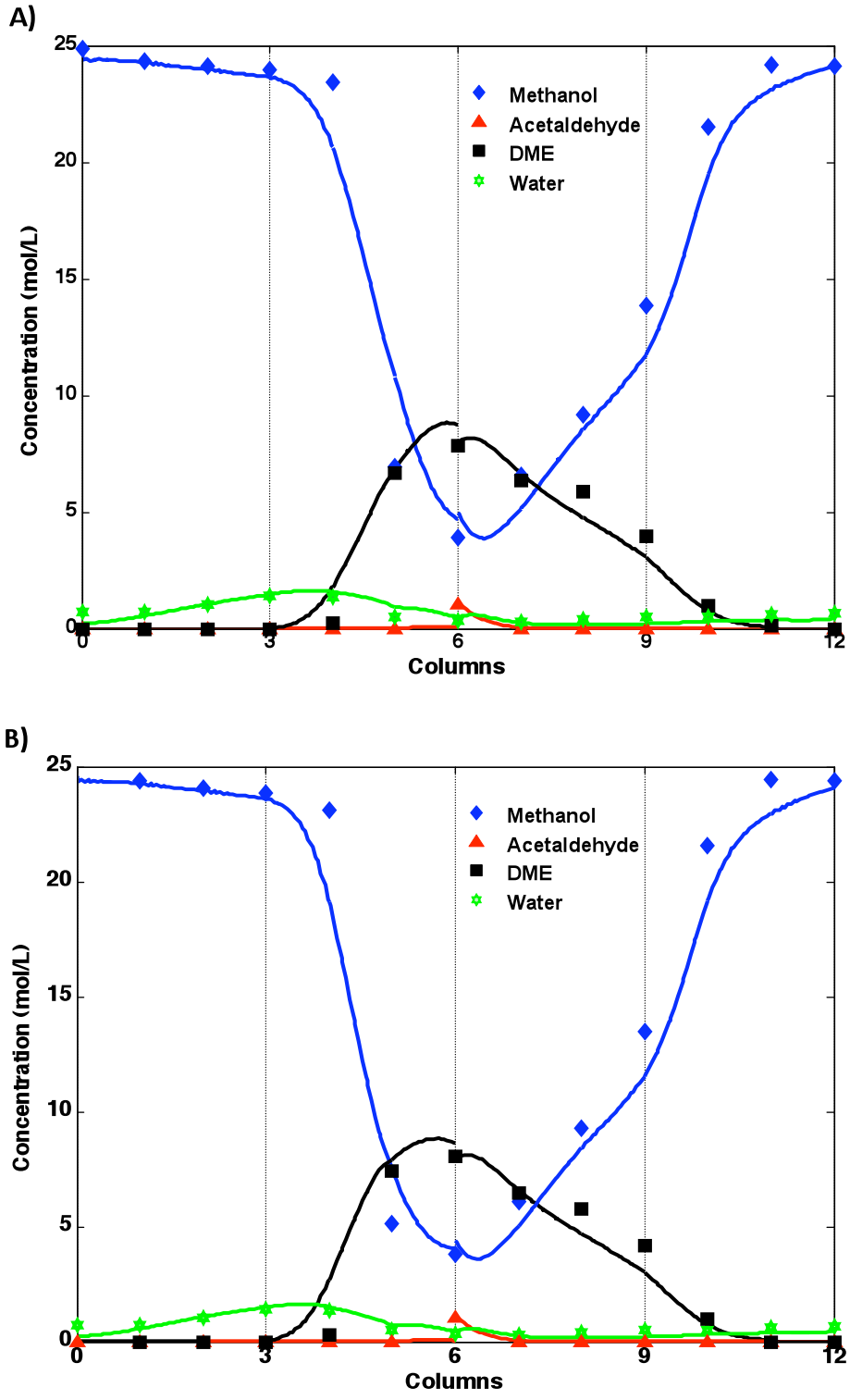

Figure 3.6 Bulk concentration profile during (A) the fifth and (B) the eighth cycles in a SMBCR modeled with the Maxwell-Stefan approach. Data are from Gandi et al, (2008).

The production of ethyl lactate in membrane reactors have been studied by Jafar et al. (2002) and Benedict et al. (2003, 2006). In this process, the membrane selectively removes the water in order to displace the reaction equilibrium. This technology uses a reactor coupled with a pervaporation membrane unit for water removal followed by separation of the reaction mixture in two consecutive distillation columns. The SMBCR is an attractive alternative technology for the production of the ethyl lactate because it combines the reaction and separation steps in a single unit.

3.3.2.1 Model Validation for SMBCR

The case study is a reactive chromatographic system based on the synthesis of ethyl lactate developed by Pereira et al. (2008). The ethyl lactate synthesis will be simulated at 50°C in a SMBCR unit with a three-columns-per-section configuration. The feed composition will be a mixture of ethanol ($C_{A,F}$ = 10.75 mol/L) and water ($C_{D,F}$ = 9.48 mol/L), and the desorbent to be used is pure ethanol. Table 3.6 shows the operating conditions and characteristics of the SMBCR columns. The reaction is reversible and the reaction rate equation proposed by the authors is given by:

$$\mathcal{R} = k_c \frac{a_A a_B - \frac{a_C a_D}{K_{eq} a_A}}{(1 + K_A a_A + K_D a_D)^2}$$

with parameters given by:

$$\ln K_{eq} = -\frac{515.13}{T} + 2.9625 \tag{3-38}$$

$$k_c = 2.7 \times 10^7 exp\left[\frac{-6011.55}{T}\right] (mol\ g^{-1} min^{-1}) \tag{3-39}$$

Table 3.6 Operating conditions and characteristics of the SMBCR (Pereira et al., 2008).

Parameter	**Value**
Feed Flow Rate	1.8 mL/min
Raffinate Flow Rate	8.8 mL/min
Desorbent Flow Rate	27.4 mL/min
Recycle Flow Rate	24.7 mL/min
Switching Time (t_C)	2.9 min
Configuration	3-3-3-3
Feed Concentration C_{AF} C_{DF}	 10.75 mol/L 9.48 mol/L
Length of the packed bed (L)	0.23 m
Internal diameter of the columns (D)	0.026 m
Radius of the particles (r_P)	342.5μm
External void fraction (ε_b)	0.4
Internal void fraction (ε_P)	0.36
Peclet number ($u_j L/D_{ax,j}$)	300
Bulk density (ρ_b)	390kg/m^3
Solid Velocity (US)	L/t_C = 0.07931 m/min
Temperature	50˚C

$$K_A = 1.22exp\left[\frac{359.63}{T}\right] \tag{3-40}$$

$$K_D = 15.19exp\left[\frac{12.01}{T}\right] \tag{3-41}$$

The activity coefficients were computed by the UNIQUAC method. The parameters needed for its use (relative molecular volume and surface area of pure species and the interaction parameters) are presented in Table 3.7 (Poling et al., 2001; Pereira et al., 2008).

Table 3.7 Relative molecular volume and surface area of pure species parameters.

	ethanol	lactic acid	ethyl lactate	water	R	Q
ethanol	0	-35.008	-152.319	-17 + 0.2797T(K)	2.5755	2.588
lactic acid	33.741	0	219.89	213.19	3.1793	2.884
ethyl lactate	264.99	-20.986	0	207.789	4.4555	3.928
water	-17 + 0.2797T(K)	-99.183	-13.093	0	0.92	1.4

The adsorption equilibrium relationship for this case was shown to follow the Langmuir isotherm model for multicomponent adsorption, equation (2-34), and the parameters are presented in Table 3.8 (Pereira et al., 2008).

Table 3.8 Adsorption equilibrium isotherms and component parameters at 323.15 K.

Components	Q (mol/L_r)	b (L/mol)	density (kg/m^3)	η (Cp)	Φ	$\bar{V}$ (cm^3/mol)	T_b K	T_c K	P_c bar
ethanol (A)	6.299	3.068	756.9	0.745	1.5	60.87	351.8	513.9	61.48
lactic acid	4.943	4.085	1160.1	14.01	1	77.56	363.2	557	48
ethyl lactate	3.237	1.815	995.9	1.426	1	118.44	418.1	586.1	28.45
water (D)	20.584	7.055	966.87	0.547	2.6	18.63	373.1	647.1	220.6

- **Modeling of the SMBCR with Maxwell-Stefan Approach.**

The Maxwell-Stefan approach model is validated when the experimental results obtained by Pereira et al. (2009) are compared with the simulation results, as shown in Figure 3.7. It is observed that the model predicts very well the experimental results. The breakthroughs of the different transitions, as well as the shape of the profile concentration peaks at the steady state in the middle of switching time are well predicted. Similar results, with reasonable accuracy, were obtained by Pereira et al. (2009) using a model with the LDF approximation. The LDF

results are good except in the third section where significant differences with the experimental data are observed, as shown in Figure 3.8.

3.4 Conclusions

A new SMBCR model with a detailed particle approach was presented introducing the formulation of the mass balance based on the Maxwell-Stefan equations. Model equations include film mass transfer and intra-particle diffusion resistance using the Maxwell-Stefan equation. The capabilities of the proposed model have been illustrated using two different case studies taken from the literature on SMBCR systems. The first system is for the production of methylacetal from the reversible reaction between methanol and acetaldehyde catalyzed by the acid resin Amberlyst 15 with nonlinear multicomponent adsorption isotherms. The second system is the synthesis of ethyl lactate from the reversible reactions, starting from ethanol and lactic acid catalyzed by the acid resin Amberlyst 15 with nonlinear multicomponent adsorption isotherms. The reaction occurs, for both syntheses, inside the particle. In both cases, our model proved to be robust and in all cases accurately predicted the experimental data. This new model based on the Maxwell-Stefan approach was compared with previous approximations for reactive chromatographic systems based on the LDF model. The numerical solution of all equations was obtained using MATLAB®7.

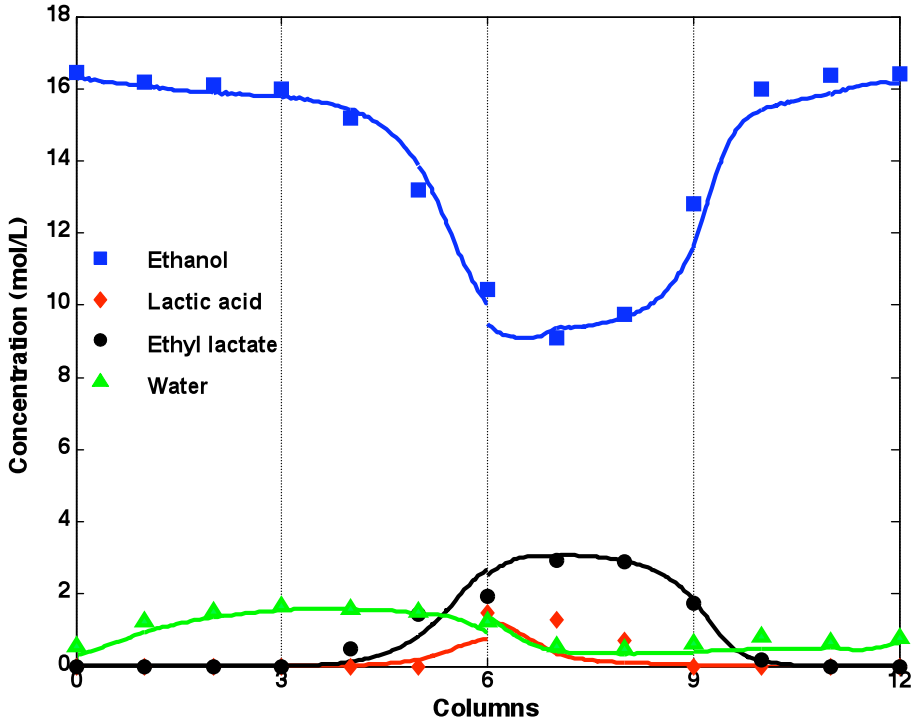

Figure 3.7 Bulk concentration profile in a TMBCR at cycle steady state modeled with the

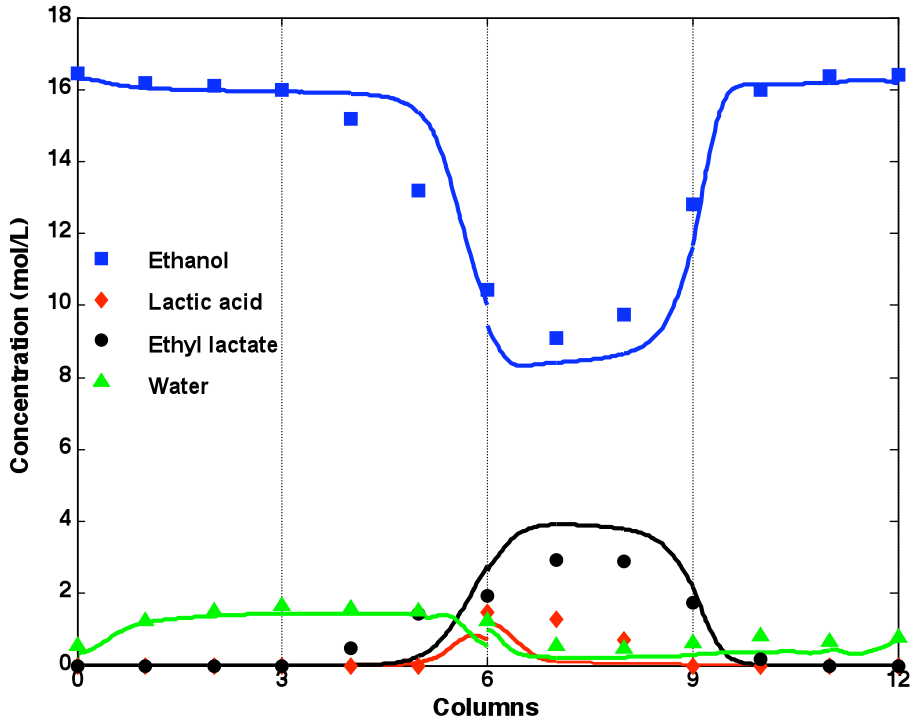

Figure 3.8 Bulk concentration profile in a TMBCR at cycle steady state modeled with the LDF approach. Experimental data are from Pereira et al., 2009.

C H A P T E R 4

4. Modeling SMBCR Performance Using the True Moving Bed Chromatographic Reactor (TMBCR) Approach

4.1 Introduction

In Chapter 3, modeling with the Maxwell-Stefan approach described very well the dynamic behavior of the SMBCR in two different experiments. However, the SMBCR analysis requires calculating the transient response of the system in order to reach the steady state solution. This may take as long as 12 cycles and a cycle is completed when the number of switches is equal to the number of columns (the case study has 12 columns). Also, Chapter 3 introduced the two main strategies of modeling an SMBCR process. In this chapter, the method known as the moving-bed approach will be used; this treats the simulated counter current process as equivalent to a true countercurrent system. The countercurrent motion of the solid is simulated with a velocity equal to the length of a column divided by the switching time. The inlet and outlet streams divide the TMBCR unit in four sections, which are Raffinate, Feed, Extract, and Desorbent as explained in Chapter 1. Figure 4.1 shows the schematic diagram of a TMBCR for the reversible reaction $A + B \leftrightarrow C + D$.

The TMBCR approach has the advantage of reducing the analysis to the examination of the countercurrent sections, because the concentration profiles build up around the feed node within the equipment and a single band profile is obtained at steady state simply setting the time dependent terms in the model equations equal to zero and solving it. In this chapter, the

Maxwell-Stefan approach will be used to describe the film and intraparticle mass transfer effects in the TMBCR.

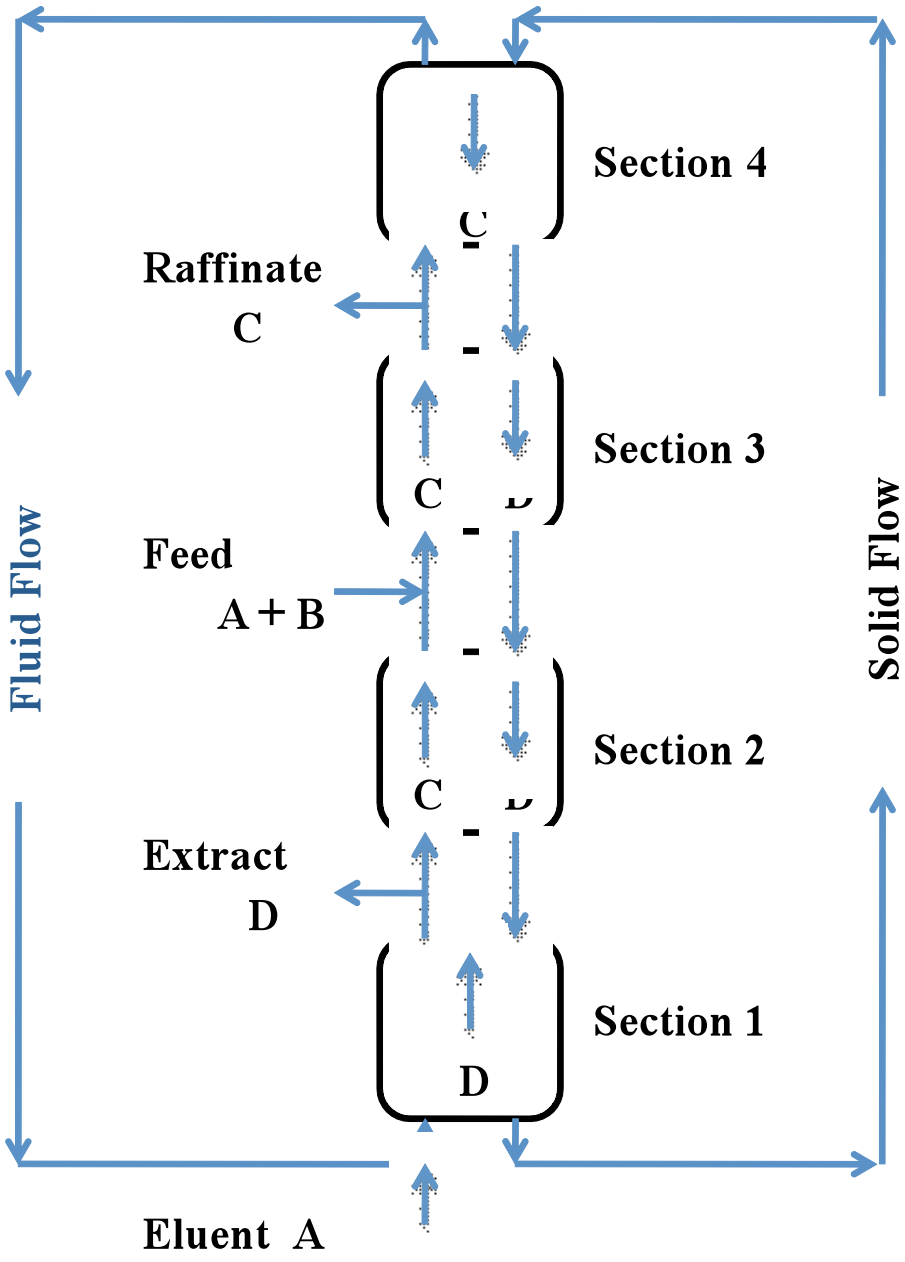

Figure 4.1. True moving bed chromatographic reactor; reaction A + B ⇔ C + D.

4.2 Transient and Steady State Models for the TMBCR Strategy

The following partial differential equations are proposed to represent the mass balance of species *i* at the section *j* of a true countercurrent bed. The analogy between SMBCR and the equivalent TMBCR is possible by the introduction of the relative velocity concept

$$u_j = u_j^{TMBCR} + u_s \tag{4-1}$$

where u_j^{TMBCR} is the fluid interstitial velocity in the equivalent TMBCR and u_s is the solid velocity in the TMBCR (representing the countercurrent solid motion). The solid velocity is evaluated from the switch time interval value t_c in the SMBCR as

$$u_s = \frac{L_c}{t_c} \tag{4-2}$$

The internal flow rates in both models are not the same, but they are related by

$$Q_j = Q_j^{TMBCR} + \frac{\varepsilon_b V_{col}}{t_c} \tag{4-3}$$

For the bulk fluid mass balance of component *i* in section *j*:

$$\varepsilon_b \frac{\partial C_{b_{i,j}}}{\partial t} = \varepsilon_b D_{ax_j} \frac{\partial^2 C_{b_{i,j}}}{\partial z^2} - \varepsilon_b u_j^{TMBCR} \frac{\partial C_{b_{i,j}}}{\partial z} - (1-\varepsilon_b) N_{film_{i,j}}\Big|_{r=r_p} \qquad i = 1 \cdots n \tag{4-4}$$

The particle mass balance must account for plug flow of the solid phase; the pellet mass balance of component *i* in section *j* is:

$$\varepsilon_p \frac{\partial C_{p_{i,j}}}{\partial t} + (1-\varepsilon_p) \frac{\partial C_{p_{i,j}}}{\partial t} = u_s \left(\varepsilon_p \frac{\partial C_{p_{i,j}}}{\partial z} + (1-\varepsilon_p) \frac{\partial C_{q_{i,j}}}{\partial z} \right) + \frac{1}{r^2} \frac{\partial}{\partial r} \left\{ r^2 \left[\varepsilon_p \left[\Gamma\left(x_{p_{i,j}}\right) \right] \left[B_p\left(x_{p_{i,j}}\right) \right]^{-1} \frac{\partial C_{p_{i,j}}}{\partial r} \right] \right\} + \sum_{d=1}^{N_R} \nu_{i,d} r_d^{het} \tag{4-5}$$

Initial condition:

$$t = 0: \qquad C_{b_{i,j}} = C_{i,0} \quad \text{for} \quad i = 1 \cdots n \tag{4-6}$$

$$C_{p_{i,j}} = C_{i,0} \quad \text{for} \quad i = 1 \cdots n \tag{4-7}$$

The standard Danckwerts boundary conditions

$$z = 0: \qquad u_j^{TMBCR} C_{b_{i,j}} - \varepsilon_b D_{ax_j} \frac{\partial C_{b_{i,j}}}{\partial z}\bigg|_{z=0} = u_j^{TMBCR} C_{i,F} \tag{4-8}$$

$$z = L_j: \qquad \frac{\partial C_{b_{i,j}}}{\partial z}\bigg|_{z=L_j} = 0 \tag{4-9}$$

$$z = L_j: \qquad \begin{cases} C_{p_{i,j}}\Big|_{z=L_j} = C_{p_{i,j+1}}\Big|_{z=0} & \text{for } j = 1, 2, 3 \\ C_{p_{i,4}}\Big|_{z=L_4} = C_{p_{i,1}}\Big|_{z=0} \end{cases} \tag{4-10}$$

$$r = 0: \qquad \frac{\partial C_{p_{i,j}}}{\partial r}\bigg|_{r=0} = 0 \tag{4-11}$$

$$r = r_p: \qquad N_{film_{i,j}} = N_{p_{i,j}} \tag{4-12}$$

Introducing the dimensionless variables:

Space (axial): $\xi = {}^{z}/_{L_j}$ (4-13)

Space (radial): $\Theta = {}^{r}/_{r_p}$ (4-14)

Time: $\theta = {}^{t}/_{t_c}$ (4-15)

Velocity ratio: $\varphi_j^{TMBCR} = {}^{u_j^{TMBCR}}/_{u_s}$ (4-16)

Peclet number: $$Pe_j = {u_j^{TMBCR} L_j}/{D_{ax_j}} \tag{4-17}$$

Damköehler number: $$Da = {\rho_b k_c L_j}/{(1-\varepsilon_b) u_j^{TMBCR}} \tag{4-18}$$

Mass transfer number: $$K_L = {3 L_j K_t}/{(r_p) u_j^{TMBCR}} \tag{4-19}$$

Diffusivity number: $$D_L = {\varepsilon_p L_j D_t}/{(r_p)^2 u_j^{TMBCR}} \tag{4-20}$$

Here, n_j is the number of columns per section. Equations (4-4) and (4-5) can be written as follows:

$$\frac{\partial C_{b\,i,j}}{\partial \theta} = \frac{\varphi_j^{TMBCR}}{n_j}\left[\frac{1}{Pe_j}\frac{\partial^2 C_{b\,i,j}}{\partial \xi^2} - \frac{\partial C_{b\,i,j}}{\partial \xi} - K_{L_j}\frac{(1-\varepsilon_b)}{\varepsilon_b} N_{film,ij}\Big|_{r=r_p}\right] \quad i = 1 \cdots n \tag{4-21}$$

$$\left(\varepsilon_p + (1-\varepsilon_p) J\left(C_{p_{i,j}}\right)\right)\frac{\partial C_{p_{i,j}}}{\partial \theta} = \frac{1}{n_j}\frac{\partial C_{p_{i,j}}}{\partial \xi}\left(\varepsilon_p + (1-\varepsilon_p) J\left(C_{p_{i,j}}\right)\right) + \frac{\varphi_j^{TMBCR}}{n_j}\left[D_{L_j}\frac{1}{\Theta^2}\frac{\partial}{\partial \Theta}\left\{\Theta^2\left[\left[\Gamma\left(x_{p_{i,j}}\right)\right]\left[D_t B_p\left(x_{p_{i,j}}\right)\right]^{-1}\frac{\partial C_{p_{i,j}}}{\partial \Theta}\right]\right\} + Da_j \sum_{d=1}^{N_R} \nu_{i,d} r_d^{het}\right] \tag{4-22}$$

with initial and boundary conditions:

$$\theta = 0: \qquad C_{b_{i,j}} = C_{p_{i,j}} = C_{i,0} \tag{4-23}$$

$$\xi = 0: \qquad C_{b_{i,j}} - \frac{1}{Pe_j}\frac{\partial C_{b_{i,j}}}{\partial \xi}\Big|_{\xi=0} = C_{i,F} \tag{4-24}$$

$$\xi = 1: \qquad \left.\frac{\partial C_{b\,i,j}}{\partial \xi}\right|_{\xi=1} = 0 \tag{4-25}$$

$$\Theta = 0: \qquad \left.\frac{\partial C_{p\,i,j}}{\partial \Theta}\right|_{\Theta=0} = 0 \tag{4-26}$$

$$\Theta = 1: \qquad N_{film_{i,j}} = N_{p_{i,j}} \tag{4-27}$$

$$\xi = 1: \qquad \begin{cases} \left.C_{p_{i,j}}\right|_{z=L_j} = \left.C_{p_{i,j+1}}\right|_{\xi=0} & \text{for } j = 1,2,3 \\ \left.C_{p_{i,4}}\right|_{z=L_4} = \left.C_{p_{i,1}}\right|_{\xi=0} \end{cases} \tag{4-28}$$

Mass balance at the nodes of the inlet and outlet lines of the TMBCR:

Desorbent node:

$$C_{b\,i,(j=4,z=L)} = \frac{u_1^{TMBCR}}{u_4^{TMBCR}} C_{b\,i,(j=1,z=0)} + \frac{u_D}{u_4^{TMBCR}} C_D \tag{4-29}$$

$$u_1^{TMBCR} = u_4^{TMBCR} + u_D \tag{4-30}$$

Extract node:

$$C_{b\,i,(j=1,z=L)} = C_{b\,i,(j=2,z=0)} = C_X \tag{4-31}$$

$$u_2^{TMBCR} = u_1^{TMBCR} - u_X \tag{4-32}$$

Feed node:

$$C_{b\,i,(j=2,z=L)} = \frac{u_3^{TMBCR}}{u_2^{TMBCR}} C_{b\,i,(j=3,z=0)} - \frac{u_F}{u_2^{TMBCR}} C_F \tag{4-33}$$

$$u_3^{TMBCR} = u_2^{TMBCR} + u_F \tag{4-34}$$

Raffinate node:

$$C_{b\,i,(j=3,z=L)} = C_{b\,i,(j=4,z=0)} = C_R \tag{4-35}$$

$$u_4^{TMBCR} = u_3^{TMBCR} - u_R \tag{4-36}$$

The steady state formulation is obtained by setting the time derivatives to zero:

$$\left.\frac{\partial C_{b\,i,j}}{\partial \theta}\right|_{steady\ state} = 0 \tag{4-37}$$

$$\left.\frac{\partial C_{p\,i,j}}{\partial \theta}\right|_{steady\ state} = 0 \tag{4-38}$$

4.3 TMBCR Simulation with the Maxwell-Stefan Approach

In this section, the use of the Maxwell-Stefan approach model for TMBCR is illustrated by means of an application example. It describes the process for the production of acetal (diethylacetal) presented in detail in Chapters 2 and 3. This process has been the subject of several studies (Silva and Rodrigues 2001, 2002, and 2005). They employ a linear driving force model (LDF) in the description of mass transfer effects in the columns while using the TMBCR modeling approach. The results of modeling the TMBCR using the Maxwell-Stefan approach will be compared to the simulation results and experimental data presented by Silva and Rodrigues (2005) obtained in a SMBCR system.

4.3.1 Model Validation for TMBCR at Steady State.

The diethylacetal synthesis in a SMBCR will be simulated at 10°C as if it were a TMBCR unit with a three-columns-per-section configuration. The feed composition will be a mixture of ethanol ($C_{A,F}$ = 8.57 mol/L) and acetaldehyde ($C_{B,F}$ = 8.96 mol/L), and the desorbent to be used is pure ethanol. Table 4.1 shows the operating conditions and characteristics of the columns used in the SMBCR. The reaction rate, activity coefficients, and adsorption isotherm parameters were presented in Chapter 2.

Table 4.1 Operating conditions and characteristics of the SMBCR (Run 1 of Silva and Rodrigues, 2005).

Parameter	**Value**
Feed Flow Rate	3 mL/min
Raffinate Flow Rate	8 mL/min
Desorbent Flow Rate	23.5 mL/min
Recycle Flow Rate	20.5 mL/min
Switching Time (t_C)	3.5 min
Configuration	3-3-3-3
Feed Concentration C_{AF} C_{BF}	 8.57 mol/L 8.96 mol/L
Length of the packed bed (L)	0.23 m
Internal diameter of the columns (D)	0.026 m
Radio of the particles (r_P)	400μm
External void fraction (ε_b)	0.4
Internal void fraction (ε_P)	0.4
Peclet number ($u_j L/D_{ax,j}$)	300
Bulk density (ρ_b)	390kg/m^3
Solid Velocity (u_s)	L/t_C = 0.0657 m/min
Temperature	10˚C

- **Modeling of TMBCR with LDF utilized by Silva and Rodrigues (2005).**

This model assumes that intraparticle mass transfer is described in terms of a simple linear driving force (LDF) approximation. The results of bulk concentration profiles in steady state with this model are presented in Figure 4.2. This figure shows that the proposed model predicted the bulk concentration profile with reasonable accuracy, except in the second section where significant differences with the experimental data exist.

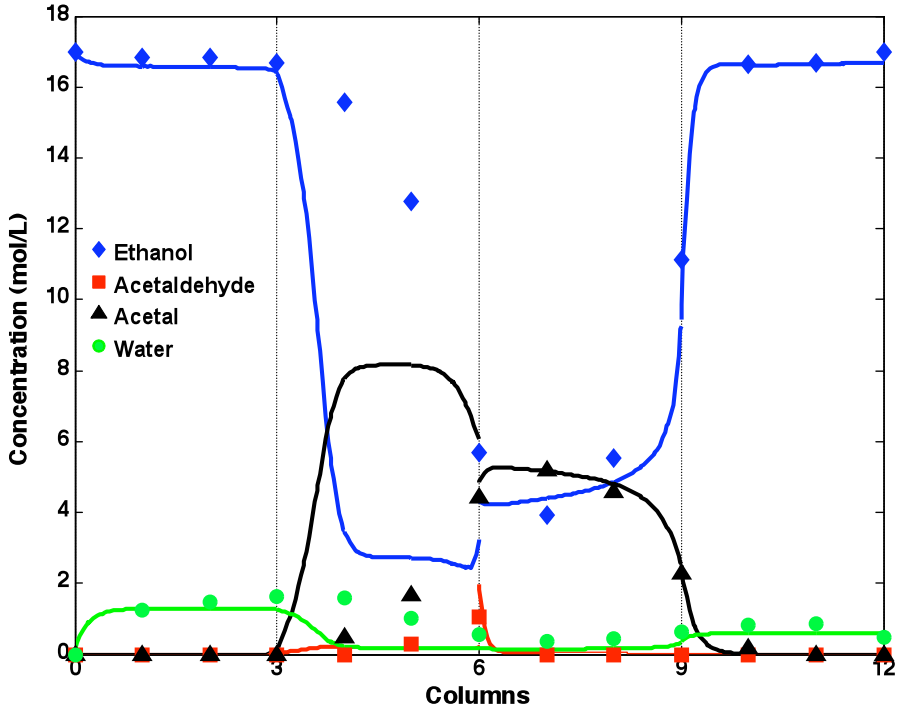

Figure 4.2 Bulk concentration profile in a TMBCR at steady state modeled with the LDF approach. Experimental data are for the SMBCR from Silva and Rodrigues (2005).

- **Modeling of TMBCR with Fick's Law (Fickian Diffusion)**

This model assumes that intraparticle mass transfer is described in terms of a Fickian diffusivity approximation. The results of this model are presented in Figure 4.3. This figure shows that the proposed model predicted the bulk concentration profile with reasonable accuracy, except in the second section where significant differences with the experimental data are observed. These differences in the second section are probably due to the fact that the multicomponent mass transfer effects are the ones that control the process are and not the reaction rate as the Fickian model implies. Besides, the Fickian model assumes that the diffusion coefficients for the liquid mixtures are not functions of concentration, and that there is no interaction between the diffusivity coefficients of the various components. Similar

results were obtained by Silva and Rodrigues (2005) using a model with the LDF approximation as was shown in Figure 4.2.

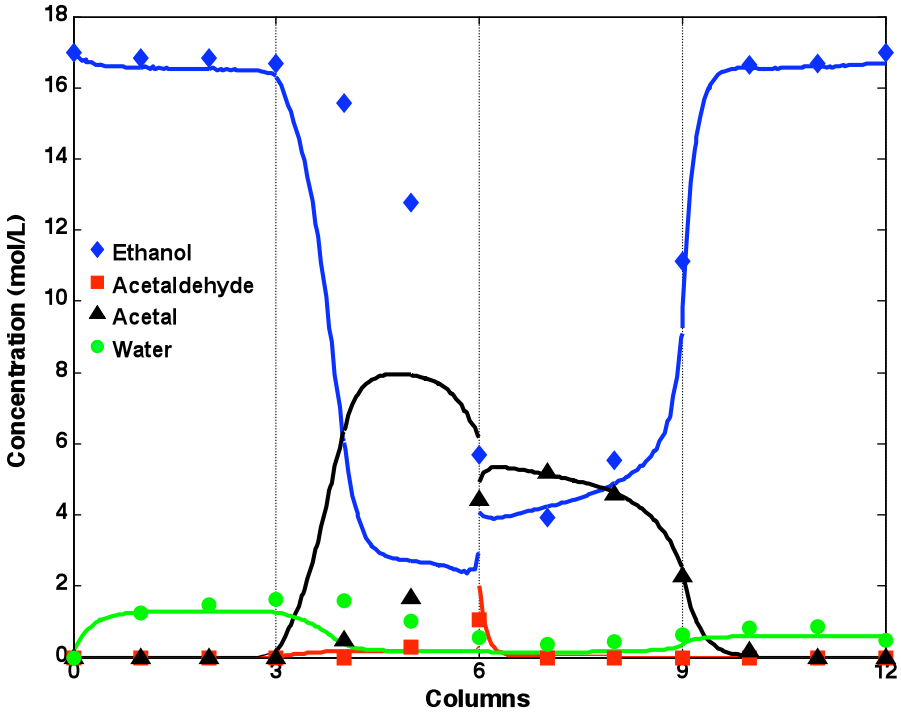

Figure 4.3 Bulk concentration profile in a TMBCR at steady state modeled with the Fickian diffusion approach. Experimental data are for the SMBCR from Silva and Rodrigues (2005).

- **Modeling of the TMBCR with the Maxwell-Stefan Approach**

This model assumes that the intraparticle mass transfer effects are described in terms of the Maxwell-Stefan approach. As can be seen from Figure 4.4, this model predicts with excellent accuracy the experimental data composition profiles at the reactor outlet. The breakthroughs of the different transitions, as well as the shape of the profile concentration peaks are very well predicted.

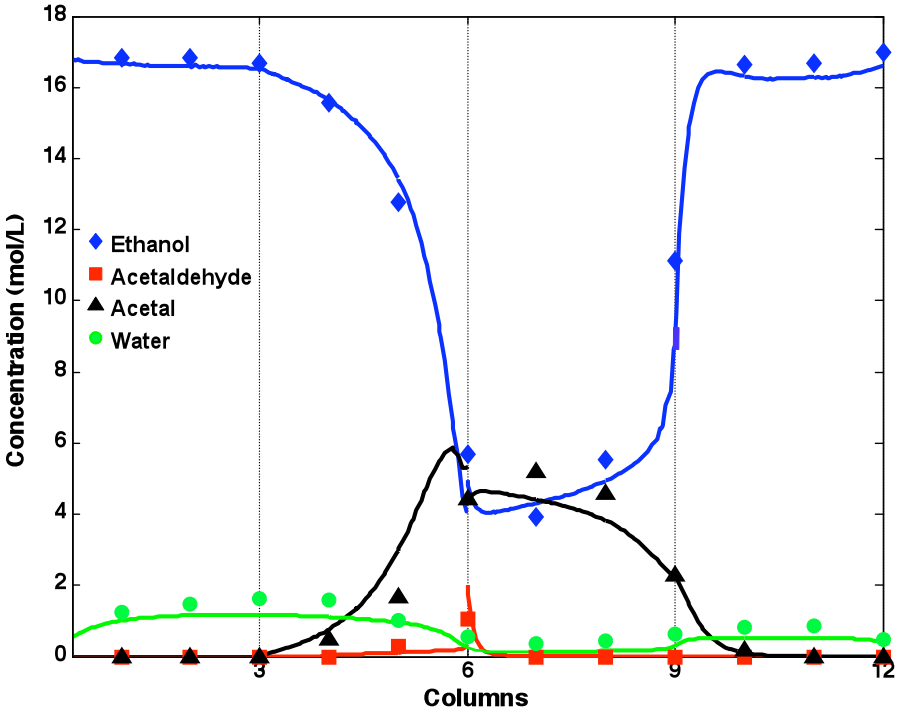

Figure 4.4 Bulk concentration profile in a TMBCR at steady state modeled with the Maxwell-Stefan approach. Experimental data are for the SMBCR from Silva and Rodrigues (2005).

In a different experimental run, Silva and Rodrigues (2005) analyzed the same reaction at different conditions in the SMBCR. They changed the flows and the switch time conditions as described in Table 4.2. The model based on the Maxwell-Stefan approach is validated again as shown in Figure 4.5. It is observed that our model predicts the experimental results with excellent accuracy as shown in Figure 4.5. The transient bulk concentration profile evolution is presented in Figure 4.6 and the steady state is obtained θ = 55, about 4 complete cycles.

Table 4.2 Operating conditions and characteristics of the SMBCR (Run 3 of Silva and Rodrigues, 2005).

Operation Conditions and Characteristics of the Simulated Moving Bed Columns	**Value**
Feed Flow Rate	3 mL/min
Raffinate Flow Rate	8 mL/min
Desorbent Flow Rate	24 mL/min
Recycle Flow Rate	20 mL/min
Switching Time (t_C)	4 min
Configuration	3-3-3-3
Feed Concentration C_{AF} C_{BF}	 8.57 mol/L 8.96 mol/L
Length of the packed bed (L)	0.23 m
Internal diameter of the columns (D)	0.026 m
Radio of the particles (r_P)	400µm
External void fraction (ε_b)	0.4
Internal void fraction (ε_P)	0.4
Peclet number ($u_j L/D_{ax,j}$)	300
Bulk density (ρ_b)	390kg/m^3
Solid Velocity (u_s)	L/t_C = 0.0657 m/min
Temperature	10˚C

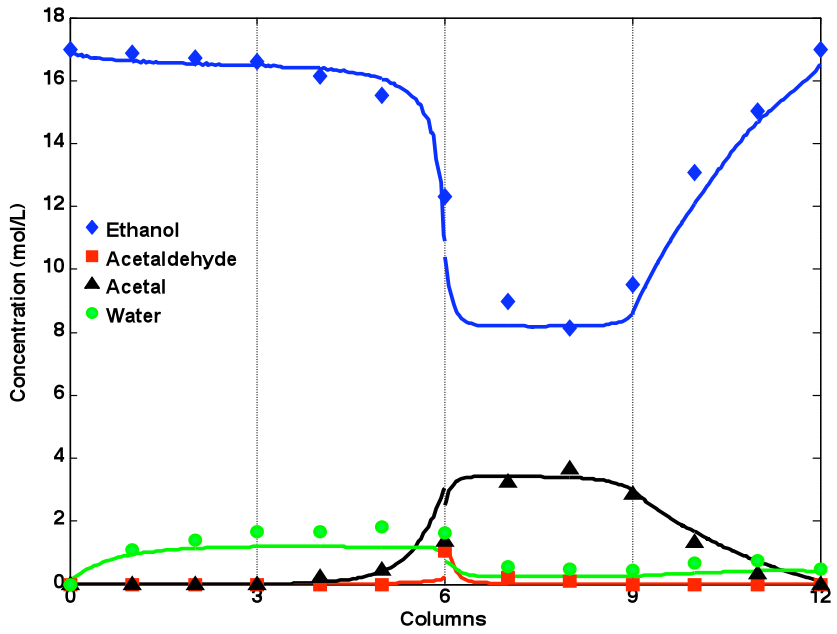

Figure 4.5 Bulk concentration profile in a TMBCR at cycle steady state modeled with the Maxwell-Stefan approach. Experimental data are from Silva and Rodrigues (2005, Run 3).

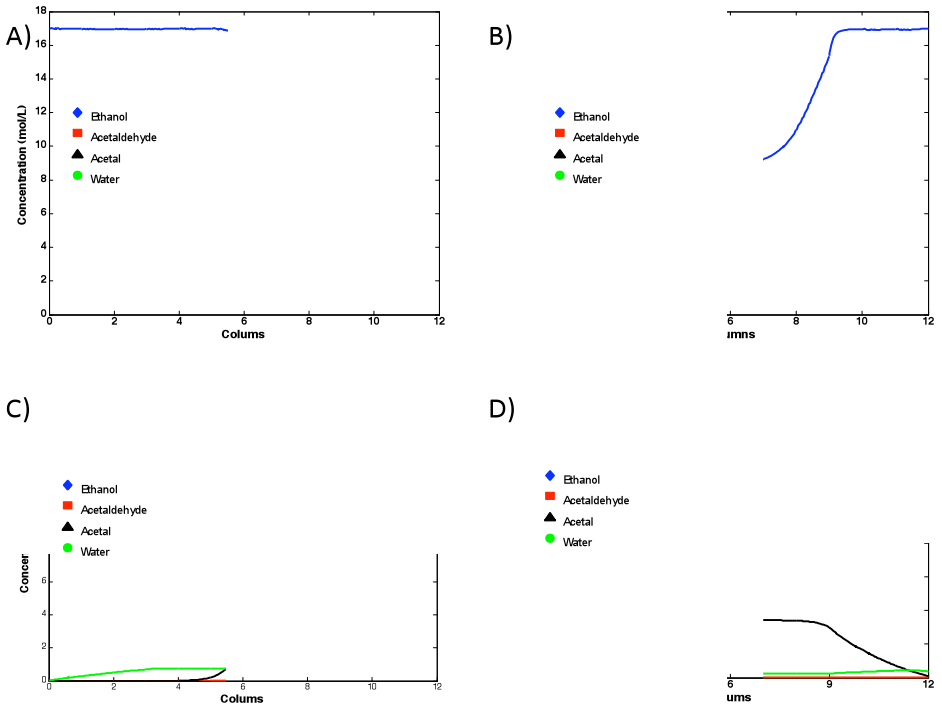

Figure 4.6 Transient bulk concentration profile in a TMBCR (A) θ = 1; (B) θ = 6; (C) θ = 12; and (D) steady state modeled with the Maxwell-Stefan approach at θ = 55. Experimental data are from Silva and Rodrigues (2005).

4.4. Comparison of True and Simulated Moving Bed Chromatographic Reactor

In this section, the Maxwell-Stefan approach will be used to compare the predictions of the TMBCR and SMBCR modeling alternatives for four application examples. The first two examples are the production of diethylacetal (Silva and Rodrigues, 2005) and dimethylacetal (Gandi et al., 2008) where a linear driving force model (LDF) is used to compare the TMBCR and SMBCR predictions. The third example is a process for the synthesis of methylacetate (Lode et al., 2003) where the equilibrium theory is used to compare true and simulated MBCR. The last example is a process for the synthesis of ethyl lactate (Pereira et al., 2009) where the linear driving force model (LDF) is also used to compare true and simulated MBCR. In all four cases, we will compare the true and simulated MBCR predictions using the Maxwell-Stefan approach model.

4.4.1 Comparison of True and Simulated Moving Bed Chromatographic Reactor Predictions with the LDF Model

The results obtained for each of the comparisons of the steady state concentration profiles between true and simulated MBCR models at the middle of the switching time using the LDF model are presented in Figure 4.7 (diethylacetal), Figure 4.8 (dimethylacetal), Figure 4.9 (methylacetate), and Figure 4.10 (ethyl lactate). Small differences between the equivalent TMBCR and the real SMBCR concentration profiles were predicted in all cases for the LDF model. These small differences are probably due to flow changes in each of the ports (raffinate, feed, and extract), and these differences are most significant in the sections with the smallest liquid flows (section 2 and section 42) as shown in each of the figures mentioned above.

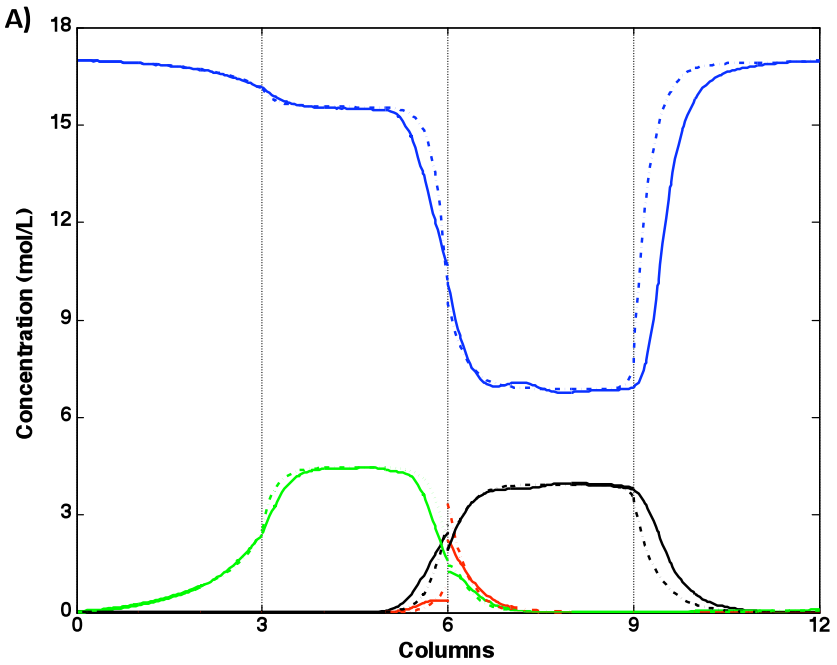

Figure 4.7 Comparison in steady state of the TMBCR model (dashed lines) and SMBCR (solid lines) in the middle of the switching time using the LDF model for the production of diethylacetal.

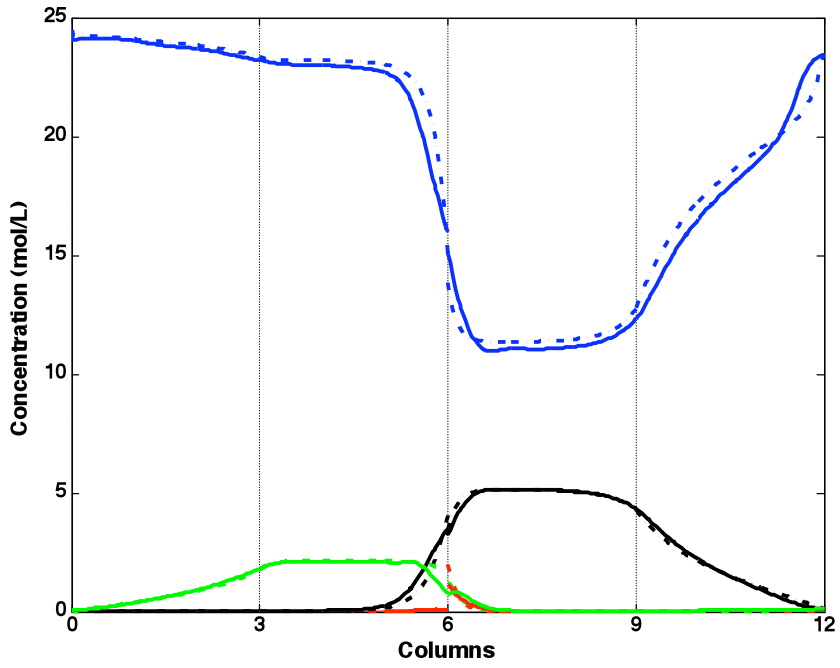

Figure 4.8 Comparison in steady state of the TMBCR model (dashed lines) and SMBCR (solid lines) at the middle of the switching time using the LDF model for the production of dimethylacetal.

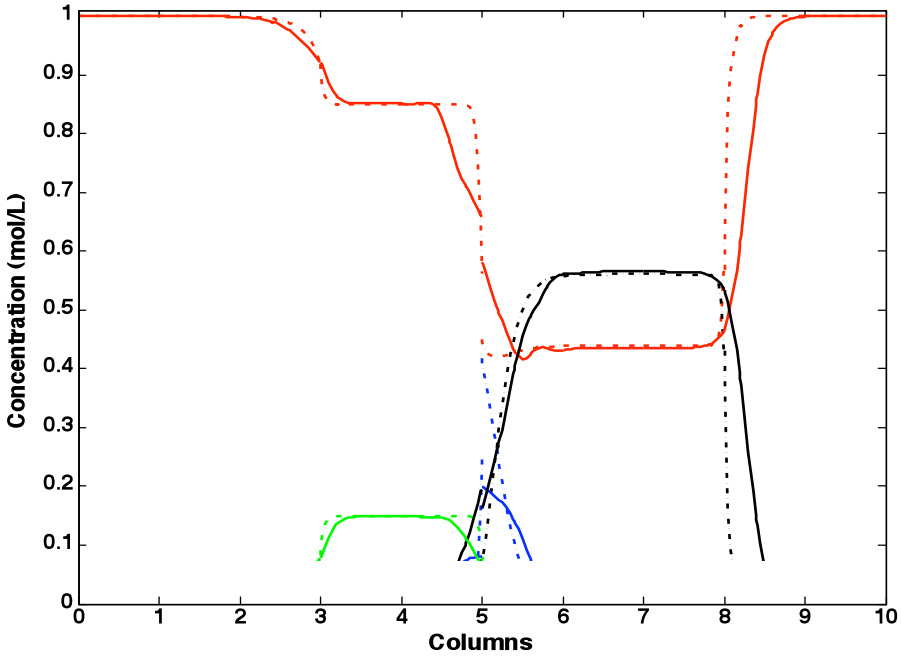

Figure 4.9 Comparison in steady state of the TMBCR model (dashed lines) and SMBCR (solid lines) at the middle of the switching time using equilibrium theory for the synthesis of

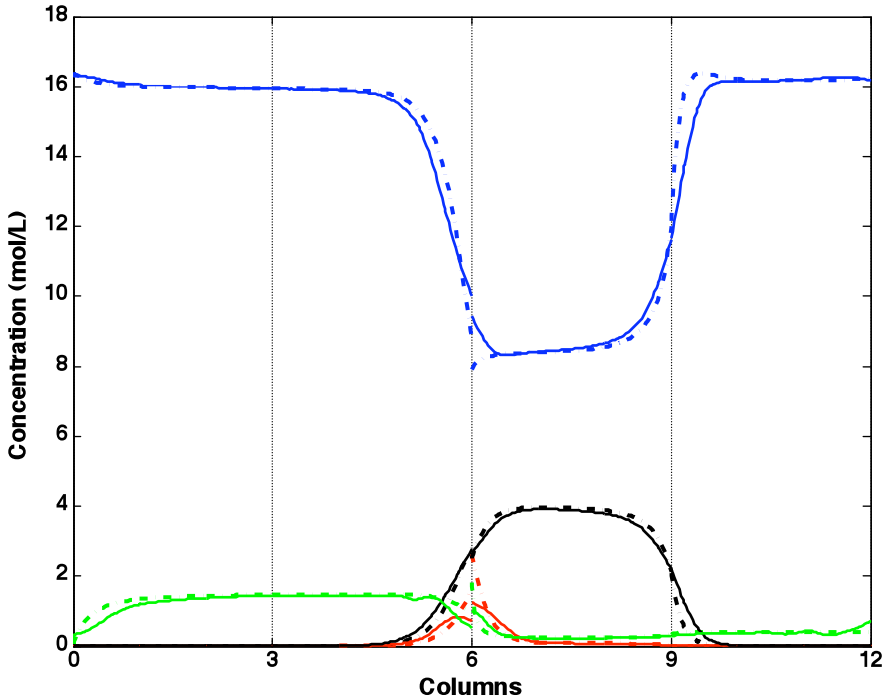

Figure 4.10 Comparison in steady state of the TMBCR model (dashed lines) and SMBCR (solid lines) at the middle of the switching time using the LDF model for the synthesis of ethyl lactate.

4.4.2 Comparison of True and Simulated Moving Bed Chromatographic Reactor Using the Maxwell-Stefan Approach Model.

In most reactive chromatography models presently used, the intra-particle diffusion process is usually simplified using linear driving force expressions or is characterized by a Fickian-like diffusion law with a parameter called the effective diffusivity; the inter-particle mass transfer rate in all cases is simplified using LDF expressions. Complex models, such as the one we propose (Maxwell-Stefan approach), incorporate details of most or all possible phenomena occurring both inter-particle and intra-particle, and hence the solution gives greater and more accurate details of the transport phenomena taking place as a function of the system parameters. The Maxwell-Stefan approach model was applied to the four cases mentioned above and under the same operation conditions. The results obtained for each of the comparisons of the steady state concentration profiles between true and simulated MBCR models at the middle of the switching time are presented in Figure 4.11 (diethylacetal), Figure 4.12 (dimethylacetal), Figure 4.13 (methylacetate), and Figure 4.14 (ethyl lactate). Again, only small differences between the equivalent TMBCR and the real SMBCR concentration profiles were observed in the cases of the production of diethylacetal and dimethylacetal using the Maxwell-Stefan model, similar to those observed with the LDF model. On the other hand, significant differences between the equivalent TMBCR and the real SMBCR concentration profiles were observed in the cases of the synthesis of methylacetate (Figure 4.13) and synthesis of ethyl lactate (Figure 4.14) using the Maxwell-Stefan model, contrary to the results obtained with the LDF model for these two cases. Figure 4.14 demonstrates that the TMBCR model does not describe the experimental data of Pereira et al. (2009) for synthesis of ethyl lactate as accurately as the actual SMBCR.

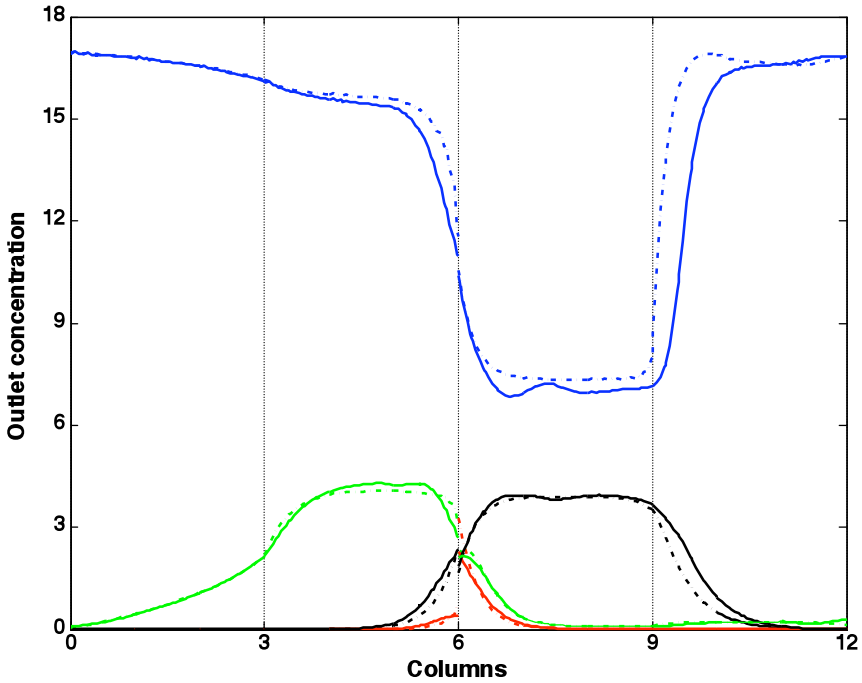

Figure 4.11 Comparison in steady state of the TMBCR model (dashed lines) and SMBCR (solid lines) in the middle of the switching time using the Maxwell-Stefan approach model

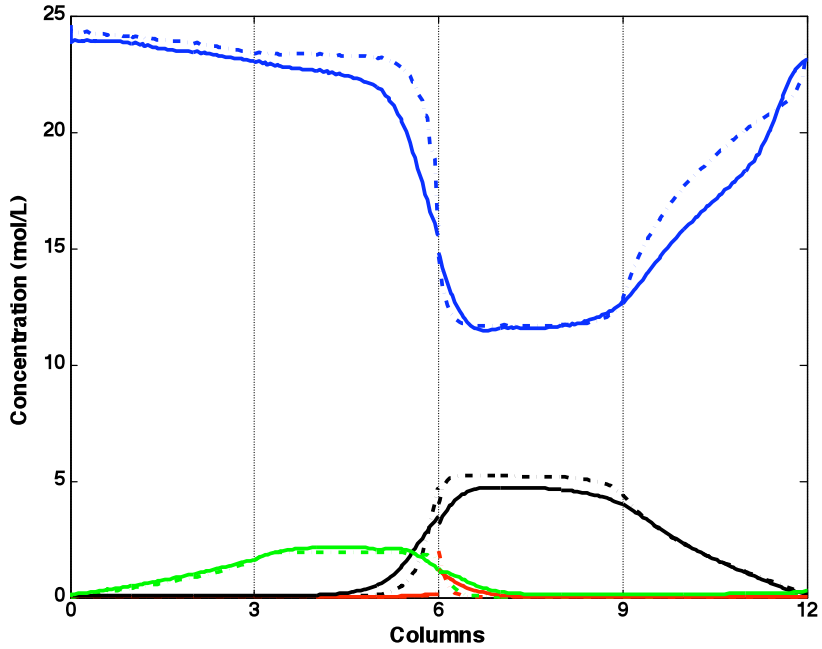

Figure 4.12 Comparison in steady state of the TMBCR model (dashed lines) and SMBCR (solid lines) at the middle of the switching time using the Maxwell-Stefan approach model for the production of dimethylacetal.

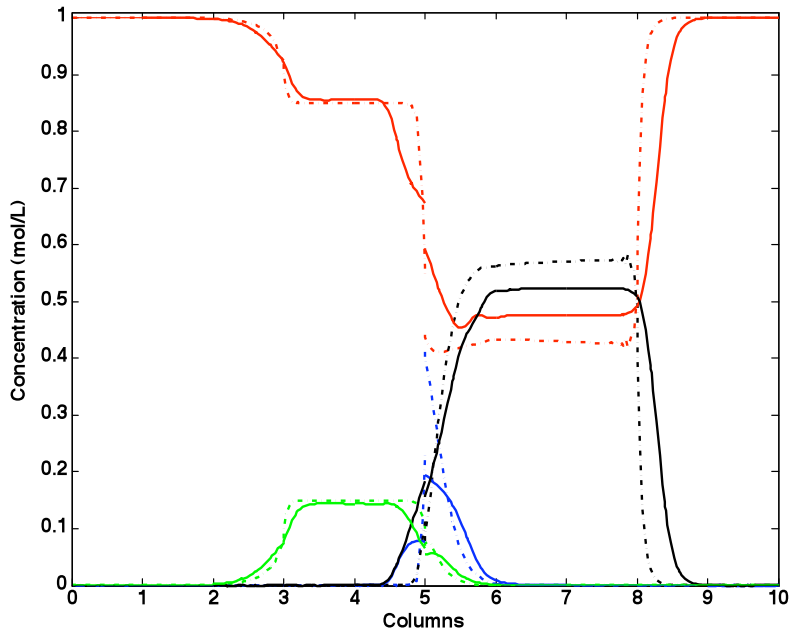

Figure 4.13 Comparison in steady state of the TMBCR model (dashed lines) and SMBCR (solid lines) at the middle of the switching time using the Maxwell-Stefan approach model for the synthesis of methylacetate.

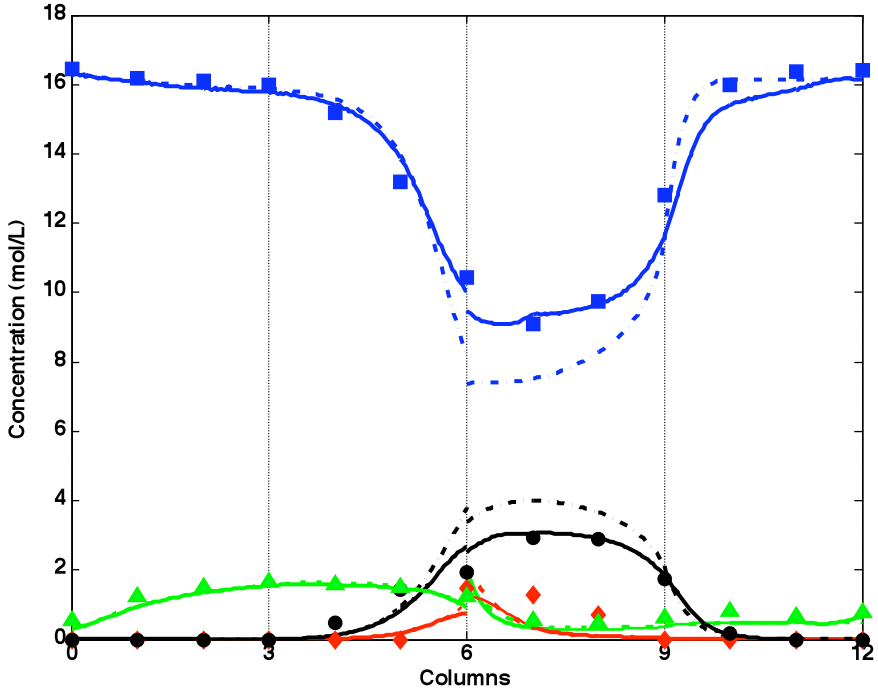

Figure 4.14 Comparison in steady state of the TMBCR model (dashed lines) and SMBCR (solid lines) at the middle of the switching time using the Maxwell-Stefan approach model for the synthesis of ethyl lactate (experimental data are from Pereira et al., 2009).

4.5 Conclusions

The synthesis of diethylacetal in a SMBCR was successfully modeled using the TMBCR approach when the mass-transfer effects were described in terms of the Maxwell-Stefan approach. The results obtained using this approach were in much better agreement with the SMBCR experimental results than those obtained using the LDF and Fickian modeling approaches.

The Maxwell-Stefan approach was used to compare the predictions of the TMBCR and SMBCR modeling alternatives for four application examples. The SMBCR modeling strategy was found to be somewhat more precise than the TMBCR model for two of the cases considered and significantly more precise for the other two cases; however, it requires considerably higher computational effort, especially when many columns are involved. Therefore, the actual SMBCR modeling strategy using the Maxwell-Stefan approach should be considered as the simulation tool of choice for detailed optimization analysis of simulated moving bed chromatographic reactors for practical applications, if computational effort is not a main concern.

C H A P T E R 5

5. Performance Assessment of SMBCR Operational Parameters

5.1 Introduction

In Chapters 3 and 4, modeling with the Maxwell-Stefan approach described very well the dynamic behavior of SMBCRs and TMBCRs, respectively. In this chapter, we study, by simulation, the effect of feed composition, switching time, and flow ratio on the SMBCR performance. The performance criteria will be raffinate and extract purity, conversion, raffinate productivity, and desorbent consumption.

5.2 Criteria for Performance Assessment of SMBCR Parameters

Successful operation of a SMBCR depends on the correct choice of internal flow rates, the switching time, and the feed composition in order to obtain the best performance of the system in terms of productivity, desorbent required, and raffinate and extract purity. Productivity is defined as the amount of product formed in the raffinate port per unit of time per adsorbent volume; desorbent required is defined as the amount of component consumed in the eluent port per unit of product generated. Performance parameters in the SMBCR will be evaluated for each period of switching time according to the following equations:

Raffinate Purity

$$PU_{Raffinate}(\%) = \frac{\int_t^{t+t_C} c_{C,R}(t)dt}{\int_t^{t+t_C} c_{B,R}+c_{C,R}+c_{D,R}} \times 100 \qquad (5.1)$$

Extract Purity (%)

$$PU_{Extract}(\%) = \frac{\int_t^{t+tC} C_{C,X}(t)dt}{\int_t^{t+tC} C_{B,X}+C_{C,X}+C_{D,X}} \times 100 \quad (5.2)$$

Conversion (%)

$$X(\%) = 1 - \frac{Q_R \int_t^{t+tC} C_{B,R}(t)dt + Q_X \int_t^{t+tC} C_{B,X}(t)dt}{Q_F C_{B,F}} \times 100 \quad (5.3)$$

Raffinate Productivity $\left(\frac{kg_{product}}{day \cdot L_{adsorbent}}\right)$

$$PR = \frac{Q_R \int_t^{t+tC} C_{C,R}(t)dt}{(1-\varepsilon_b)V_{unit}} \quad (5.4)$$

Desorbent consumption $\left(\frac{L_{desorbent}}{Kg_{product}}\right)$

$$DC = \frac{[Q_D C_{A,D} + Q_F(C_{A,F} - 2XC_{B,F})]V_{ml,A}}{Q_R \int_t^{t+tC} C_{C,R}(t)dt} \quad (5.5)$$

The correct internal flow rates in the SMBCR are such that in section I complete regeneration of the adsorbing phase by the incoming desorbent stream is achieved, and in section IV the light product (or less adsorbed) is completely removed from the fluid phase in order to recycle the solvent. In sections II and III complete separation of the products must be achieved and sufficient time provided for chemical reaction to occur. Stori et al. (1993) showed that performance of a non-reactive SMB depends only on the flow rate ratios $\gamma_i = {u_i}/{u_s}$. This result is also sufficient for the case of a reactive SMB under conditions of very fast reaction kinetics, because the reactant is completely consumed close to the feed port and most of the solid in the system is used for separation of the products. In the case of slow reaction kinetics this procedure is not valid (Lode et al., 2001) and additional design parameters such as feed composition and switching time are needed (Migliorini et al., 1999).

With the application of the ideal model or equilibrium theory, neglecting axial dispersion and mass transfer resistance, it is possible find an analytical solution of the model

equations (Lode et al., 2001; Gomes et al., 2007). The solution of this model allows defining the flow rate ratios γ_i based in the follow inequalities, which are valid for linear adsorption:

$$\gamma_1 > \frac{1-\varepsilon_b}{\varepsilon_b}(K_B + \varepsilon_p) \tag{5.6}$$

$$\frac{1-\varepsilon_b}{\varepsilon_b}(K_C + \varepsilon_p) < \gamma_2 < \gamma_3 < \frac{1-\varepsilon_b}{\varepsilon_b}(K_B + \varepsilon_p) \tag{5.7}$$

$$\frac{1-\varepsilon_b}{\varepsilon_b}(K_C + \varepsilon_p) > \gamma_4 \tag{5.8}$$

where K_C and K_B are, respectively, the higher and lower affinity constants from the linear isotherm. The region of complete separation for section II and III is illustrated in Figure 5.1.

In recent years, it is common to encounter the case of nonlinear adsorption isotherms in practical applications, where the regions in Figure 5.1 change and additional parameters are needed to find the best performance of a SMBCR. Therefore, although with equilibrium theory and the TMB model it is possible to determine the flows in sections I and IV (Helfferich, 1970), the equilibrium or ideal models cannot be utilized to predict the best performance for complex systems (nonlinear adsorption isotherm, mass transfer resistances, and flow rates in the complete separation region).

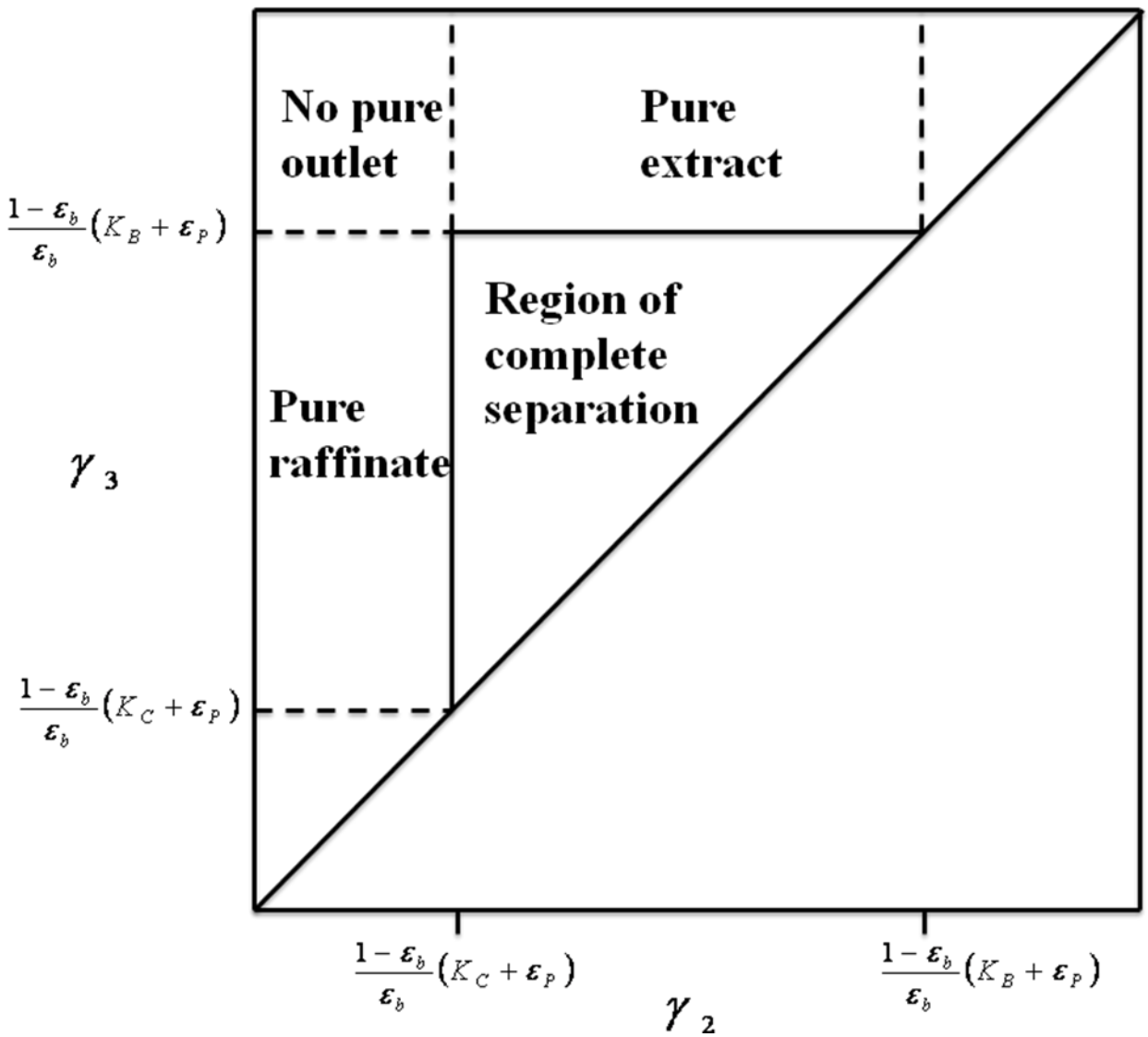

Figure 5.1 γ2–γ3 plane for linear isotherms (Lode et al., 2001)

The results of the ideal system can be used as an initial trial for a SMBCR optimization. The best performance conditions of a SMBCR (flow rates, switching time, and feed concentration) are obtained using the more robust model developed in this work, which describes mass transfer effects, both inter-particle and intra-particle, using the Maxwell-Stefan equations. Previous publications have used the TMBCR modeling strategy for optimization of SMBCR units operating parameters. However, in this work we have found

that the TMBCR model not always represents accurately the SMBCR performance. In the following sections, all performance parameters will be assessed using the SMBCR modeling strategy, specifying a minimum purity of 97% for both the raffinate and extract ports.

5.3 Performance of a SMBCR: synthesis of diethylacetal as case study

The performance of a SMBCR is investigated through numerical simulation, using as a case study the synthesis of diethylacetal from ethanol and acetaldehyde, catalyzed by the acid resin Amberlyst®15. The effects of feed composition, switching time, and flow rate are investigated based on a dynamic model of a SMBCR developed previously in Chapter 3. Each of these operational parameters is investigated for a unit configuration 3-3-3-3.

5.3.1 Effect of feed composition

In order to study the influence of the feed composition, the other operation conditions are held constant as shown in Table 5.1. In this system, ethanol is used simultaneously as desorbent to ensure complete regeneration in section I and as reactant. The influence of the feed composition on the acetal purity, acetaldehyde conversion, productivity, and ethanol consumption are shown in Figures 5.2 and 5.3. These figures show that a feed containing 80 mol% acetaldehyde results in the best performance, with productivity and desorbent consumption of 20.9 kg/L-day and 6.34 L/kg respectively. They also show that the raffinate purity remains practically constant over 97%. On the other hand, the extract purity drops below 97% when the feed is over 80% acetaldehyde because it becomes contaminated with diethylacetal and acetaldehyde.

A better understanding of the system is possible by analyzing the internal concentration profile in cyclic steady state as shown in Figures 5.4 to 5.11. In these figures, for feed

concentrations up to 70 mol% acetaldehyde, this species is completely consumed near the feed port and the SMBCR unit functions like an SMB to separate diethylacetal and water. On the other hand, for feed concentrations over 80 mol% acetaldehyde, the reaction in section III is not complete and the unreacted acetaldehyde goes to the raffinate stream leading to impure acetal.

The feed concentration that gives the best performance will be the reference point used to analyze the switching time effect in the next section.

Table 5.1 Operational conditions and characteristics of the SMBCR for diethylacetal synthesis (Silva and Rodrigues, 2005).

Parameter	**Value**
Feed Flow Rate	10 mL/min
Raffinate Flow Rate	27 mL/min
Desorbent Flow Rate	79 mL/min
Recycle Flow Rate	27 mL/min
Switching Time (t_C)	3.6 min
Configuration	3-3-3-3
Variable Feed Concentration C_{AF} C_{BF}	 8.57 mol/L 8.96 mol/L
Length of the packed bed (L)	0.23 m
Internal diameter of the columns (D)	0.026 m
Radio of the particles (r_P)	400µm
External void fraction (ε_b)	0.4
Internal void fraction (ε_P)	0.4
Peclet number ($u_j L/D_{ax,j}$)	300
Bulk density (ρ_b)	390kg/m^3

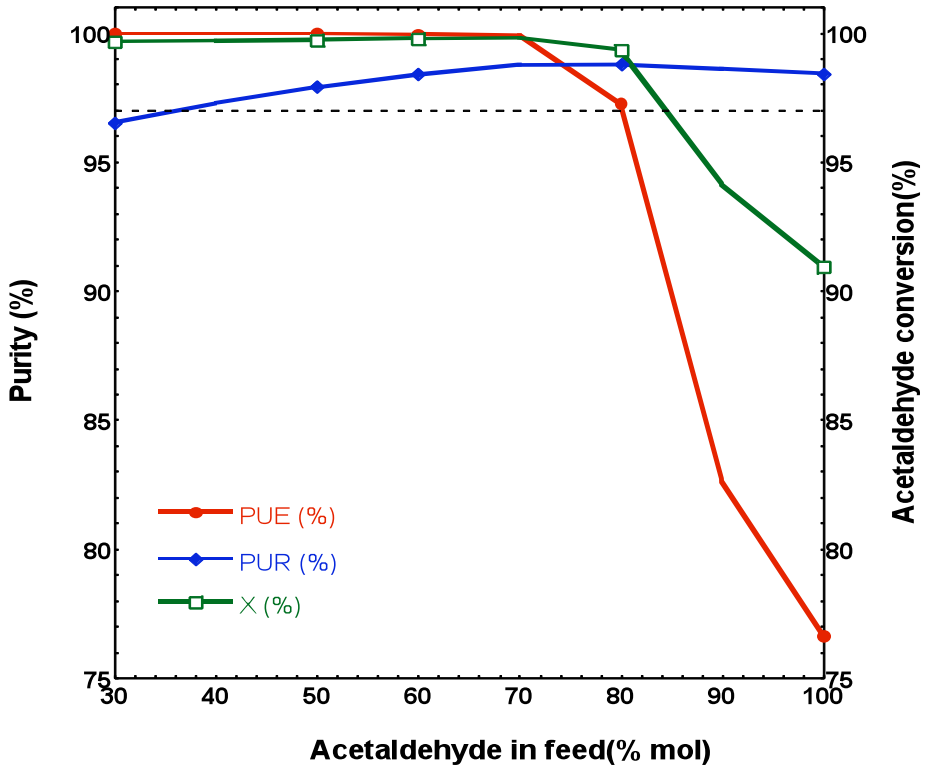

Figure 5.2 Effect of the feed composition on purity and acetaldehyde conversion.

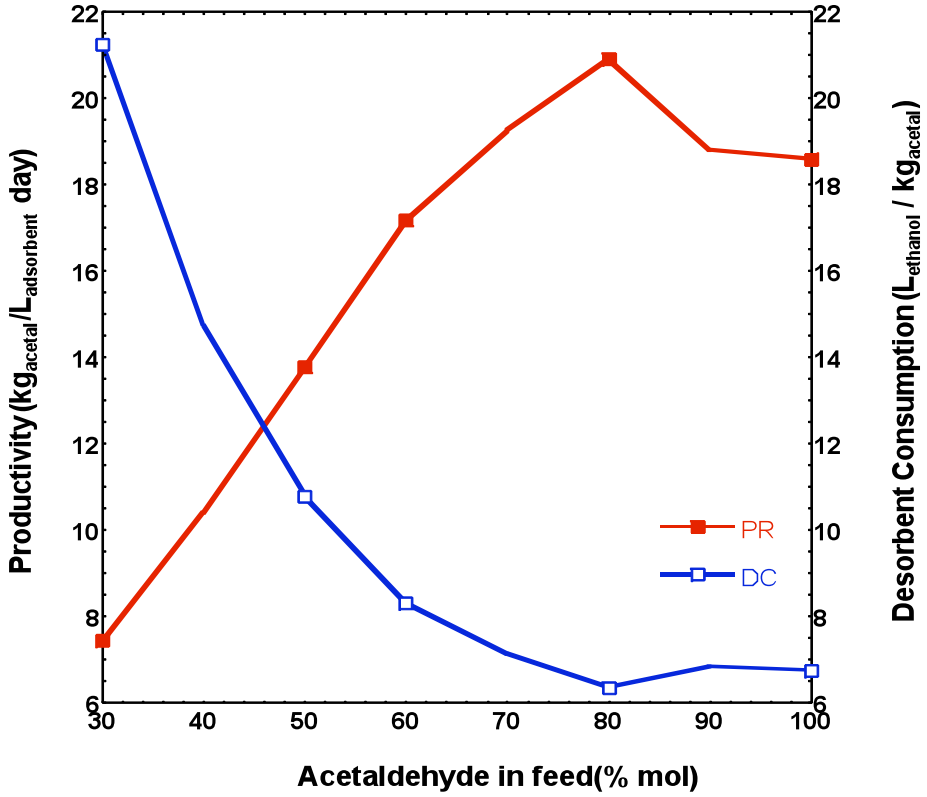

Figure 5.3 Effect of the feed composition on productivity and desorbent consumption.

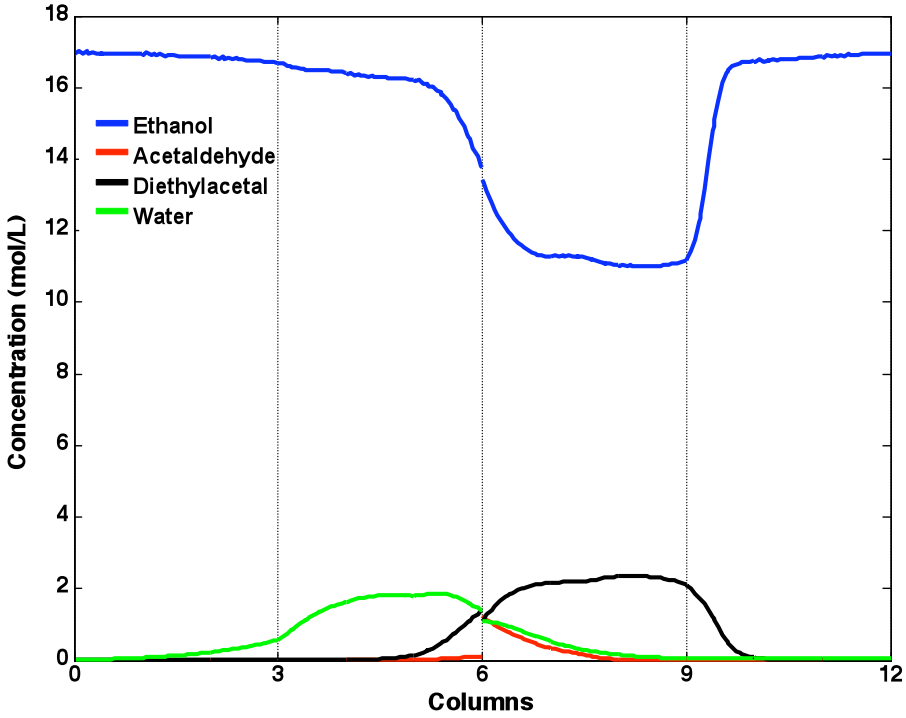

Figure 5.4 Effect of the feed composition (30 mol% acetaldehyde) in the middle of

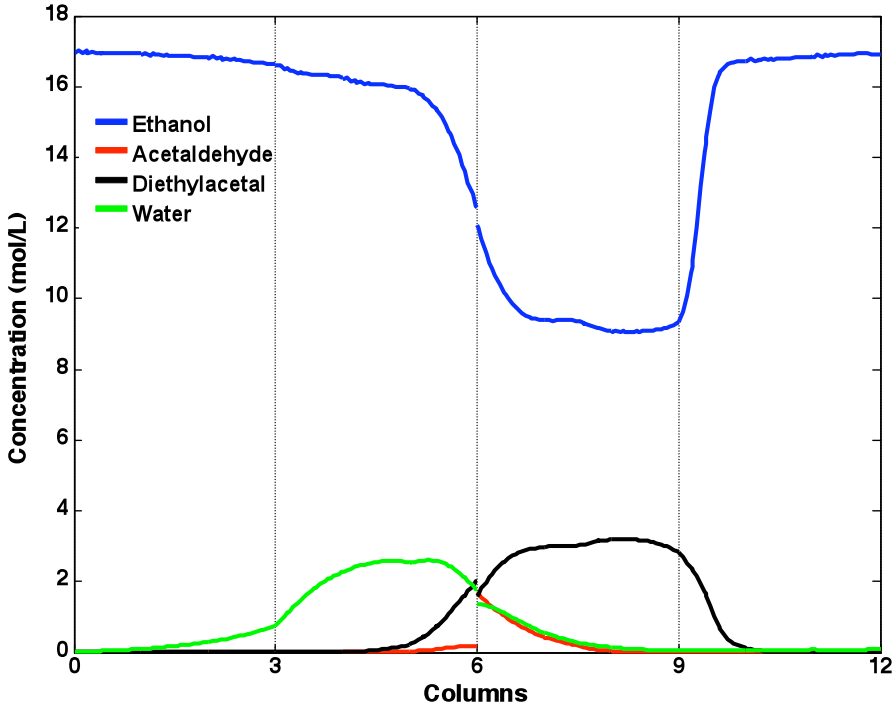

Figure 5.5 Effect of the feed composition (40 mol% acetaldehyde) in the middle of switching time at cyclic steady state.

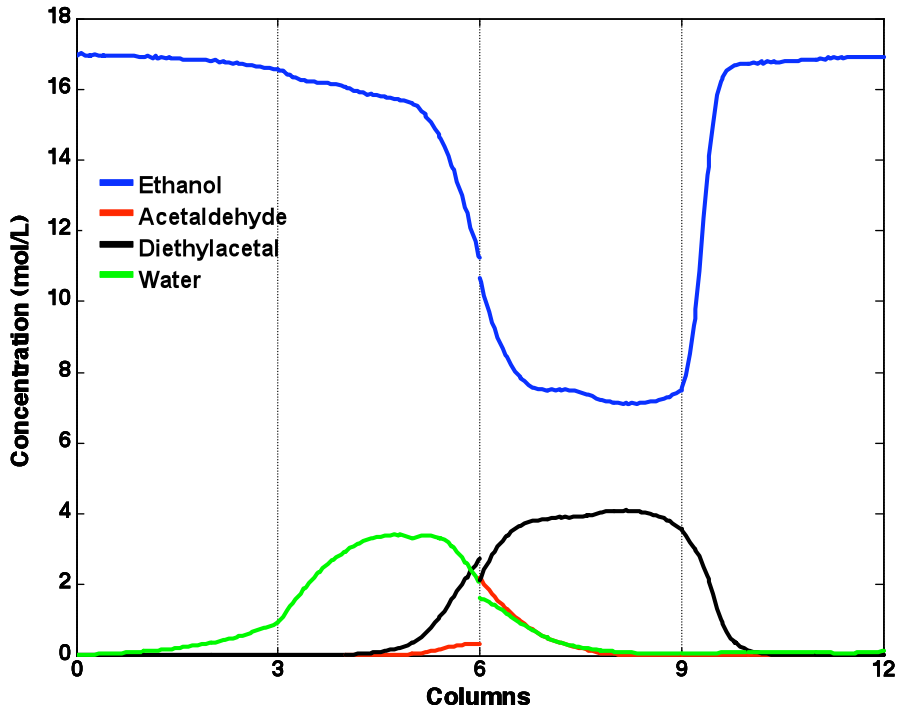

Figure 5.6 Effect of the feed composition (50 mol% acetaldehyde) in the middle of

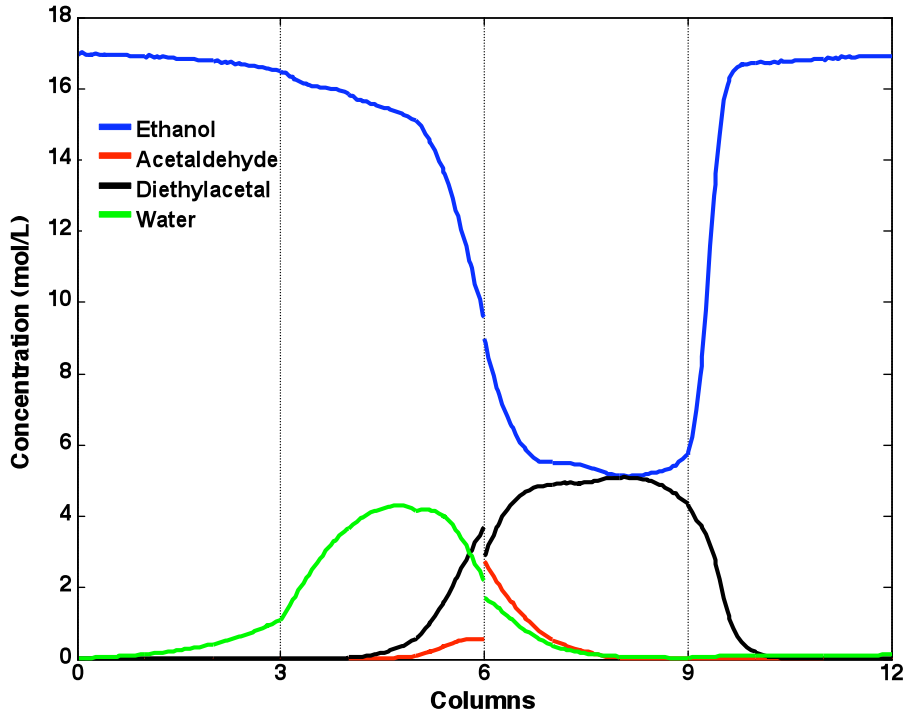

Figure 5.7 Effect of the feed composition (60 mol% acetaldehyde) in the middle of switching time at cyclic steady state.

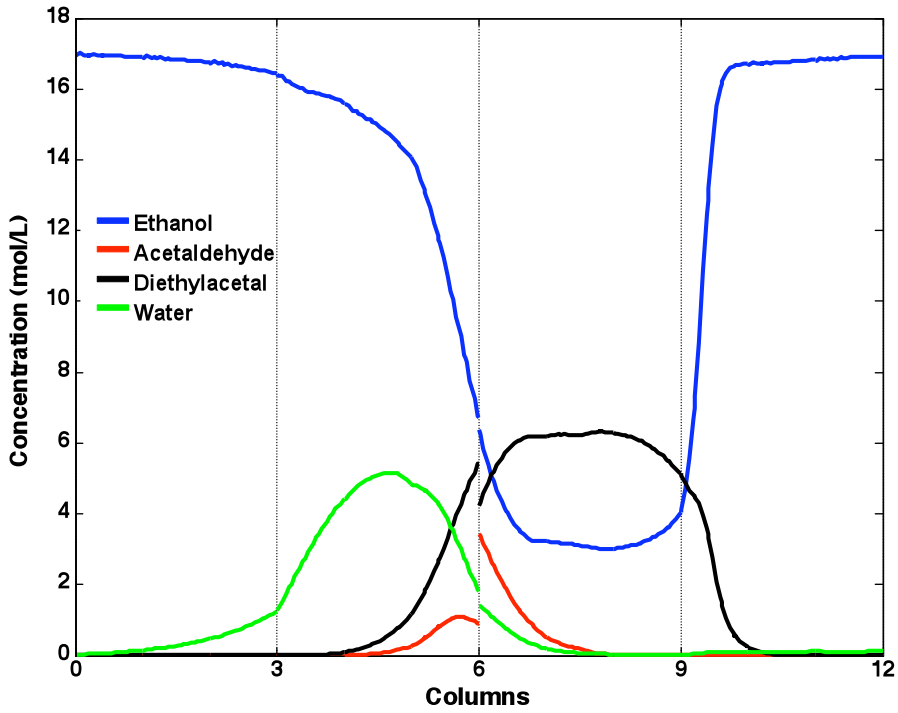

Figure 5.8 Effect of the feed composition (70 mol% acetaldehyde) in the middle of

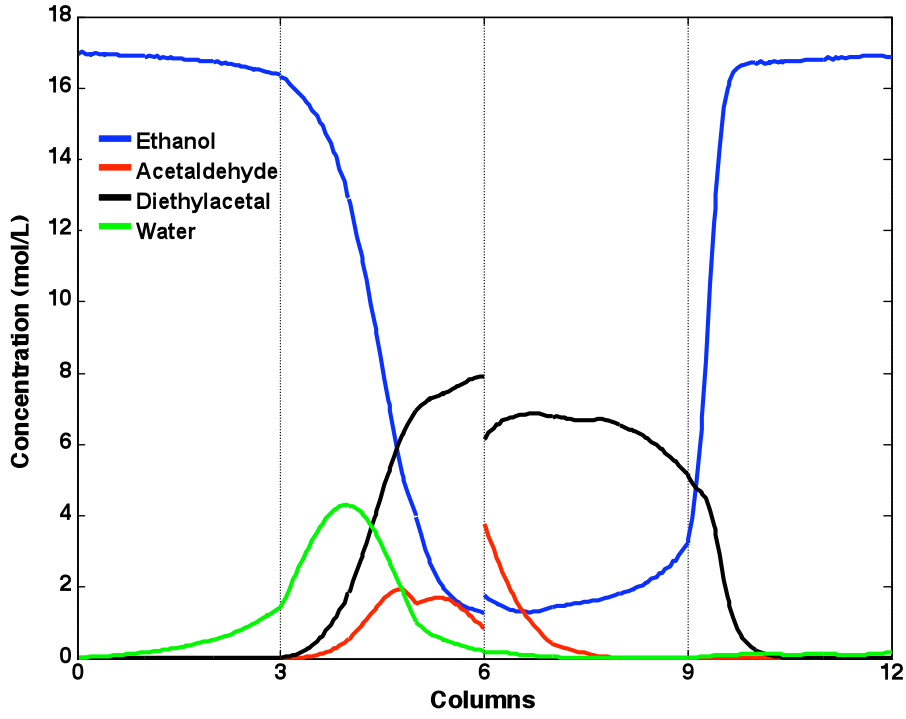

Figure 5.9 Effect of the feed composition (80 mol% acetaldehyde) in the middle of switching time at cyclic steady state.

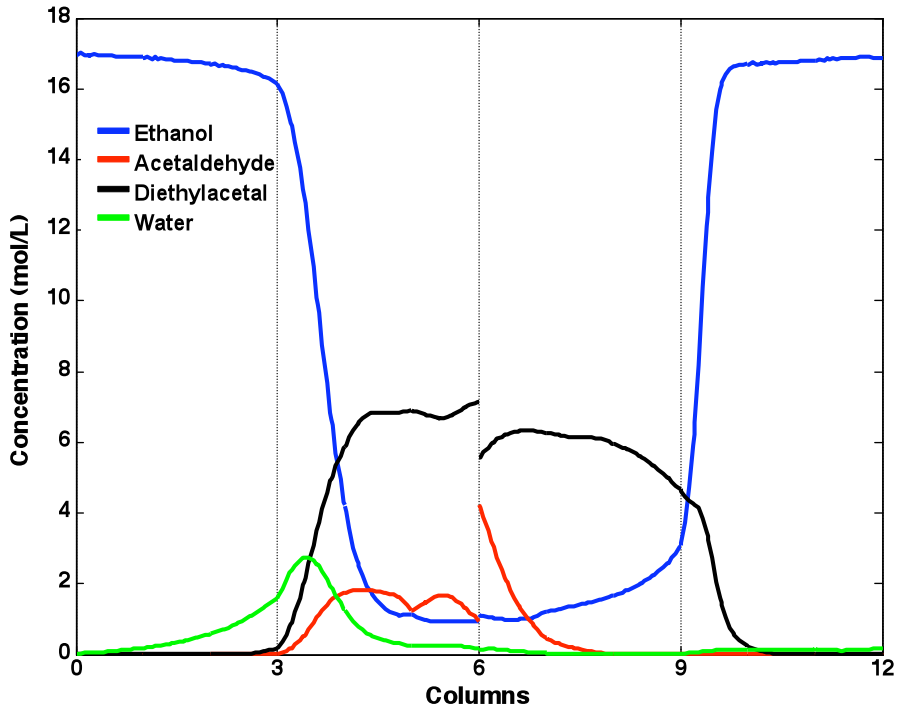

Figure 5.10 Effect of the feed composition (90 mol% acetaldehyde) in the middle of

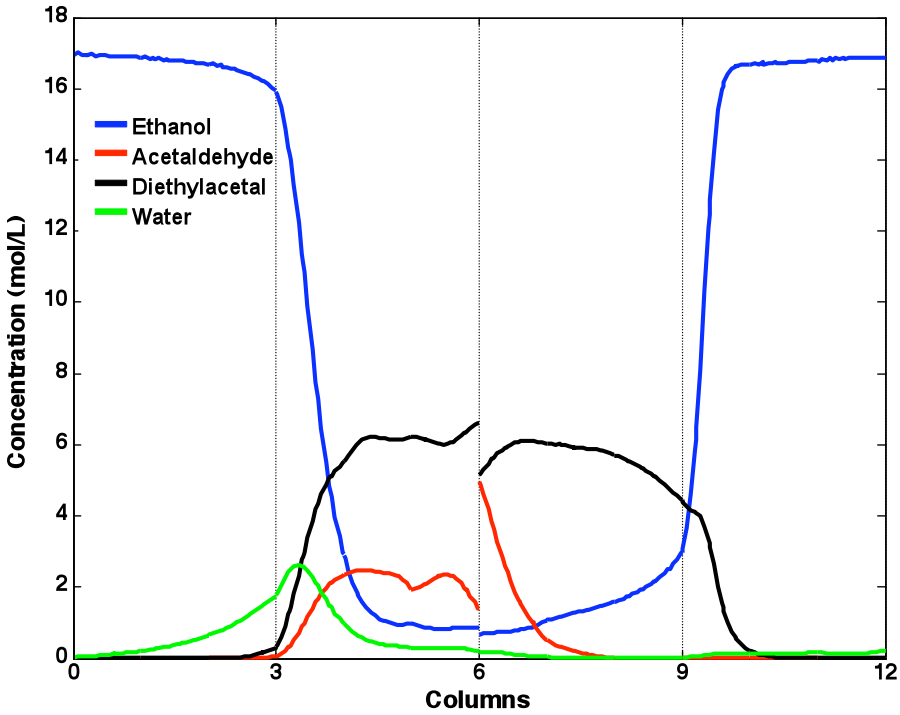

Figure 5.11 Effect of the feed composition (100 mol% acetaldehyde) in the middle of switching time at cyclic steady state.

5.3.2 Effect of switching time

The effect of switching time on the performance of the SMBCR is studied by simulating different switching times from 2.5 to 4.5 min, using the best feed concentration obtained above (80 mol% acetaldehyde), keeping constant the other operational conditions in Table 5.1. The influence of the switching time on the raffinate and extract purities, acetaldehyde conversion, productivity, and ethanol consumption are shown in Figures 5.12 and 5.13. Figure 5.12 shows that for switching times between 3.6 and 4 min the acetaldehyde conversion as well as the raffinate and extract purities are over the specified minimum limit of 97%. For the same range of switching times, Figure 5.13 shows a maximum productivity de 22.7 kg/L- day and a minimum desorbent consumption of 5.82 L/kg for a switching time of 3.75 min. For switching times below 3.6 min, the extract port begins to show significant contamination. As the switching time is further reduced, both extract and raffinate ports are contaminated. On the other hand, as the switching time is increased beyond the optimal level the raffinate port is significantly contaminated.

A better understanding of the system is obtained by analyzing the profiles of internal concentration in steady state as shown in Figures 5.14 to 5.21. They show that water and ethanol are moving from section II to section III with increasing switching time. This is due to the fact that when switching time increases the simulated solid velocity decreases (solid velocity = length/switching time). The reaction slows down in section II because acetaldehyde must displace water in order to react with the ethanol. When the reaction is slow, the mass transfer effects are dominant. These results show how robust the model based on the Maxwell-Stefan approach is. On the other hand, the linear and Fickian models cannot describe well this process taking place in section II.

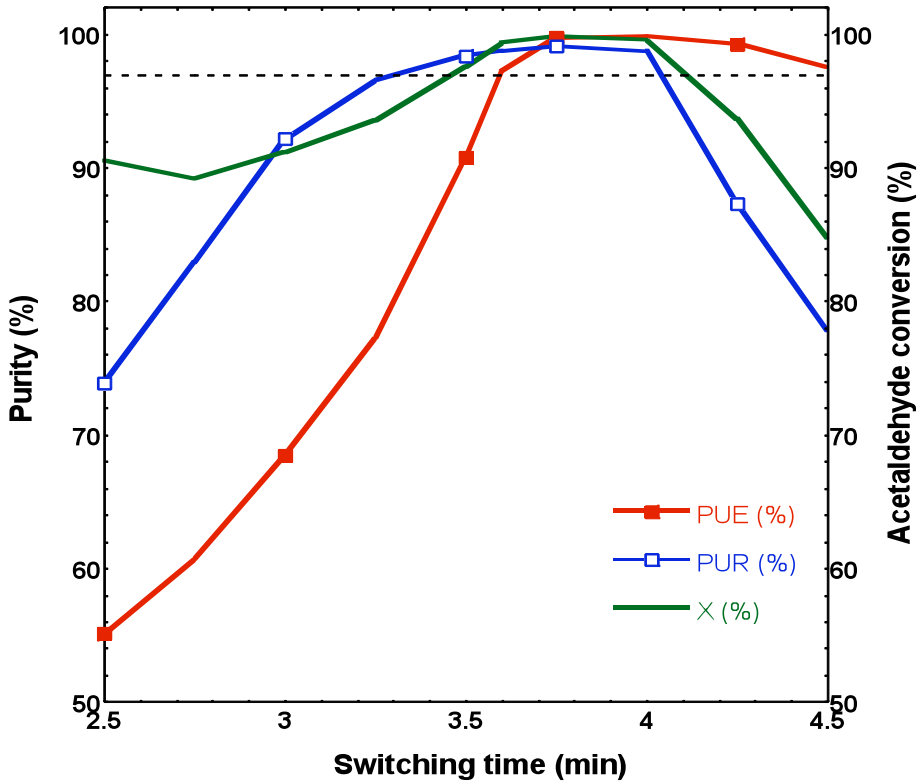

Figure 5.12 Effect of switching time on purity and acetaldehyde conversion.

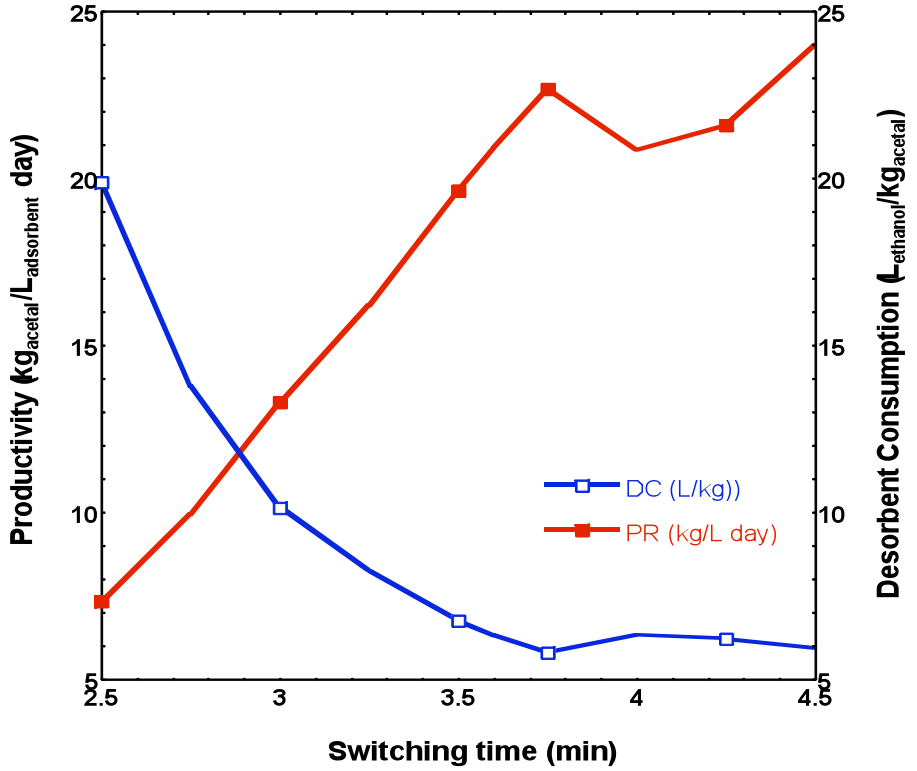

Figure 5.13 Effect of switching time on productivity and desorbent consumption.

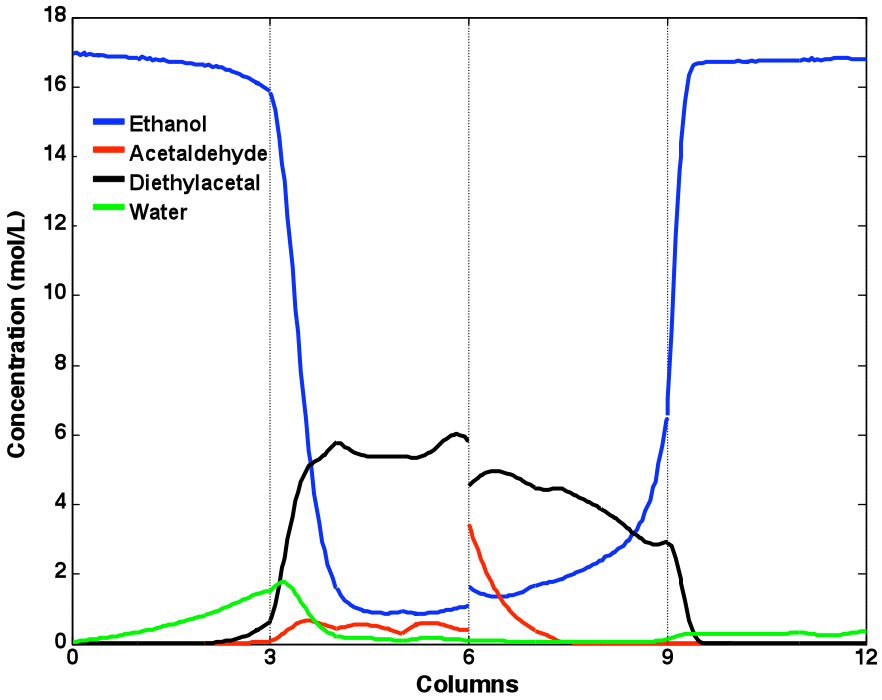

Figure 5.14 Cyclic steady state concentration profiles in the middle of switching time of 2.75

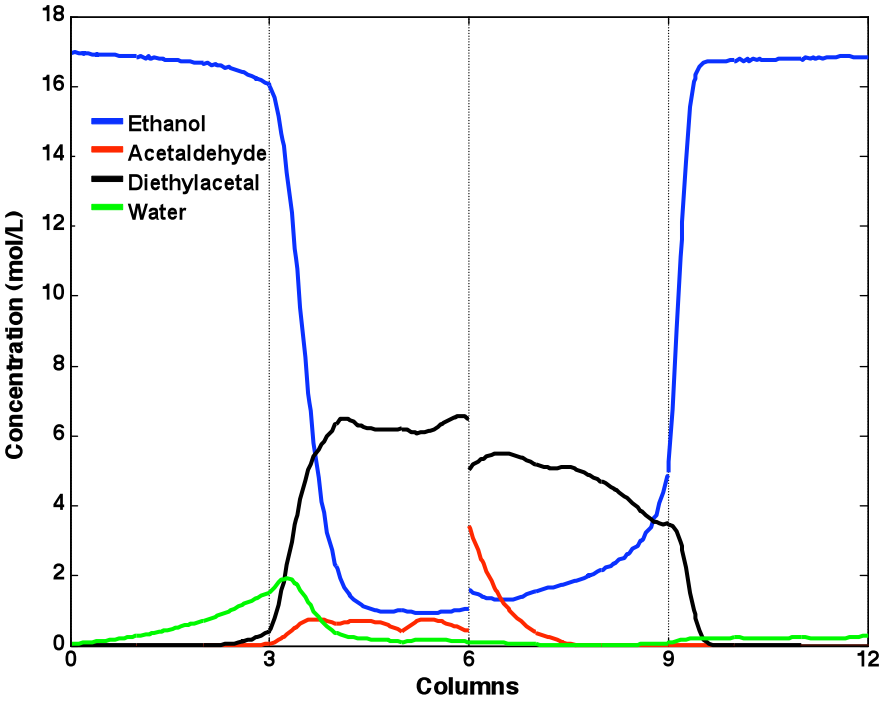

Figure 5.15 Cyclic steady state concentration profiles in the middle of switching time of 3 min for a feed composition 80 mol% acetaldehyde.

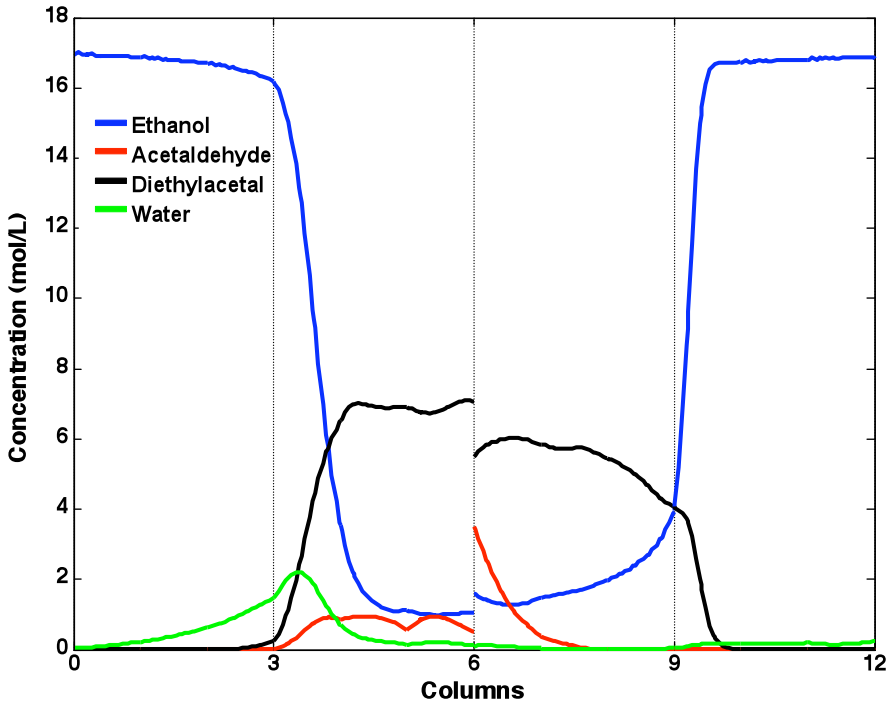

Figure 5.16 Cyclic steady state concentration profiles in the middle of switching time of 3.25

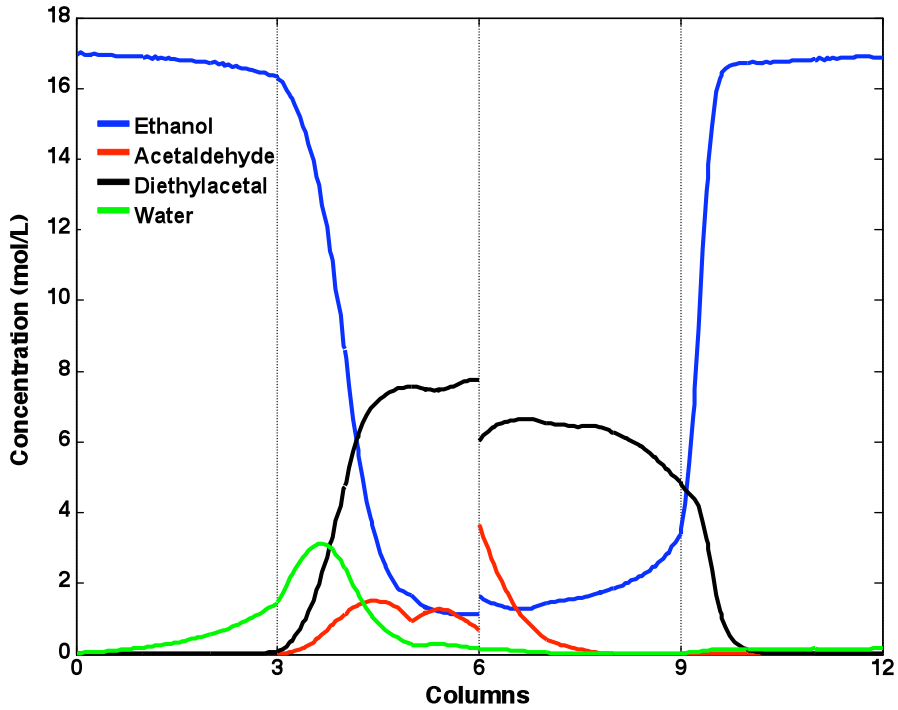

Figure 5.17 Cyclic steady state concentration profiles in the middle of switching time of 3.5 min for a feed composition 80 mol% acetaldehyde.

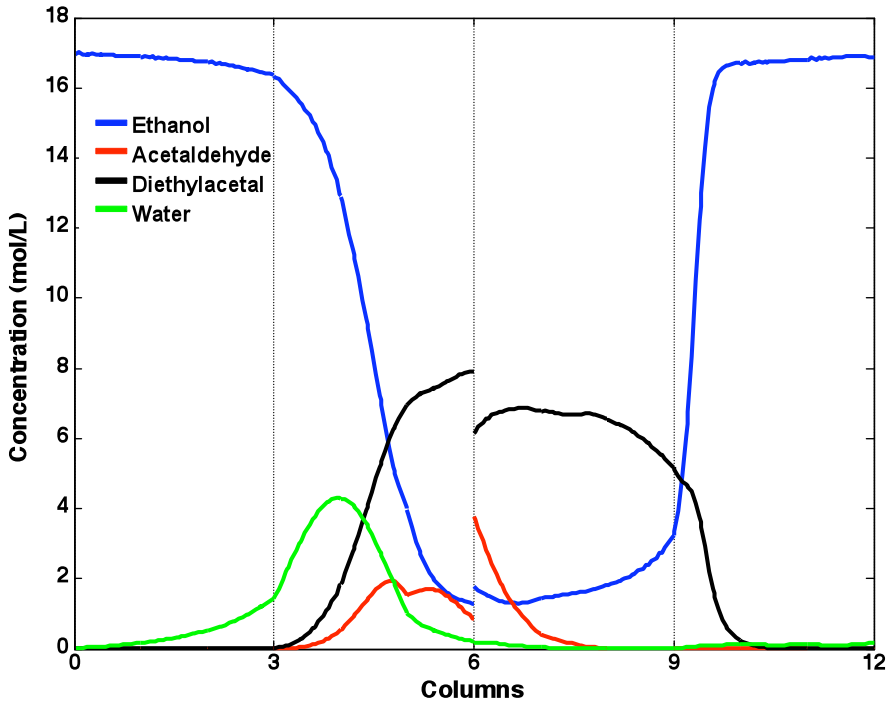

Figure 5.18 Cyclic steady state concentration profiles in the middle of switching time of 3.6

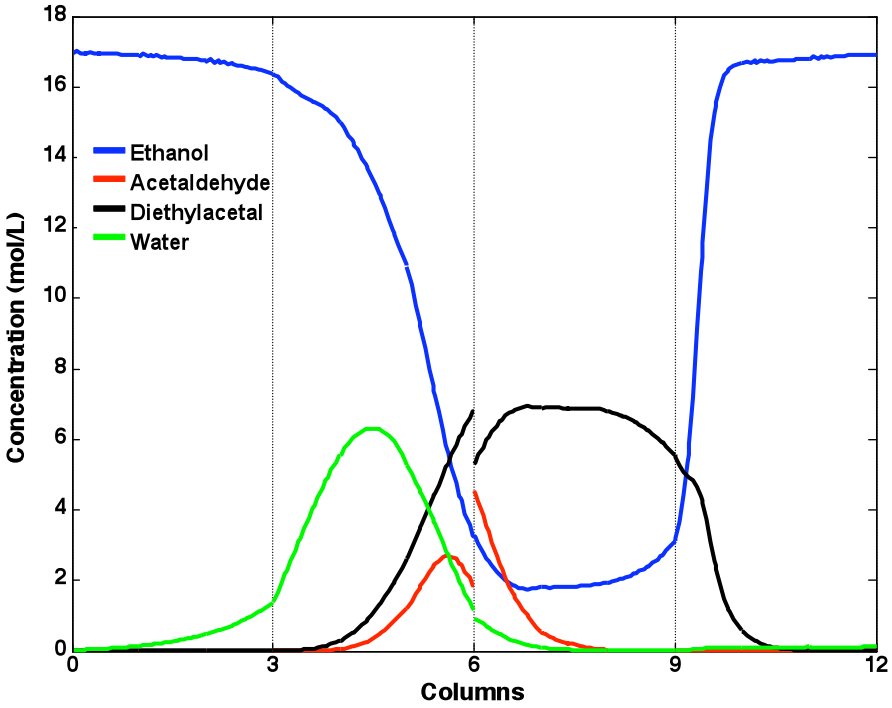

Figure 5.19 Cyclic steady state concentration profiles in the middle of switching time of 3.75 min for a feed composition 80 mol% acetaldehyde.

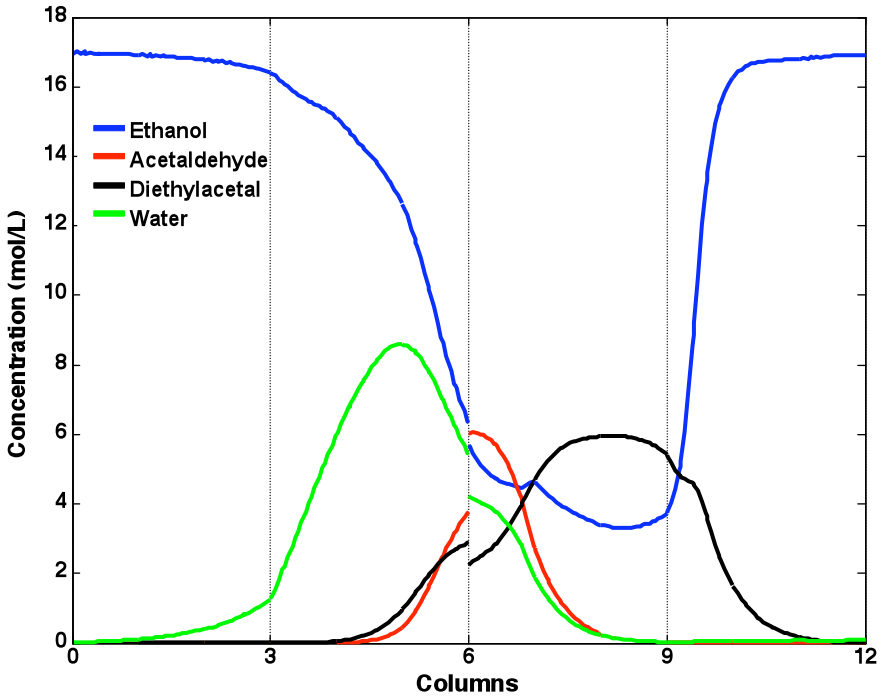

Figure 5.20 Cyclic steady state concentration profiles in the middle of switching time of 4 min for a feed composition 80 mol% acetaldehyde.

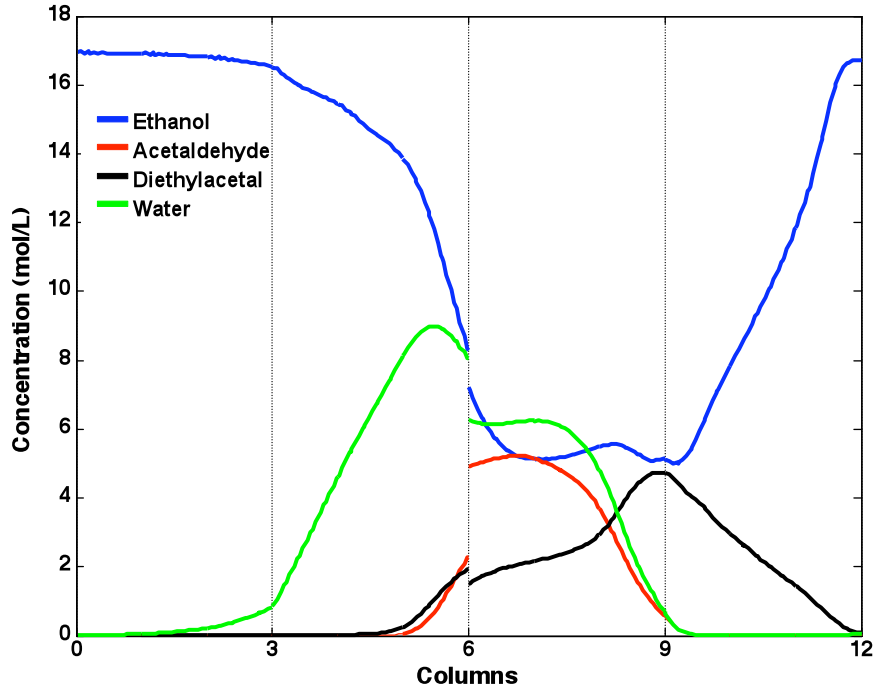

Figure 5.21 Cyclic steady state concentration profiles in the middle of switching time of 4.5 min for a feed composition 80 mol% acetaldehyde.

5.3.3 Effect of flow rate ratios on development of reaction/separation region

Lode et al. (2001) defined the reaction/separation region as the operation region where the product specifications are achieved, as shown in Figure 5.1. In our case, the criteria of purity and conversion were set at a minimum of 97%. To choose the proper design of the SMBCR system, it is necessary to find the major condition of the flow rates in each section of the system utilizing the best switching time (3.75 min in our case) and the best feed composition (80 mol% acetaldehyde in our case) found in Sections 5.3.1 and 5.3.2, respectively. To locate the reaction/separation region for the synthesis of diethylacetal, perform the following steps:

- Fix the feed concentration and switching time at the optimal values found in Sections 5.3.1 and 5.3.2, respectively.
- Fix the fluid/solid velocity ratio $\left(\gamma_i = {u_i}/{u_s}\right)$ in section I and IV. These values can be obtained using the equilibrium theory as explained previously. The values are $\gamma_1 = 8.7521$ and $\gamma_4 = 1.3819$.
- Consider different values of the fluid/solid velocity ratios $\left(\gamma_i = {u_i}/{u_s}\right)$ in sections II and III and build a γ_{II} - γ_{III} plane to find the reaction/separation region guarantying the minimum of purity of 97% in both raffinate and extract ports.

The reaction/separation region is located above the diagonal $\gamma_{II} = \gamma_{III}$. The condition of $\gamma_{II} = \gamma_{III}$ corresponds to zero feed flow rate; therefore γ_{III} must be higher than γ_{II} as shown by equation 5.7. To construct the reactive/separation region, after fixing $\gamma_{II} = \gamma_{IV} = 1.3819$, the values of γ_{II} and γ_{III} were increased by steps of 0.15. For each value of γ_{II} and γ_{III} the feed

flow rate was calculated from the mass balance in the feed port and for each combination of these flows the purities in the raffinate and extract ports were calculated. The simulation procedure ends with the last value of the maximum feed rate which gives extract and raffinate purities of 97%. Above that feed flow rate value the purity requirements cannot be fulfilled for any pair of values of (γ_{II}, γ_{III}).

Figure 5.22 shows the reaction/separation region for 97% of purity in the extract and raffinate ports. It shows that the region of complete reaction/separation is near the diagonal and is indicated by the solid circles. Figure 5.22 shows that, beyond the region of complete reaction/separation, increases of both flow rates in sections II and III yields contamination of the raffinate port (represented by up triangles in Figure 5.22). On the other hand, when the flow rates in sections II and III are reduced the extract port is contaminated (represented by down triangles in Figure 5.22).

The region of complete separation shown in Figure 5.1 usually has triangular form and the vertex represents the optimal performance. The vertex in Figure 5.22 is the circle without color which represents the best operational point in terms of productivity (24.29 kg/L-day) and desorbent consumption (5.15 L/kg) as shown in Figure 5.23. This figure was generated using the (γ_{II}, γ_{III}) pairs in the region of reaction/separation of Figure 5.22. As an example, Figure 5.24 shows the concentration profiles in the middle of the switching time of 3.75 min and feed concentration of 80% mol of acetaldehyde with γ_{II} = 2.625 and γ_{III} =3.5.

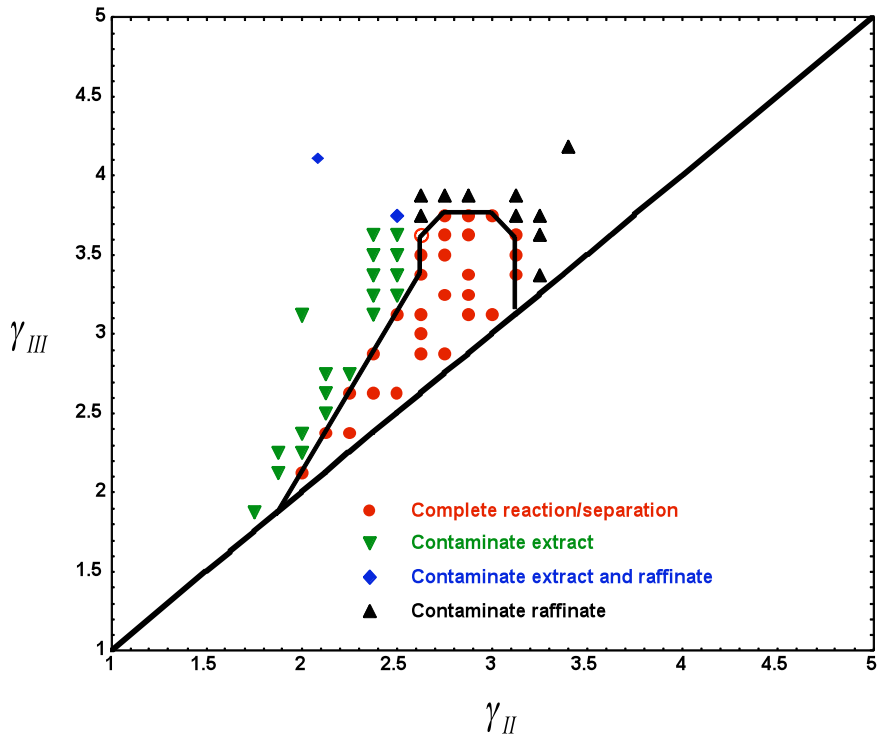

Figure 5.22 Flow rate ratios that describe the reaction/separation region for a switching time of 3.75 min and a feed composition 80 mol% acetaldehyde.

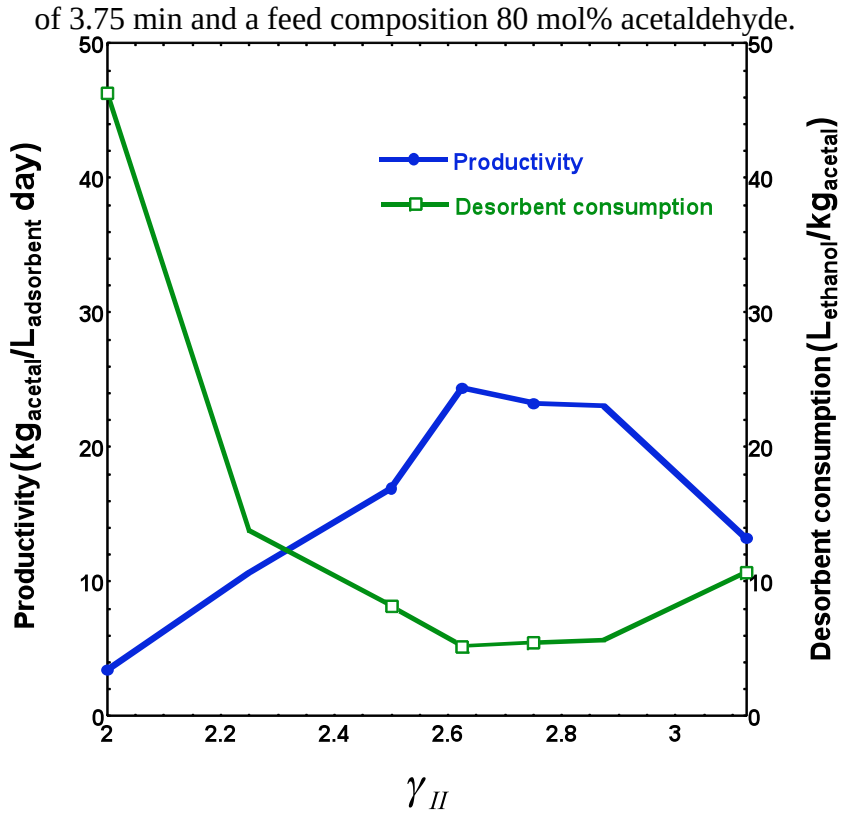

Figure 5.23 Effect of the flow rate ratios on productivity and desorbent consumption for a switching time of 3.75 min and a feed composition 80 mol% acetaldehyde.

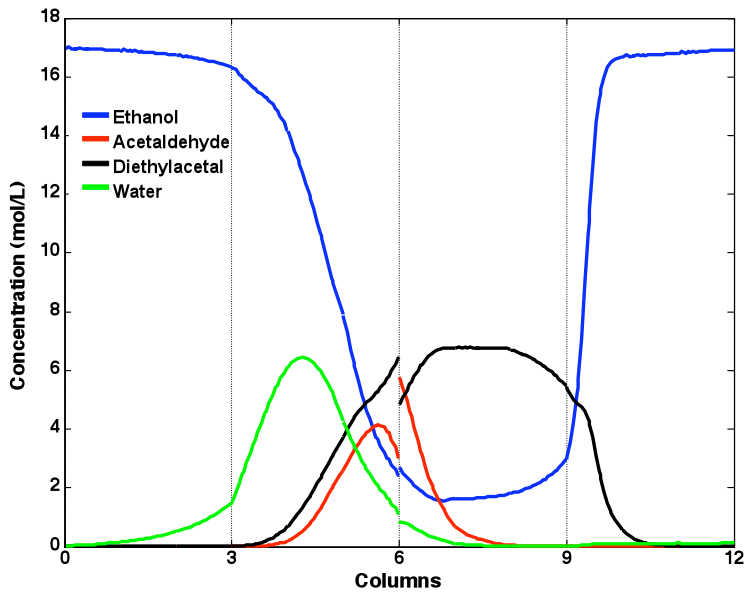

Figure 5.24 Cyclic steady state concentration profiles in the middle of switching time of 3.75 min for a feed composition 80% mol acetaldehyde (γ_{II} = 2.625 and γ_{III} = 3.5).

C H A P T E R 6

6. Conclusions and Recommendations for Further Research

6.1 Conclusions

The following conclusions are the result of detailed and careful analysis of inter-particle and intra-particle mass-transfer effects in chromatographic reactors:

1. Three different modeling and simulation approaches for chromatographic reaction processes have been presented and analyzed, starting with the rigorous model based on the Maxwell-Stefan approach for multicomponent mass transfer effects. Two simplified modeling approaches to describe the mass transfer effects have also been presented, the first based on the Fickian diffusivity concept, and the second based on the LDF approximation. The suitable modeling and simulation approach has to be chosen depending on the specific application.
2. The capabilities of the proposed model have been illustrated using two different case studies taken from the literature on FBCR systems. The first system is for the production of diethylacetal (acetal) from the reversible reaction between ethanol and acetaldehyde catalyzed by the acid resin Amberlyst 15 and 18 with nonlinear multicomponent adsorption isotherms. The second system is the production of triacetine from the reversible reactions, starting from glycerol and acetic acid catalyzed by the acid resin Amberlyst 15 with nonlinear multicomponent adsorption isotherms. In both cases, the Maxwell Stefan model proved to be robust and in all cases accurately predicted the experimental data.

3. In the acetal process, the intra-particle effects apparently had little effect on the process kinetics because the LDF model represented the experimental data almost as well as the rigorous Maxwell-Stefan model. In the triacetine process, however, the intra-particle effects are highly significant and neither one of the simplified models represented the experimental data nearly as well as the rigorous model proposed in this work.
4. The MATLAB®7 programming environment based on matrices proved to be very good for applications of this type. Using MATLAB®7 matrix notation and matrix processing routines it is possible to write a very compact code easy to understand, debug, and modify.
5. The Maxwell-Stefan approach can provide a useful tool for the exploration of the possible performance of more efficient continuous units, such as annular chromatography reactors or simulated moving bed reactors, and for their scale-up, which is needed to assess the economic performance that can be expected from these processes. In this work, we utilized this approach to successfully simulate the TMBCR and SMBCR configurations.
6. The synthesis of diethylacetal in a SMBCR was successfully modeled using the TMBCR approach when the mass-transfer effects were described in terms of the Maxwell-Stefan approach. The results obtained using this approach were in much better agreement with the SMBCR experimental results than those obtained using the LDF and Fickian modeling approaches.
7. The Maxwell-Stefan approach was used to compare the predictions of the TMBCR and SMBCR modeling alternatives for four application examples. The SMBCR

modeling strategy was found to be somewhat more precise than the TMBCR model for two of the cases considered and significantly more precise for the other two cases; however, it requires considerably higher computational effort, especially when many columns are involved. Therefore, the actual SMBCR modeling strategy using the Maxwell-Stefan approach should be considered as the simulation tool of choice for detailed optimization analysis of simulated moving bed chromatographic reactors for practical applications, if computational effort is not a main concern.

8. The optimal performance of a SMBCR was investigated through numerical simulation, using as a case study the synthesis of diethylacetal from ethanol and acetaldehyde, catalyzed by the acid resin Amberlyst®15. The effects of feed composition, switching time, and flow rate were investigated based on the dynamic model of a SMBCR developed in this work. The optimal operational conditions were found to be a switching time of 3.75 min and feed concentration of 80 mol% acetaldehyde.
9. The reaction/separation region for the previous case study was evaluated. The best operational point in terms of productivity (24.29 kg of acetal/L of adsorbent-day) and desorbent consumption (5.15 L ethanol/kg acetal) was found to be a switching time of 3.75 min, feed concentration of 80% mol of acetaldehyde, and γ_{II} = 2.625, γ_{III} =3.5 for 97% purity of both raffinate and extract.

6.2 Recommendations for further research

Throughout all the simulations in this work, it was assumed that the chromatographic reaction process was isothermal. The experimental results of all the case studies used to

validate the model confirmed this assumption. However, chemical reactions as well as adsorption-desorption processes frequently involve substantial heat effects. In many chromatographic reaction processes of industrial interest, the assumption of isothermal operation might not be valid. Therefore, one direction in which to continue this research could be adding to the Maxwell-Stefan model the heat balance equation and solving the coupled heat and mass balance system of differential equations that would result.

Another direction for further research is the investigation of increasingly complex reaction systems; enzymatic systems, systems with multiple reactions, some of which could be equilibrium-limited and others subject to product or reactant inhibition. More concentrated feed streams could be considered once the isothermal restriction is removed and substituted for adiabatic operation.

Identification of other reaction systems that might benefit from combined separation and reaction and the closely allied subject of discovering or developing new adsorbent-catalyst solids will form an important direction for further research. Heat recapture, energy efficiency, effects of particle size, and economic analysis of separating reactors are currently virgin topics.

REFERENCES

Agar D. W. (1999), Multifunctional reactors: Old preconceptions and new dimensions. *Chem. Eng. Sci., 54*, 1299.

Agreda V.H., and L.R. Partin (1984), Reactive distillation process for the production of methty acetate *U.S. patent 4,435,595* to Eastman Kodak.

Aizawa T., Nakamura H., Wakabayashi K., Kudo T., and Hasegawa H. (1994), Process for producing acetaldehyde dimethyl acetal, U.S.Patent No. 5,362, 918.

Akanni K., and Evans J. (1987), Effective transport coefficients in heterogeneous media, *Chem. Eng. Sci.*, 42, 1945.

Azevedo D.C.S., and Rodrigues A.E. (2001), Design methodology and operation of a SMBCR for the inversion of sucrose and glucose-fructose separation, *Chem. Eng. J.*, 82:95-107.

Backhaus A. (1923), Continuous process for the manufacture of esters. *U.S. Patent 1,400,849*.

Barker P.E., Ganetsos G., Ajongwen J., Akintoye A. (1992), *Chem. Eng. J.* 50 pp. 23-28.

Bart H.J, Kaltenbrunner W, Landschützer H. (1996), Kinetics of esterification of acetic acid with propyl alcohol by heterogeneous catalysis, *Int. J. Chem. Kin.*, 28, pp. 649-656.

Bart H.J. (2001), *Reactive Extraction*, Springer, Berlin.

Benedict D.J., Parulekar S.J., Tsai S.P. (2003), Esterification of lactic acid and ethanol with/without pervaporation, *Ind. Eng. Chem. Res.*, 42, 2282-2291.

Benedict D.J., Parulekar S.J., Tsai S.P. (2006), Pervaporation-assisted esterification of lactic and succinic acids with downstream ester recovery, *J. Membr. Sci.*, 281, 435-445.

Benitez J. (2002), *Mass Transfer Operations*. John Wiley & Sons, New York.

Berman S., Isbenjian H., Sedo A., and Othmer D. F. (1948), Esterification; continuous production of dibutyl phthalate in a distillation column, *Ind. Eng. Chem.*, 40, 2139-2148.

Bird R.B, Stewart W.E, and Lightfoot, E.N. (2002), *Transport Phenomena*, 2nd Ed., Wiley-New York.

Borren T., Fricke J. (2005), *Chromatographic reactors* in *Preparative Chromatography of Fine Chemicals and Pharmaceutical Agents* edited by Schmidt-Traub, H., Wiley-VCH Verlag, Weinheim, Germany.

Broughton D.B., and Gerhold C.G. (1961), *U.S. Patent 2,985,589*, to Universal Oil Products Company.

Chung S. F., and Wen C. Y (1968). Longitudinal dispersion of liquid flowing through fixed and fluidized beds. *A.I.Ch.E. Journal*, *17*, 857-874.

Dinwinddie J.A., and Morgan W.A. (1961), *U.S. Patent 2,976,132*, to Esso Research and Engineering Company.

Do D. D. (1998), *Adsorption Analysis: Equilibria and Kinetics*; Imperial College Press: London.

Dünnebier G, Fricke J, and Klatt K-U. (2000), Optimal design and operation of simulated moving bed chromatographic reactors, *Ind. Eng. Chem. Res.*, 39, 2290-2304.

Falk T., Seidel-Morgenstern A. (2002), Analysis of a discontinuously operated chromatographic reactor, *Chem. Eng. Sci.*, 57, pp. 1599-1606.

Finlayson B.A. (1980), *Nonlinear Analysis in Chemical Engineering*, McGraw-Hill, New York.

Fish B., Carr R., and Aris R. (1989), The continuous countercurrent moving-bed separator, *AIChE J.*, 25, 737-745.

Fredeslund A., Gmehling J., and Rasmussen P. (1977), *Vapor-liquid equilibria using UNIFAC*, Elsevier Science Publishers, Amsterdam.

Fricke J., Meurer M., Dreisorner J., and Schmidt-Traub H. (1999), Effect of process parameters on the performance of a simulated moving bed chromatographic reactor. *Chemical Engineering Science*, *54*, 1487-1492.

Gandi G. K.; Silva V. M. T. M.; and Rodrigues A. E. (2005), Process development for the dimethylacetal synthesis: thermodynamics and reaction kinetics, *Ind. Eng. Chem. Res.*, 44, 7287.

Gandi G. K.; Silva V. M. T. M.; and Rodrigues A. E. (2006), Synthesis of 1,1-dimethoxyethane in a fixed bed adsorptive reactor, *Ind. Eng. Chem. Res.*, 45, 2032.

Gelosa D., Ramaioli M., Valente G., and Morbidelli M. (2003), Chromatographic reactors: esterification of glycerol with acetic acid using acidic polymeric resins. *Ind. Eng. Chem. Res*., *42*, 6536-6544.

Gomes L, Leao C, Rodrigues A. (2007), Simulation of true moving bed adsorptive reactor: detailed particle model and linear driving force approximation. *Chemical Engineering Science*, 62, 1026-1041.

Gu T. (1995), *Mathematical modeling and scale-up of liquid chromatography*, Springer Velag, Berlin, Germany.

Guiochon G., Golsham-Shirazi S., and Katti A.M. (1994), *Fundamentals of preparative and nonlinear chromatography*, Academic Press, New York.

Hashimoto K, Adachi S, Noujima H, and Ueda Y. (1983), A new process combining adsorption and enzyme reaction for producing higher-fructose syrup, *Biotech. Bioeng.*, 25 Nr. 10, pp. 2371-2393.

Helfferich F.G. (1970), *Multicomponent chromatography*, Marcel Dekker, New York.

Herbsthofer R., and Bart H.-J. (2003), Influence of reaction kinetics on the performance of a chromatographic reactor, *Chem. Eng. Technol.*, 26, 874-879.

Higler A., Taylor R., and Krishna R. (2000), Nonequilibrium modeling of reactive distillation: a dusty fluid model for heterogeneously catalyzed process. *Ind. Eng Chem. Res.*, 39, 1596.

Jafar J.J., Budd P.M., and Hughes R. (2002), Enhancement of esterification reaction yield using zeolite A vapor permeation membrane, *J. Membr. Sci.*, 199, 117-123.

Juza M., Mazzotti M., and Morbidelli M. (2000), Simulated moving-bed chromatography and its application to chirotechnology. *Trends in Biotechnology*, *18*, 108-118.

Kaczmarski K., and Antos D. (1996), Fast finite difference method for solving multicomponent adsorption-chromatography models, *Comput. Chem. Eng.*, 20, 1271-1276.

Kaczmarski K., Mazotti M., Storti G., and Morbidelli M. (1997), Modeling fixed-bed adsorption columns through orthogonal collocation on moving finite elements, *Comput. Chem. Eng.*, 21, 641-660.

Kaufhold M., and El-Chabawi M. (1996), Process for preparing acetaldehyde diethyl acetal, U.S. Patent No. 5,527,969.

Kawase M., Pilgrim A., Araki T., and Hashimoto K. (2001), Lactosucrose production using simulated moving bed reactor. *Chemical Engineering Science*, 51, 2971-2976.

Kawase M., Inoue Y., Araki, T., and Hashimoto, K. (1999), The simulated-moving-bed reactor for production of bisphenol A. *Catalysis Today*, *48*, 199-209.

Kawase M., Suzuki T. B., Inoue K., Yoshimoto, K., Hashimoto, K. (1996), Increased esterification conversion by application of the simulated moving bed reactor. *Chem. Eng. Sci.*, *51*, 2971-2981.

Kelly J., Chapman S., Brereton P., Bertrand A., Guillou C., and Wittskowski R. (1999), Gas chromatographic determination of volatile congeners in spirit drinks; interlaboratory study, *J. AOAC Int.*, 82, 1375.

Kenig E.Y, and Górak A. (2005), *Reactive absorption*, in: *Integrated Chemical Processes: Synthesis, Operation, Analysis, and Control*, Wiley-VCH, Weinheim, Germany, pp. 265-311.

Kohlpaintner C., Schulte M., Falbe J., Lappe P., and Weber J. (1999), Aldehydes, aliphatic and araliphatic, *Ullmann's Encyclopedia of Industrial Chemistry*, Wiley-VCH, Weinheim, Germany.

Krishna R., and Wesselingh J. (1997), The Maxwell-Stefan approach to mass transfer. *Chemical Engineering Science*, 52, 861-911.

Lang F. (2003), A continuous annular chromatograph, Ph.D. Thesis, ETH, Zurich, Switzerland.

Liapis A.I., and Rippin D.W.T. (1979), Simulation of binary adsorption in continuous counter-current operation in comparison with other operating modes, *A.I.Ch.E. Journal*, 25, 455-460.

Lode F, Francesconi G, Mazzitti M, and Morbidelli M. (2003), Synthesis of methylacetate in a simulated moving-bed reactor: experiments and modeling, *A.I.Ch.E. Journal*, 49, 1516.

Lode F., Houmard M., Migliorini C., Mazzotti M., and Morbidelli M. (2001) Continuous reactive chromatography. *Chem. Eng. Sci*., *56*, 269-291.

Martin A.J.P. (1949), *Summarizing paper*, Discuss. Faraday Soc., 7, pp. 332.

Mathworks (2007), Using MATLAB® Version 7. The Mathworks, Massachusetts

Mazotti M., Storti G., and Morbidelli M. (1997), Optimal operation of simulated moving bed units for nonlinear chromatographic separations, *J. Chromatogr*., 769.

Mazzotti M., Kruglov A., Neri B., Gelosa D., and Morbidelli M. (1996), A continuous chromatographic reactor: SMBR. *Chemical Engineering Science*, *51*, 1827-1836.

Mazzotti M., Neri B., Gelosa D., and Morbidelli M. (1997b), Dynamics of a chromatographic reactor: esterification catalyzed by acidic resins. *Industrial and Engineering Chemistry Research*, *36*, 3163-3172.

Meurer M., Altenhoner U., Strube J., and Schmidt-Traub H. (1997), Dynamic simulation of SMBCRs, *Chem. Eng. Sci.*, 52, 71-79.

Migliorini C., Fillinger M., Mazzotti M., and Morbidelli M. (1999), Analysis of simulated moving bed reactors, *Chem. Eng. Sci.*, 54, 2475-2480.

Minceva M., and Rodrigues A.E. (2005), Simulated moving-bed reactor: reactive separation regions. *A.I.Ch.E. Journal*, 51, 2737–2751.

Oost C, and Hoffmann U. (1996), The synthesis of tertiary amyl methyl ether (TAME): microkinetics of the reactions. *Chem. Eng. Sci*., 51, 329-340.

Oudshoorn O. L., Janissen M., Van Kooten W.E.J., Van Bekkum H., Van Den Bleek C.M., and Calis H.P.A. (1999), A novel structured catalyst packing for catalytic distillation of ETBE. *Chem. Eng. Sci*., 54, 1413-1418.

Pais L.S., Loureiro J.M., and Rodrigues A.E. (1998), Modeling strategies for enantiomeres separation by SMB chromatography, *A.I.Ch.E. Journal*, 44, 561-569.

Pereira C.S.M., Gomes P.S., Gandi G.K., Silva V.M.T.M., and Rodrigues A.E. (2008), Multifunctional reactor for the synthesis of dimethylacetal, *Ind. Eng. Chem. Res.*, 47, 3515-3524.

Pereira C.S.M., Zabka M., Silva V.M.T.M., and Rodrigues A.E. (2009), A novel process for the ethyl lactate synthesis in a simulated moving bed reactor (SMBR), *Chem. Eng. Sci.*, 64, 3301-3310.

Perry's Chemical Engineers Handbook (1984), McGraw-Hill: New York.

Petroulas T., Aris R., and Carr R. (1985), Analysis and performance of a counter-current moving-bed chromatographic reactor, *Chem. Eng. Sci.*, 40, 2233-2240.

Poling B., Prausnitz J., and O'Connell J. (2001), *The properties of gases and liquids*; 5th Ed., McGraw-Hill: New York.

Reissner A., Priot A., Wolfgang J., Bart H.J., and Byers C.H. (1997), Preparative desalting of bovine serum by continuous annular chromatography, *J. Chrom. A.*, 763, 49-56.

Rice R, and Do D. (1995), *Applied Mathematics and Modeling for Chemical Engineers*. John Wiley & Sons: New York.

Ruthven D. M. (1984), *Principles of Adsorption and Adsorption Processes*; John Wiley & Sons: New York.

Sardin M, Schweich D., and Villermaux J. (1993), *Preparative Fixed-Bed Chromatographic Reactor* in *Preparative and Production Scale Chromatography* edited by Ganetsos, G., and Barker, P.E., Marcel Dekker, New York, USA, pp. 477-522.

Sarmidi M. R., and Barker P. (1993), Simultaneous biochemical reaction and separation in a rotating annular chromatograph. *Chem. Eng. Sci., 48*, 2615-2623.

Schweich D., and Villermaux J. (1982), Evidence for a transient promoting catalytic effect in a chromatographic reactor, *Ind. Eng. Chem. Fundam.*, 21, 51-55.

Shieh M. T., and Barker P. (1995), Saccharification of modified starch to maltose in a semi-continuous counter-current chromatographic reactor-separator (SCCR-S). *Journal of Chemical Techniques in Biotechnology*, 63, 125-134.

Shieh M. T.,and Barker P. (1996) Combined bioreaction and separation in a simulated counter-current chromatographic bioreactor-separator for the hydrolysis of lactose. *Journal of Chemical Techniques in Biotechnology*, 66, 265-278.

Silva V. M. T. M., and Rodrigues A. E. (2002), Dynamics of fixed-bed adsorptive reactor for the synthesis of diethylacetal, *AIChE J.*, 48, 625.

Silva V. M. T. M.; and Rodrigues A. E. (2005), Novel process for dimethylacetal synthesis, *A.I.Ch.E. J.*, 51, 2752.

Silva V. M. T. M.; and Rodrigues A. E. (2001), Novel syntesis of diethylacetal: thermodynamic and kinetic studies. *Chem. Eng. Sci., 56*, 1255-1263.

Smith J. M.; and Van Ness H. C. (1987), *Introduction to chemical engineering thermodynamics*; 4th Ed., McGraw-Hill: New York, 1987.

Sneesby M.G., Tadé M.O., and Smith T.N. (1998), Multiplicity and pseudo-multiplicity in MTBE and ETBE reactive distillation, *Trans I. Chem. E.*, 76A, 525-531.

Storti G., Mazzotti M., Morbidelli M., and Carra S. (1993), Robust design of binary countercurrent separation processes, *A.I.Ch.E. Journal*, 39, 471-492.

Storti G., Massi M.,Paludetto R., Morbidelli M., and Carra S. (1988), Adsorption separation processes; countercurrent and simulated countercurrent operations, *Computers in Chemical Engineering*, 12, 475.

Ströhlein G, Assuncao Y, Dube N, Bardow A, Mazzotti M, and Morbidelli M. (2006), Esterification of acrylic acid with methanol by reactive chromatography: Experiments and simulations. *Chem. Eng. Sci.*, 61, 5296-5306.

Sundamacher K, Uhde G, and Hoffmann U. (1999), Multiple reactions in catalytic distillation processes for the production of the fuel oxygenates MTBE and TAME. *Chem. Eng. Sci*., 54, 2839-2847.

Takahashi Y., and Goto S. (1992) Continuous separation of fructoligosaccharides using annular chromatography, *J. Chem. Eng. Japan*, 25, 403.

Takeuchi K., and Uraguchi Y. (1977), Experimental studies of a chromatographic moving-bed reactor: catalytic oxidation of carbon monoxide on activated alumina as a model reaction. *Journal of Chemical Engineering Japan*, 10, 455-460.

Tanaka K., Yoshikawa R., Ying C., Kita H., and Okamoto K. (2002), Application of zeolite T membrane to vapor-permeation-aided esterification of lactic acid with ethanol, *Chem. Eng. Sci.*, 57, 1577-1584.

Taylor R., and Krishna R. (1993), *Multicomponent mass transfer*, John Wiley & Sons, New York.

Teja A. S., and Rice P. (1981), Generalized corresponding states method for the viscosities of liquid mixtures. *Ind. Eng. Chem. Fundam*., *20*, 77.

Toumi A., and Engell S. (2004), Optimization-based control of a reactive SMB process for glucose isomerization. *Chem. Eng. Sci.*, 59, 3777-3792.

Van Der Wielen L., Potters J., Straathof A., and Luyben K. (1990), Integration of bioconversion and continuous product separation by means of counter-current adsorption, *Chem. Eng. Sci.*, *45*, 2397-2404.

Waller F.J., Weist E.L., Brown, D.M., and Tijm P.J.A. (1999), Diesel fuel composition comprising dialkoxy alkanes for increased cetane number, U.S. Patent 5,858,030.

Villermaux J. (1981), *The chromatographic reactor* in *Percolation Processes: Theory and Application* edited by Rodrigues A.E., and Tondeur D., Sijthoff en Noordhoff, Alpena an den Rijn, The Netherlands, pp. 539-588.

Zhang Z., Hidajat K., and Ray A.K. (2001), Application of simulated countercurrent moving bed chromatographic reactor for MTBE synthesis, *Ind Eng Chem Res*., 40, 5305-5313.